A GENERALIZED ELECTRONIC DIABATIC MODEL APPLIED TO TWO-STATE REACTIONS

by

Laura Bray Laverdure

A thesis submitted in partial fulfillment
of the requirements for the degree of
Master of Science (MSc) in Chemical Sciences

The Faculty of Graduate Studies
Laurentian University
Sudbury, Ontario, Canada

THESIS DEFENCE COMMITTEE/COMITÉ DE SOUTENANCE DE THÈSE
Laurentian Université/Université Laurentienne

Faculty of Graduate Studies/Faculté des études supérieures

Title of Thesis Titre de la thèse	A GENERALIZED ELECTRONIC DIABATIC MODEL APPLIED TO TWO-STATE REACTIONS
Name of Candidate Nom du candidat	Laverdure, Laura Bray
Degree Diplôme	Master of Science
Department/Program Département/Programme	Chemical Sciences
Date of Defence Date de la soutenance	January 16, 2015

APPROVED/APPROUVÉ

Thesis Examiners/Examinateurs de thèse:

Dr. Gustavo Arteca
(Supervisor/Directeur de thèse)

Dr. Jeffrey Shepherd
(Committee member/Membre du comité)

Dr. M'hamed Chahma
(Committee member/Membre du comité)

Dr. Paul Mezey
(External Examiner/Examinateur externe)

Approved for the Faculty of Graduate Studies
Approuvé pour la Faculté des études supérieures
Dr. David Lesbarrères
M. David Lesbarrères
Acting Dean, Faculty of Graduate Studies
Doyen intérimaire, Faculté des études supérieures

ACCESSIBILITY CLAUSE AND PERMISSION TO USE

Abstract

A generalized electronic diabatic model for chemical reactions includes a physical mechanism for the transition from a reactant-like to a product-like quantum state, namely, an external field. In our model, an external electric field couples states and modifies effective potential energy surfaces thereby allowing to treat a reaction as a fully quantum process. Through semi-classical models of two-state reactions, we show that we can control the identity of the most stable nuclear configuration by varying the form and intensity of the external field's coupling potential. We group topologically equivalent potential energy curves in phase diagrams for a manifold of simple two-state models. We also illustrate the method's implementation in a fully quantum-mechanical approach by considering two diabatic states in the radical HBN⇄BNH isomerization. To ensure diabaticity, these states are built on a grid of floating Gaussian orbitals and the potential energy curves are constructed by moving the nuclei.

Keywords

Diabatic functions, potential energy surfaces, external fields, semi-classical models

Acknowledgements

The author thanks the following people and organizations:

The National Science and Engineering Research Council of Canada and Laurentian University for supporting this research financially,

Dr. G.A. Arteca for his patient supervision of this research project,

Dr. J. Shepherd and Dr. M. Chahma, the committee members,

Louise Bray and Paul Laverdure for their humorous revisions of the first completed draft,

Table of Contents

Table of Figures

1. Introduction

Introductory chemistry courses present chemical reactions as processes that unfold on a single potential energy surface.[1] Within this interpretation, by way of collisions with other molecules or by interacting with photons, the reaction system gains enough energy to overcome reaction barriers and rearrange electronically. These semi-classical concepts, an inaccurate quantum representation at best, can be traced to the separate treatment of nuclei and electrons given in the Born-Oppenheimer (BO) approximation.[2] This approximation works well for vibrational frequencies and simple thermal processes. It does not work well, however, where electronic and nuclear motions are coupled such as in the formation or dissociation of bonds. The failure is complete where the motions are strongly coupled, for example, at conical intersections where electronic states cross.[3] On a more fundamental level, the BO approximation lacks a 'reaction driver' that is to say an external force that 'makes a reaction go'. When we consider the possibility of reaction control with lasers or more generally with external fields [4-7], the need for an adequate explanation becomes more pressing.

In this thesis, we employ an alternative approach based on a generalized electronic diabatic model.[8-16] For this model, the external force is an electric field. This external electric field is the 'driving force' lacking in the BO approximation. With this field, we will be able to account for many of the features that characterize a chemical process as a change in quantum state taking place over an effective surface. Using semi-classical potential energy curves, we can determine general trends in how the external field via its coupling potential can change an effective potential energy surface.

The various models of energy surfaces can be grouped into 'phases' where each region would represent an archetypical shape of a total energy surface as characterized by a topological criterion. One of the main objectives of this thesis is to predict these possible 'phases' over an entire ensemble of model diabatic potentials for two-state chemical processes. The diagrams, or 'topology maps', help illustrate the subtle variations in the effective potential energy curve as the model parameters and the field coupling's potential's shape and intensity are varied.

As a complement, we present a quantum-mechanical approach to build diabatic electronic eigenfunctions on a grid of orbitals that are not centred on any nuclei. This methodology, recently used for a three-state process [8], is adapted here to study a simple two-state radical isomerization. From an optimal grid, we then extract the potential energy surfaces by moving the nuclei along different plausible reaction trajectories.

1.1 Review of the Born-Oppenheimer Approximation

The BO approximation represents a cornerstone in quantum mechanics and remains a standard to which new approaches are compared.[17] This thesis is no exception. A brief overview of the BO approximation and its deficiencies shall serve as a motivation for developing a more physical description of chemical reactions consistent with the quantum nature of the process.

In the analysis of any quantum mechanical problem, the starting point is to find a solution to a Schrödinger equation, either time dependent or independent. The BO approximation attempts a solution of the time-independent Schrödinger equation for systems with several degrees of freedom, written as follows:

$$\hat{H}_{mol}(\mathbf{r},\mathbf{R})\Psi(\mathbf{r},\mathbf{R}) = E(\mathbf{R})\Psi(\mathbf{r},\mathbf{R}) \qquad \text{Equation 1}$$

where **r** represents the electronic position operator, while **R** is a vector of nuclear coordinates in the laboratory frame. Both act as variables for the set of basis functions, $\{\Psi\}$, for the Hilbert space of quantum states. $\hat{H}_{mol}$, as given in Equation 2, is the molecular Hamiltonian operator and consists of the electronic and nuclear kinetic energy operators as well as the system's potential energy operator. This last operator includes the electronic, the nuclear and electronuclear potential operators:

$$\hat{H}_{mol} = \hat{T}_e + \hat{T}_N + \hat{U}(\mathbf{r},\mathbf{R})$$

$$= -\frac{1}{2}\sum_i \nabla_{\mathbf{r}_i}^2 - \frac{1}{2}\sum_\alpha \frac{\nabla_{\mathbf{R}_\alpha}^2}{M_\alpha} + \sum_{i<j}\frac{1}{\|\mathbf{r}_i - \mathbf{r}_j\|} + \sum_{\alpha<\beta}\frac{Z_\alpha Z_\beta}{\|\mathbf{R}_\alpha - \mathbf{R}_\beta\|} - \sum_{i,\alpha}\frac{Z_\alpha}{\|\mathbf{r}_i - \mathbf{R}_\alpha\|} \qquad \text{Equation 2}$$

where α and β refer to the nuclei and i and j refer to the electrons. Furthermore, we use atomic units, equivalent to $\frac{\hbar^2}{|e|^2 m_e} = 1$, and measure distances in Bohrs, nuclear masses in terms of the electron's mass m_e and charges in electron charges |e|. The BO approach begins by introducing the expansion of the total time-independent molecular eigenfunction of $\hat{H}_{mol}$, Ψ, as the superposition of the product of two functions [18,19]:

$$\Psi = \sum_i \varphi_i(\mathbf{r};\mathbf{R})\chi_i(\mathbf{R}) \qquad \text{Equation 3}$$

The so-called electronic eigenfunctions φ_i depend on the electronic coordinates and also parametrically on the nuclear coordinates. The part of the molecular eigenfunction that is associated to the dynamics of the nuclei as quantum particles is given as $\chi_i(\mathbf{R})$. Due the great difference between nuclear and electronic masses ($M_\alpha \geq 1836$ in electron masses $m_e = 1$), their coordinates are treated differently in the BO approximation. The electrons form the fast coordinates and the nuclei are the slow coordinates. With this separation, the nuclear kinetic energy operator is then neglected. The effect of this is physically equivalent to keeping the nuclear coordinates fixed, thereby defining an electronic Hamiltonian [19,20]:

$$\hat{H}_e = \hat{T}_e + \hat{U}(\mathbf{r},\mathbf{R}) \qquad \text{Equation 4}$$

From a semi-classical point of view, this separation of coordinates would no longer be justified if the classical nuclear velocities were substantial. However, in this range of velocities, the very notion of a "classical" molecule is inappropriate; the nuclei and electrons form a quantum plasma. On the other hand, fixing the nuclear positions is unfeasible in chemical reactions where bonds are broken and formed. The nuclear coordinates change and the electronic eigenfunctions, being parametrically dependent on these, must change as well.

Born and Oppenheimer expanded the expression for a system's energy, $\langle\Psi|\hat{H}_{mol}\Psi\rangle_{\mathbf{r}}$, as a power series in $(m_e/M)^{1/4}$ where m_e is the electronic mass and M is a nuclear mass.[19,21] The terms comprising vibration, translation and rotation, correspond to different powers in $(m_e/M)^{1/4}$; where these motions can be separated, as usual, using nuclear coordinates denoted by **Q**, and coordinates referring to the centre of mass, $\mathbf{R_{CM}}$.[18,19]

At this point there are two main options on how to deal with nuclear dynamics. The first option is to continue the quantum mechanical treatment. One can solve for the nuclear portion of the molecular Hamiltonian's eigenfunction under the assumption that the separation of coordinates is valid:

$$\left\langle \varphi_i(\mathbf{r};\mathbf{R}) \middle| \hat{H}_{mol} \Psi(\mathbf{r},\mathbf{R}) \right\rangle_{\mathbf{r}} = U_i(\mathbf{R})\chi_i(\mathbf{R}) \qquad \text{Equation 5}$$

where $U_i(\mathbf{R})$, the electronic potential energy, is the eigenvalue of the electronic Hamiltonian.[18] The second choice is to take the electronic potential energy, $U_i(\mathbf{R})$, as the surface on which nuclear trajectories are treated classically via Newtonian or Langevin dynamics.[22,23]

Both the electronic and nuclear parts contain nuclear coordinates and hence they are affected by the nuclear kinetic energy operator. This gives rise to what are called non-adiabatic coupling terms (NACTs) which measure the nuclear dependence of the electronic part of the molecular Hamiltonian's eigenfunction. The BO approximation, which is also called adiabatic, lies in neglecting the non-adiabatic coupling terms.[18] If the coupling terms are small, the expression for the molecular energy can be improved by their reintroduction. The reintroduction helps account for transitions between potential energy surfaces, for example between the electronic ground and excited states. However, a central complication arises: the non-adiabatic coupling terms diverge at points where the probability for a transition is highest, that is the set of points where the potential energy surfaces cross. These terms are given by [18]:

$$\langle \varphi_j(\mathbf{r};\mathbf{R}) | \nabla_{\mathbf{R}} \varphi_i(\mathbf{r};\mathbf{R}) \rangle_{\mathbf{r}} = \frac{\left\langle \varphi_j(\mathbf{r};\mathbf{R}) \middle| \nabla_{\mathbf{R}} \hat{H}_e \middle| \varphi_i(\mathbf{r};\mathbf{R}) \right\rangle_{\mathbf{r}}}{U_i(\mathbf{R}) - U_j(\mathbf{R})} = \mathbf{F}_{ij}(\mathbf{R}) \qquad \text{Equation 6}$$

where $\nabla_{\mathbf{R}}$ is the gradient in nuclear coordinates. These crossings, known as conical intersections, represent the ultimate breakdown of the BO approximation.

1.2 Conical Intersections

As stated above, the adiabatic approximation is invalid whenever two or more potential energy surfaces cross within the BO approximation (see Equation 6).[18] Unfortunately, previous and ongoing research demonstrates the ubiquitous nature of conical intersections.[3, 18,24-26] What was initially thought to be a exoticism of highly symmetrically systems – such as with N_3 radical

or alkali triatomics which have D_{3h} symmetry – is now shown to occur in non-symmetric systems as well.[27-29] In both cases, conical intersections affect reaction kinetics by offering radiationless pathways – a 'spontaneous' jump from one energy surface to another.

Let us take the example of a bond dissociation or formation reaction with an energy barrier. By following the adiabatic reaction coordinate, the electronic eigenfunction changes considerably at the reaction barrier. At this point, if the separation between two surfaces is small, the reaction may not proceed adiabatically to the product configuration. Instead of taking on the product's characteristics, the electronic eigenfunction may retain those of the reactant. The molecule would then have made a non-adiabatic 'hop' to the upper bound surface. The non-adiabatic recrossing of the energy barrier will reduce the rate constant for that reaction. Situations such as these, where there is a decoupling between nuclear configuration and electronic structure, are well-known in the active site for several proteins involved in hydrogen transfer and electron transfer.[30-32]

These conical intersections need not even be along the minimum energy reaction path (see Figure 1) for the non-adiabatic terms to become significant.[33] The influence of the conical intersection extends far beyond the point of intersection because the derivative couplings remain large for a volume surrounding that point in nuclear configuration space. For this reason, even though the conical intersections take up virtually no volume of coordinate space, they influence nuclear motion to a large extent. In other words, if they are energetically accessible, they must be accounted for.

In the context of eliminating the shortcomings of the BO approximation, conical intersections must be included for a complete description of a reaction's evolution. It is, therefore, important either to know where they occur or how to avoid diverging non-adiabatic coupling terms they produce with post-BO methods. We explain below some basic concepts to locate conical intersections. These notions provide a proper context to understand the alternative procedure we follow, based on diabatic functions as opposed to correcting the adiabatic BO solutions by including non-adiabatic coupling terms near conical intersections.

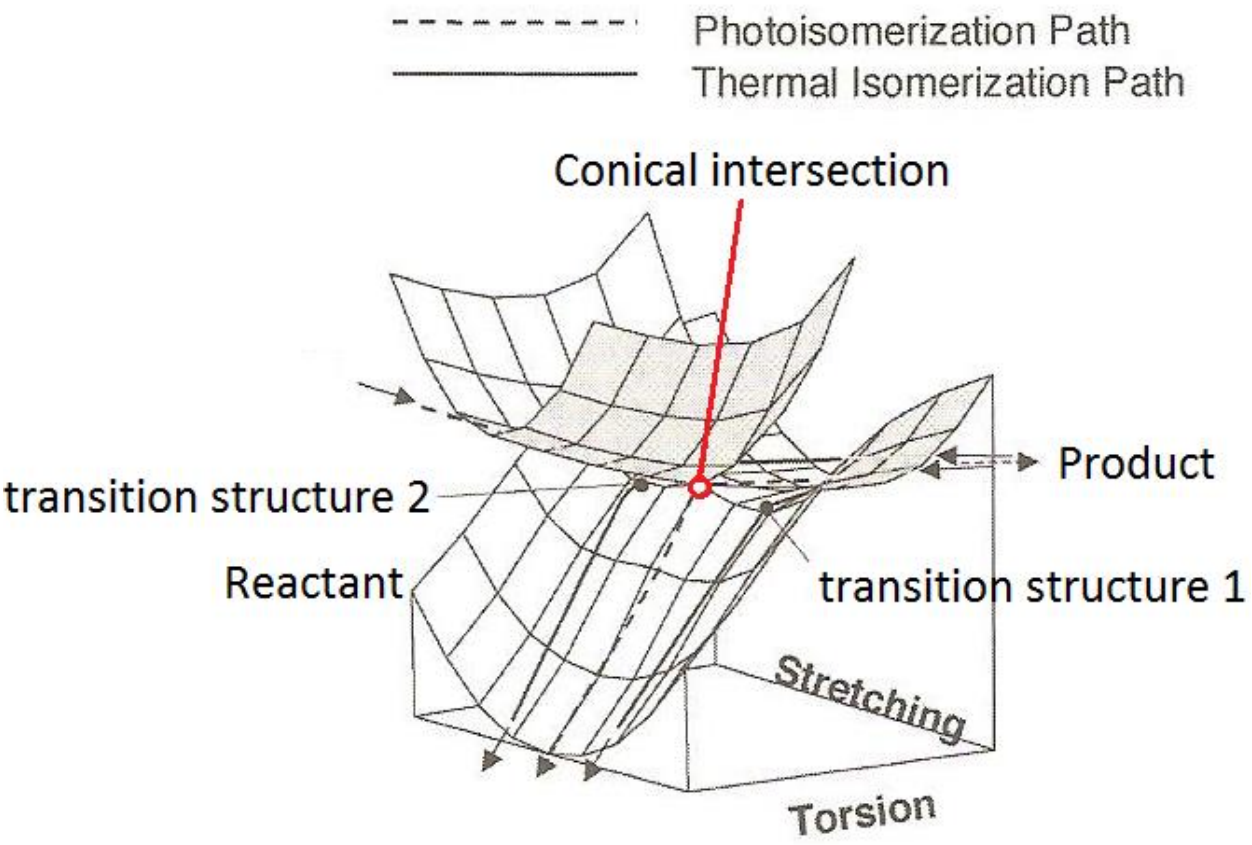

Figure 1. Example of a conical intersection

Figure 1 shows a conical intersection between the excited and ground state potential energy surfaces for the isomerization of a polyeniminium cation. On the photoisomerization path, the electronically excited species reaches the product state through the conical intersection. The transition structures along the thermal isomerization path are in the vicinity of the conical intersection. Significant non-adiabatic effects are thus expected for both isomerization paths. Figure adapted from [34]

Symmetry is generally used to classify conical intersections:

1. The first known type of conical intersections is called symmetry-required intersections. These occur in highly symmetrical molecules between states belonging to the same degenerate irreducible representation.[35] The symmetry-required conical intersections occur when the nuclear configuration reaches an energetically unstable point of higher symmetry and this degeneracy is lifted by linear displacements in nuclear coordinates thus giving rise to the Jahn-Teller effect.[36]

2. The other two types of conical intersections are called "accidental" since their presence is not caused by symmetry and cannot be predicted from simple properties of the molecular Hamiltonian. Accidental symmetry-allowed conical intersections involve the crossing of two states of distinct symmetry, that is belonging to different irreducible representations.[25] The accidental same-symmetry conical intersections are, as the name implies, the crossing of two states belonging to the same symmetry. The states may have the same symmetry, that is they may belong to the same irreducible representation, but they do not necessarily belong to the solutions of the same attractor equilibrium geometry.[25,26]

Apart from causing divergence in the derivative couplings, conical intersections have another distinguishing feature, a wave function phase known as the Berry phase.[37] The Berry phase changes sign for electronic eigenfunctions that have completed a loop around an odd number of conical intersections.[26] This phase must be carefully monitored in post-BO schemes to ensure that one stays in the correct reaction channel during nuclear dynamics. Conical intersection location schemes are based either on locating derivative divergences or the change in sign in the Berry phase.[25]

1.3 Methodologies beyond the Born-Oppenheimer approximation

To provide context and contrast to the non-adiabatic methodology used in this thesis, we will briefly describe other methods of solving potential energy curve problems near conical intersections. The usual method to overcome the divergent non-adiabatic coupling terms is to consider a transformation from the adiabatic basis to a diabatic basis, that is a set of functions

that are strictly independent of nuclear coordinates.[37] We briefly show that through such transformations, one can, at best, only achieve a quasi-diabatic basis set, nearly independent of nuclear coordinates for a region of configurational space.

Can one get rigorously diabatic states through a transformation of adiabatic states? The answer is a very restricted "yes". It is possible to build diabatic states from an orthogonal transformation of a small subset of adiabatic states such that the derivative couplings vanish, at least in a finite region of configurational space.[38] This small subset would typically contain strongly coupled states, well-separated from all others in a relevant range of nuclear coordinates. The transformation matrix can then be applied to the strongly coupled adiabatic basis functions. For instance in the case of a two-state problem, the diabatic basis functions, $(\varphi_1^{\mathrm{d}}, \varphi_2^{\mathrm{d}})$, would be obtained from the strongly coupled adiabatic solutions, (φ_1, φ_2) by applying a transformation matrix:

$$\begin{pmatrix} \varphi_1^{\mathrm{d}} \\ \varphi_2^{\mathrm{d}} \end{pmatrix} = \mathrm{S}^{\mathrm{T}}(\mathbf{Q}) \begin{pmatrix} \varphi_1 \\ \varphi_2 \end{pmatrix} \qquad \text{Equation 7}$$

where the "rotation" transformation matrix is given as:

$$\mathrm{S}(\mathbf{Q}) = \begin{pmatrix} \cos\alpha(\mathbf{Q}) & \sin\alpha(\mathbf{Q}) \\ -\sin\alpha(\mathbf{Q}) & \cos\alpha(\mathbf{Q}) \end{pmatrix} \qquad \text{Equation 8}$$

where the mixing angle, $\alpha(\mathbf{Q})$, rotates the system in the two states' internal coordinate space, $\mathbf{Q}$. The purpose of this transformation is to eliminate the derivative couplings $\mathbf{F}_{\mathrm{ij}}$,[38] at least over some region of the Q-space. This is achieved by choosing the rotational angle, $\alpha(\mathbf{Q})$, as follows [39]:

$$\mathbf{F}_{\mathrm{ij}}^{\mathrm{d}} = -\nabla_{\mathbf{Q}}\alpha(\mathbf{Q}) + \mathbf{F}_{\mathrm{ij}} = 0 \qquad \text{Equation 9}$$

If we restrict ourselves to a single nuclear coordinate, the mixing angle obtained by the integration of Equation 9 produces a set of basis functions that are diabatic along that nuclear coordinate.[38] Most reactions require multiple coordinates for their description and therefore the applicability of this procedure is restricted to diatomic molecules.

If we do not restrict integration to a single dimension, the mixing angle, $\alpha(\mathbf{Q})$, may be path dependent. The path dependence can be avoided if the complete set of interacting electronic states is included in the transformation matrix $S(\mathbf{Q})$, which, for all but very simple systems, contradicts our choice of a small subset. Thus, in general, rigorously diabatic basis sets produced from a finite adiabatic basis set do not exist.[38] There are, however, several methods to create "quasi-diabatic basis sets". Indeed, the recent literature on new diabatization schemes involves quasi-diabatization schemes.[38-44] Quasi-diabatic states still give non-zero derivative couplings, but the singularity in Equation 6 is removed and the remaining couplings are considered 'small' for most applications.

There are, in general, two approaches to quasi-diabatization. The first is known as dynamical diabatization which minimizes the non-adiabatic coupling terms so they may be neglected or accounted for perturbatively.[39] The second is known as structural diabatization and it aims to find a new wave function whereby the electronic structure maintains certain characteristics throughout the region where the adiabatic solution changes rapidly.[40,41] We briefly explain the basic concepts for each approach in the following subsections.

1.3.1 Dynamical quasi-diabatization

The dynamical quasi-diabatization schemes separate the derivative coupling into a removable part and a non-removable part.[45] There will always be residual couplings due to the finite basis set; this forms the non-removable part. The schemes in the literature are distinguishable by how much of the removable coupling they eliminate.[38] An example of a dynamical quasi-diabatization scheme focuses on the vicinity of a conical intersection and restricts the coordinates to a plane, or a hyper plane, containing the conical intersection.[39] The choice of coordinate system determines in which coordinate the derivative coupling is singular. If one uses the so-called branching space, where the local degeneracy of the crossing states is removed linearly, the singularity can be removed. Equation 9 is then rearranged as [39]:

$$\mathbf{F}_{ij}^{d} = \left[-\nabla_{\mathbf{Q}}\alpha_0(\mathbf{Q}) + \mathbf{F}_{ij}\right] - \nabla_{\mathbf{Q}}\alpha_1(\mathbf{Q}) = \tilde{\mathbf{F}}_{ij} - \nabla_{\mathbf{Q}}\alpha_1(\mathbf{Q}) \qquad \text{Equation 10}$$

In this equation, the mixing angles α_0 and α_1 eliminate the singularity and the remaining removable part respectively. Since $\tilde{\mathbf{F}}_{ij}$ is not singular, one can use Helmholtz's theorem to

decompose the derivative coupling (Equation 10) into longitudinal and transverse parts.[42,43] Specifically, the Helmholtz theorem states that a vector field can be represented as the sum of two vectors, one of which has zero curl and the other has zero divergence.[46] The decomposition can be rearranged in terms of a scalar potential, β(**Q**), and a vector potential, **A**(**Q**):

$$\tilde{\mathbf{F}}_{ij} = \tilde{\mathbf{F}}_{ij}^{lon} + \tilde{\mathbf{F}}_{ij}^{tra} = \nabla\beta + \nabla \times \mathbf{A} \qquad \text{Equation 11}$$

where $\tilde{F}_{ij}^{lon}$ corresponds to the longitudinal part and $\tilde{F}_{ij}^{tra}$corresponds to the transversal part. One may take full advantage of this theorem and compute the divergence of the derivative couplings in Equation 10, by solving the following Poisson equation for β numerically [47]:

$$\nabla\tilde{F}_{ij} = \nabla\tilde{F}_{ij}^{lon} = \nabla \cdot \nabla\beta = 0 \qquad \text{Equation 12}$$

In this way, the singular and longitudinal parts of the derivative coupling are removed, but the transversal derivative coupling remains. There are also residual couplings from solving Equation 9 in a restricted coordinate space. As a result, the new basis set is not strictly diabatic. However, these remaining derivative couplings can either be considered negligible or accounted for perturbatively.[43] This method is highly accurate because it directly calculates the derivative couplings. A serious disadvantage for this method, however, is the computational expense of calculating these couplings directly.

Another dynamical scheme proposed by Thiel and Köppel only requires knowing the adiabatic potential energy surfaces.[43] The procedure relies on the assumption that the coupled states are energetically well separated from all others. They use a transformation matrix as in Equation 8 with an approximate mixing angle, assuming the residual derivative coupling is negligible.[43] This method is inherently more approximate, but the adiabatic potential energy surfaces are easier to calculate than the "exact" derivative couplings.

1.3.2 Structural quasi-diabatization

Under diabatization schemes that consider the electronic structure, we find Atchity and Ruedenberg's concept of configurational uniformity [40], furthered in the so-called 'fourfold

way' by Truhlar and co-workers.[41,44,48] They consider a set of N adiabatic states, $\{\varphi_i\}$, which are all described in terms of the same set of M orthonormal electronic configurations, $\{\gamma_j\}$ (the latter being molecular states given by Slater determinants built with molecular orbitals $\{u_{kj}\}$). That is to say, each adiabatic state is represented as a superposition of electronic configurations with expansion coefficients $\{c_{ij}\}$:

$$\varphi_i = \sum_j^M c_{ji}\gamma_j \qquad \text{Equation 13}$$

A function built in this manner resembles those used in the post-Hartree-Fock multi-configurational self-consistent field. Within the set of M configurations there are subsets that are particular to each molecular electronic state. The subset represents a small number of $\{\gamma_j\}$ configurations that dominate the electronic structure of that state.[40] Any changes in electronic structure are due to the changes in the configurational expansion coefficients. In this context, it is said that there is 'configurational uniformity' if the dominating $\{\gamma_j\}$ configurations remain the same along a given path in nuclear configurational space, thus giving rise to an electronic φ_i solution that is in practice a diabatic state.[40] The molecular orbitals, u_{kj}, that would generate these γ_j electronic configurations are found by maximizing the functional J_1 which is the sum of occupation numbers, p^j_{kk}, while varying the molecular orbitals $\{u_{kj}\}$, in an adiabatic state, φ_i:

$$J_1 = \sum_k^\eta \sum_i^M (p^j_{kk})^2, \qquad \text{Equation 14.1}$$

$$J_1^* = \max_{\{u_{kj}\}} J_1 \qquad \text{Equation 14.2}$$

Normally, occupation numbers take integer values of 0, 1 or 2 representing how many electrons are in an orbital. In cases such as in Equation 13, where there is a multi-configurational description for the electronic eigenfunction, we may have fractional occupation numbers. The occupation numbers, p^j_{kk}, in Equation 14 are the diagonal elements of the electronic population density matrix, where η is the number of molecular orbitals and M is the number of electronic configurations γ_j. The quasi-diabatization must be extended to the $\{u_{kj}\}$ orbitals themselves since

they may not always lead to clearly dominant configurations upon which the diabatic states are built.[41]

State-averaged "natural orbitals" can be used as diabatic orbitals where there is strong coupling.[49] Natural orbitals can be distinguished by the fact that they diagonalize the electron density matrix. They are not considered diabatic, however, if the diagonal elements of the density matrix are degenerate or nearly so. This problem is solved by modifying the state-state averaged natural orbital with a natural orbital diabatization functional.[41] This functional involves the diagonal elements of a density matrix that has been averaged over all states and is added to Equation 14. Maximization of the augmented functional still does not help to distinguish adiabatic from diabatic orbitals for some strongly coupled excited states because, in regions where their coupling dominates, the functionals for each type of orbitals are nearly equal.

We may recall that the diabatic basis set is constructed from a small subset of electronic configurations; the most 'diabatic' set is then the smallest subset possible. (In the case of this thesis, the set will contain only two electronic diabatic states.) One technique [41] relies on the transition density matrix to build this optimal (minimal) diabatic basis set. The transition density matrix shows how many electrons in a molecular orbital u_{km}, for an electronic configuration γ_m, also appear in the orbital u_{kn} for the γ_n configuration. A minimum diabatic basis set can then be ensured by maximizing the sum of diagonal elements in the transition density matrix. The so-called "diabatization functional", J_2, is then maximized:

$$J_2 = \left\{ \alpha_{ON} \sum_{k}^{\eta} \sum_{j}^{M} (p_{kk}^{j})^2 + \alpha_{NO} N \sum_{k}^{\eta} (\bar{p}_{kk})^2 + \alpha_{TD} \frac{2}{N-1} \sum_{k}^{\eta} \sum_{m<n}^{M} (p_{kk}^{mn})^2 \right\} \qquad \text{Equation 15.1}$$

$$J_2^* = \max_{\{u_{kj}\}} J_2 \qquad \text{Equation 15.2}$$

where the coefficients' subscripts refer to occupation number (ON), natural orbital (NO), and transition density (TD), respectively. Each of α_{ON}, α_{NO}, and α_{TD} are arbitrary fixed coefficients that determine the contribution of each term to the diabatization. Whereas the occupation number term gives the density of electrons in an orbital u_{kj} for a γ_j configuration, the transition density

term evaluates the how much electron density has been transferred from an orbital u_{km} to the orbital u_{kn}.

When the system has an odd number of electrons and the N states are strongly coupled, Equation 15 cannot differentiate between adiabatic and diabatic orbitals. In other words, the functional produces similar values for diabatic and adiabatic basis sets for certain couplings of radical excited states. As a final correction, molecular orbital uniformity is enforced explicitly. In order to do this, a reference nuclear configuration is chosen, $\mathbf{Q}_{ref}$, where diabatic states are approximately the same as adiabatic states. [41] At these nuclear coordinates, the condition that states interact weakly and Equation 15 is valid; the diabatization functional is then maximized and η diabatic molecular orbitals, $\{u_{kj}\}$, are obtained for the γ_j configuration. If there are λ pairs of molecular orbitals with degenerate occupation numbers, then molecular orbital uniformity can be achieved by maximizing the sum of the squares of the orbital overlap at the reference geometry, $\mathbf{Q}_{ref}$, and the nuclear geometry of interest. The λ molecular orbitals are a subset of the η and act as reference orbitals. Since this maximization changes the density matrices, the diabatization functional must be reapplied to the remaining η-λ molecular orbitals.[44]

1.3.3 Other alternatives for studying molecular dynamics in multiple electronic states

There are other methods that describe nuclear dynamics in a reaction by incorporating the interaction between several electronic states. For example, the surface hopping method uses classical nuclear trajectories on potential energy surfaces.[50] The trajectories may 'hop' to another surface depending on a transition probability. The usual method to determine the transition probability is to calculate the time-dependent Schrödinger equation along a trajectory.[51] It must be followed by a correction that takes into account that surface hopping tends to artificially transfer energy from the classically moving nuclei to the quantum electrons.[52] More recently, Cederbaum has devised a new method to get nuclear motions to proceed along a single potential energy surface.[8] The initial approach is still the same as in Equation 3, which is to represent the molecular Hamiltonian's eigenfunction as a product, but as a single product instead of a sum of products. In order to achieve this, one introduces a modified

'electronic' Hamiltonian, $\bar{H}_e$, that includes operators based on the nuclear part of the molecular eigenfunction as indicated in Equation 16:

$$\bar{H}_e = \hat{H}_e - \frac{\hbar}{M}\left(\nabla_{\mathbf{Q}} \ln\chi\right) \cdot \nabla_{\mathbf{Q}} + \hat{T}_N(\mathbf{Q}) + C_K \qquad \text{Equation 16}$$

All variables are defined as before in Equation 3 and Equation 4; C_K is a function of the total linear momentum. The total nuclear kinetic energy is a linear combination of the kinetic energy due to internal motions, $\hat{T}_N(\mathbf{Q})$, and the kinetic energy associated with centre of mass translation. The electronic energy on which nuclear dynamics unfolds thus depends more explicitly on the nuclear coordinates.

1.4 Generalized electronic diabatic model

We can now contrast the previous approaches with the one followed in this thesis. In our present generalized electronic diabatic (GED) model, electrons are classified as quantum particles and the nuclei as classical (that is massless) background charges.[9] The electronic Hamiltonian is defined as:

$$\hat{H}_e(\hat{\mathbf{q}}, \boldsymbol{\xi}) = \hat{T}_e(\hat{\mathbf{q}}) + \hat{V}_{ee}(\hat{\mathbf{q}}, \hat{\mathbf{q}}') + \hat{V}_{eN}(\hat{\mathbf{q}}, \boldsymbol{\xi}) + \hat{V}_{NN}(\boldsymbol{\xi}, \boldsymbol{\xi}') \qquad \text{Equation 17}$$

where $\hat{V}_{ee}(\hat{\mathbf{q}}, \hat{\mathbf{q}}')$, $\hat{V}_{eN}(\hat{\mathbf{q}}, \boldsymbol{\xi})$, and $\hat{V}_{NN}(\boldsymbol{\xi}, \boldsymbol{\xi}')$ are, respectively, the electronic, the electronuclear and the nuclear-nuclear Coulombic operators. Our notation for the coordinate systems, $\{\hat{\mathbf{q}}, \boldsymbol{\xi}\}$ differs from the previous sections to emphasize that the electronic coordinates are diabatic quantum operators, while the nuclear coordinates are classical. The set $\{\psi_j(\hat{\mathbf{q}})\}$ are eigenfunctions of the electronic Hamiltonian calculated at a single point in nuclear space. Each eigenfunction, $\psi_j(\hat{\mathbf{q}})$, is associated with a nuclear configuration $\|\boldsymbol{\xi}_j\|$. In turn this nuclear configuration corresponds to a minimum in an uncoupled diabatic potential energy curve, $\min_{\xi} U$, which we call *an attractor* [8-13]:

$$\hat{H}_e(\hat{\mathbf{q}}, \boldsymbol{\xi}_j)\psi_j(\hat{\mathbf{q}}) = E_j(\boldsymbol{\xi}_j)\psi_j(\hat{\mathbf{q}}) = \min_{\boldsymbol{\xi}}\{U_j(\boldsymbol{\xi}, [\psi_j(\hat{\mathbf{q}})])\psi_j(\hat{\mathbf{q}})\} \qquad \text{Equation 18}$$

where the diabatic potential energy function, $U_j(\boldsymbol{\xi})$, is computed from the $\psi_j(\hat{\mathbf{q}})$ function evaluated at the attractor of interest:

$$\langle \psi_j(\hat{\mathbf{q}}) | \hat{H}_e(\hat{\mathbf{q}}, \boldsymbol{\xi}) \psi_j(\hat{\mathbf{q}}) \rangle = U_j\left(\boldsymbol{\xi}, \left[\psi_j(\hat{\mathbf{q}})\right]\right) \quad \text{Equation 19}$$

There exist two types of attractors. The first is associated with bound states, with a confining potential energy functional. The second corresponds to unbound states or asymptotically separated species where the potential energy describes a continuum.[9] In our approach, the eigenfunctions calculated at geometries other than those corresponding to a given attractor, for example, at the attractor corresponding to a different electronic species, will still produce the same set, although their energy ranking may differ. These electronic eigenfunctions are strictly diabatic by construction, as they are evaluated at a single nuclear attractor configuration $\boldsymbol{\xi}_j$, and thus completely independent of nuclear coordinates. On the other hand, the potential energy functional then depends on nuclear coordinates through the electro-nuclear and nuclear-nuclear Coulombic operators.

Each resulting eigenfunction, ψ_j, represents an electronic "diabatic state" of an isolated molecule. Without some external factor, there is no physical reason for a transition to even take place between states. That factor is introduced by an external field vector potential operator, $\hat{\mathbf{A}}$.[9] Using Maxwell's equations of electromagnetism [46], we can relate this operator to an external electric field and a magnetic field with the following identities:

$$\hat{\mathbf{E}} = -\left(\frac{\partial \hat{\mathbf{A}}}{\partial t} + \nabla \hat{V}\right) \quad \text{Equation 20}$$

$$\hat{\mathbf{B}} = \nabla \times \hat{\mathbf{A}} \quad \text{Equation 21}$$

whereby $\hat{\mathbf{E}}$ is the operator for the electric field and $\nabla\hat{V}$ is the gradient of the scalar electric potential with respect to the all displacement coordinates, $\boldsymbol{\xi}$ and $\hat{\mathbf{q}}$. The external field vector potential operator couples with the electronic momentum to produce an effective kinetic energy operator [8,9]:

$$\hat{T}_e(\hat{q}) = \frac{1}{2m_e}\left(\hat{\mathbf{p}}_e - \frac{e}{c}\hat{\mathbf{A}}(\boldsymbol{\xi}, t)\right)^2 \quad \text{Equation 22}$$

In this equation, $\hat{\mathbf{p}}_e$ is a vector operator of one-electron momentum operators, that is $-i\hbar(\nabla_1, \nabla_2 \ldots \nabla_n)$. If we limit ourselves to weak fields and neglect the $\|\hat{\mathbf{A}}(\boldsymbol{\xi}, t)\|^2$ terms as being

too small, we may regain the original electronic kinetic energy operator and define an external field potential operator as [9]:

$$\hat{V}_{e-field} \approx -\frac{e}{m_e c}\hat{\mathbf{A}} \cdot \hat{\mathbf{p}}_e \qquad \text{Equation 23}$$

In the GED approach, this operator is the "external force" solely responsible for coupling the diabatic states. The actual molecular electronic states are coherent superpositions (or mixed states) of these diabatic basis functions where the coefficients depend on the nuclear coordinates and the external field:

$$\Phi(\hat{\mathbf{q}}, \boldsymbol{\xi}) = \sum_s c_s(\boldsymbol{\xi}, \hat{\mathbf{A}})\, \psi_s(\hat{\mathbf{q}}) \qquad \text{Equation 24}$$

With this formalism, reactions are represented as changes in the electronic state due to a shift in the coefficients $\{c_s(\boldsymbol{\xi}, \hat{\mathbf{A}})\}$, not the diabatic eigenfunctions $\{\psi_s(\hat{\mathbf{q}})\}$.

Since the external field potential operator, $\hat{V}_{e-field}$, involves the electronic momentum, for a pair of diabatic states to be coupled they must have different parities with respect to an inversion, rotation or reflection in $\hat{\mathbf{q}}$-coordinate space.[10] If the diabatic states have the same parities, they would remain uncoupled even in the presence of an external field. In this case, a third diabatic state with a different parity must be introduced for a reaction, that is a change in quantum state, to occur.[8-14] While there may be a manifold of diabatic states, constraints such as boundary conditions and accessible windows of energies indicate that a finite set of diabatic functions may be sufficient to describe a significant range laboratory observations.[11]

In practice, a minimalist set of diabatic functions is chosen depending on the reaction paths to be studied. In this thesis, we consider two types of transitions between two diabatic states:

1. a simple dissociation process, where the bound state's spatial parity is different from the unbound state.

2. a transition between two bound states representing an isomerization. In a reaction between two closed-shell species, the parity would be even with respect to $\hat{\mathbf{p}}_e$ and thus their coupling would

vanish. As a result, a simple two-state model of isomerization requires that we consider radical (unpaired spin) species.

The diabatic states, $\{\psi_j(\hat{\mathbf{q}})\}$, diagonalize the Hamiltonian matrix at any nuclear configuration. [9-12,14] One can represent a Hamiltonian operator at any $\boldsymbol{\xi}$ as a perturbed Hamiltonian at an attractor, say $\boldsymbol{\xi}_i$, that is, treating the difference between $\boldsymbol{\xi}$ and $\boldsymbol{\xi}_i$ as a first order perturbation ΔU. Since the set $\{\psi_j(\hat{\mathbf{q}})\}$ are eigenfunctions of $\hat{H}_e(\hat{\mathbf{q}}, \boldsymbol{\xi}_i)$, and $\Delta U(\boldsymbol{\xi}_i, \boldsymbol{\xi}, \hat{\mathbf{q}})$ has the same symmetry as $\hat{H}_e(\hat{\mathbf{q}}, \boldsymbol{\xi}_i)$ in electronic and nuclear coordinates, the following equality holds:

$$\langle\psi_j(\hat{\mathbf{q}})|\hat{H}_e(\hat{\mathbf{q}}, \boldsymbol{\xi}_i)\psi_i(\hat{\mathbf{q}})\rangle = \langle\psi_j(\hat{\mathbf{q}})|\Delta U(\boldsymbol{\xi}_i, \boldsymbol{\xi}, \hat{\mathbf{q}})\psi_j(\hat{\mathbf{q}})\rangle = 0 \Leftrightarrow i \neq j \qquad \text{Equation 25}$$

This shows that, although they may be energetically 'shuffled', that is ordered differently in their eigenvalues, the same diabatic states are found regardless of the attractor's location. In other words, we need only compute these states at a single nuclear configuration, for simplicity, the attractor configurations, $\boldsymbol{\xi}_i$, for each relevant chemical species.

The external field potential operator and the electronic Hamiltonian now define the full electronic Hamiltonian denoted by $\hat{H}_{full}$. For a two-state model in an external field, the full Hamiltonian matrix one must diagonalize in order to obtain an effective potential energy surface takes the form

$$\left[\hat{H}_{full}(\hat{\mathbf{q}}, \boldsymbol{\xi}, \hat{A})\right] = \begin{bmatrix} H_{11} & H_{12} \\ H_{12} & H_{22} \end{bmatrix}, \text{where } H_{ij} = \left\langle\psi_i(\hat{\mathbf{q}})\middle|\hat{H}_{full}(\hat{\mathbf{q}}, \boldsymbol{\xi}, \hat{A})\psi_j(\hat{\mathbf{q}})\right\rangle \qquad \text{Equation 26}$$

From the equality given in Equation 25, it is clear that the off-diagonal term H_{12}, in Equation 26, is entirely due to the external field potential operator, while the diagonal terms depend only on $\hat{H}_{mol}$. In other words, we find the following matrix elements:

$$\begin{bmatrix} H_{11} & H_{12} \\ H_{12} & H_{22} \end{bmatrix} = \begin{bmatrix} U_1 & V_{12} \\ V_{12} & U_2 \end{bmatrix} \qquad \text{Equation 27.1}$$

$$H_{ii} = U_i = \left\langle\psi_i(\hat{\mathbf{q}})\middle|\hat{H}_{mol}(\hat{\mathbf{q}}, \boldsymbol{\xi}, \hat{A})\psi_i(\hat{\mathbf{q}})\right\rangle, \left\langle\psi_i(\hat{\mathbf{q}})\middle|\hat{V}_{e-field}(\hat{\mathbf{q}}, \boldsymbol{\xi}, \hat{A})\psi_i(\hat{\mathbf{q}})\right\rangle = 0 \qquad \text{Equation 27.2}$$

$$H_{12} = V_{12} = \langle \psi_1(\hat{\mathbf{q}}) | \hat{V}_{e-field}(\hat{\mathbf{q}}, \boldsymbol{\xi}, \hat{A}) \psi_2(\hat{\mathbf{q}}) \rangle, \langle \psi_1(\hat{\mathbf{q}}) | \hat{H}_{mol}(\hat{\mathbf{q}}, \boldsymbol{\xi}, \hat{A}) \psi_2(\hat{\mathbf{q}}) \rangle = 0 \quad \text{Equation 27.3}$$

Since V_{12} is proportional to the external field vector, for simplicity, we shall call it the "external field coupling". The effective or full potential energy surface is then given by the lowest eigenvalue of Equation 27.1 [9,13,15]:

$$E_{full}(\boldsymbol{\xi}) = U_1 + \frac{1}{2}\left[\Delta U_{12} - |\Delta U_{12}| \sqrt{1 + 4\left(\frac{V_{12}}{\Delta U_{12}}\right)^2}\right] \quad \text{Equation 28}$$

where $U_i = U_i(\boldsymbol{\xi})$, while V_{12} may or may not depend on $\boldsymbol{\xi}$-configurations, depending on the chosen model. We can build effective potential energy surfaces quantum mechanically through the construction of the diabatic states and positioning of the system's nuclei as done in sections 5 and 6. To discover general trends in the effective potential energy surfaces, however, we can use semi-classical functions to represent the potential energy curves for the reactant and product. All of these ideas are developed fully in the following sections of this thesis.

2. Objectives

The main purpose of this thesis is to investigate the effects of various external field couplings on a manifold of semi-classical models associated with both simple dissociation and isomerization reactions. We will characterize some aspects of the topology of all the possible potential energy curves $E_{full}(\boldsymbol{\xi})$ (see Equation 28) in the external field, and then organize the two-state models into "phase diagrams" according to these topological features. These diagrams convey qualitatively the effective potential energy curve's dependence on the shape and intensity of the external field, as well as the uncoupled diabatic potential curves $\{U_i\}$.

To complement these semi-classical models, we shall illustrate an implementation of the generalized diabatic model by applying it to the hydrogen boronitride radical isomerization (HBN ⇄ BNH). In order to describe this concrete example from a quantum mechanical perspective, the diabatic electronic states associated with the attractors are built on an optimal grid of floating Gaussian orbitals. We focus solely on the diabatic states and potential energy curves as we consider the isomerization to be controlled by a variable external electric field. The uncoupled diabatic potential energy curves corresponding to the radical isomerization are constructed using various tentative paths in nuclear configurational space, loosely speaking "nuclear trajectories", while the Gaussian orbital positions in the grid are fixed. The different "trajectories" will permit a glimpse of which electronic state dominates the superposition of electronic eigenfunctions for different points in the nuclear configurational space. We explore how this description depends on the chosen basis set and the choices of grids for the floating Gaussian orbitals. We present those approaches as a prototype calculation that illustrates how to construct and use a diabatic basis set.

3. Semi-classical models and methodology

In the next few subsections of this section, we discuss in detail how the characterization and classification of effective semi-classical potential energy surfaces into "phase diagrams" are implemented in practice. These phase diagrams will be generated by applying various models for the external field on a manifold of chemical processes involving two diabatic quantum states. Results of this approach will be discussed in detail in section 4. In section 5, we contrast this semi-classical approach with a possible fully quantum mechanical formalism involving the construction of actual electronic diabatic eigenfunctions, that is, a nuclear coordinate independent basis set built on a grid of fixed atomic orbitals. For the sake of clarity, the methodology for the fully quantum model will be discussed in its corresponding section.

3.1 Semi-classical models

For bound states, energy minimization algorithms ensure the neighbourhood around each attractor is, in a first approximation, a harmonic minimum.[12] It is, therefore, a reasonable approximation to represent semi-classically the uncoupled diabatic potential energy surfaces as quadratic functions. In our case, the external field coupling will give rise to any anharmonicities. For the purpose of observing the trends in a large set of effective potential energy surfaces, two types of semi-classical potentials suffice. We shall denote the uncoupled reactant as U_1 and the product as U_2.

For a dissociative model, the product's diabatic potential can be represented by a decaying exponential or the repulsive part of a Lennard-Jones potential function (see Figure 2A). The exponential has convenient mathematical properties while the repulsive Lennard-Jones is empirically more reasonable. For the radical isomerization model, a shifted harmonic represents the product's diabatic potential (see Figure 2B). In both models, the reactant's diabatic potential, U_1, is given by a harmonic potential. In summary, the functions chosen to represent the diabatic potentials are:

$$U_1 = \frac{1}{2}kx^2 \qquad \text{Equation 29}$$

$$\text{Dissociative } U_2 = \begin{cases} se^{-x} + t & \text{Equation 30 .1} \\ s(x+r)^{-10} + t & \text{Equation 30 .2} \\ s(x+r)^{-12} + t & \text{Equation 30 .3} \end{cases}$$

$$\text{Isomerization } U_2 = \frac{1}{2}s(x-r)^2 + t \qquad \text{Equation 31}$$

The parameters k and s can be likened to force constants. The variable x and the constant r represent relative nuclear displacements, while t is comparable to a zero-point energy. For simplicity, we confine ourselves to the cases where both r and t are positive.

To characterize these semi-classical potentials, another useful parameter would be the height of a pseudo reaction barrier, Δ, that is to say, the energy difference between the crossing point of the uncoupled diabatic potentials, where $U_1 = U_2$, and the zero-point energy of the product, t (see Figure 2). We refer to it as a pseudo barrier because the potential curves, U_1 and U_2, are uncoupled; there can be no reaction. It does, however, provide a useful comparison to the actual reaction barrier present in the effective potential energy curve which can be modified through manipulation of the external field coupling V_{12}.

Although the position and height of the pseudo barrier is easily determined for our radical isomerization model, the same cannot be said of the dissociative model, since then equality U_1=U_2 is a transcendental equation. We can however estimate the barrier height in some limit cases. A simple mathematical analysis of Taylor series leads us to the following results [15]:

$$\text{for large k and } U_2 = se^{-x} + t, \text{we find: } \Delta \approx s - s\sqrt{\frac{2t+2s}{k}} + \frac{st+2s^2}{k} \qquad \text{Equation 32 .1}$$

$$\text{for small k, then } \Delta \approx e^{-\sqrt{\frac{2t}{k}}} \qquad \text{Equation 32 .2}$$

$$\text{for large k and } U_2 = s(x+r)^{-2p}, \text{we find: } \Delta \approx \frac{s}{r^{2p}} - 2psr^{p+3}\sqrt{\frac{2(s+t)}{k}} \qquad \text{Equation 32 .3}$$

$$\text{for small k, } \Delta \approx \frac{s}{2}\left(\sqrt{\frac{2t}{k}} + r\right)^{-2p} \quad (t \neq 0) \qquad \text{Equation 32 .4}$$

The manifolds of semi-classical models were built in one dimension in increments along the nuclear coordinate, $\Delta x = 0.05$ and $\Delta x = 0.1$, for the isomerization and the dissociative models respectively. The independent variable, x, which shall henceforth be called the nuclear coordinate, can represent distance along a vibrational mode. For example, in the dissociative model, x can be related to a bond elongation. As discussed in a following subsection, the interpretation and role of this elongation changes depending on the molecular orientation.

In the dissociative model ($\lim_{x\to\infty} U_2 < \infty$), the product's force constant, s, and the separation along the nuclear coordinate, r, in the Lennard-Jones type potentials (Equation 30.2, 30.3) are fixed as s = 1, r = 1. For the radical isomerization model ($\lim_{x\to\infty} U_2 \to \infty$), in order to make the distinction between an uncoupled potential corresponding to an excited state and an isomerization, the following inequality must be obeyed:

$$k \geq \frac{2t}{r^2} \qquad \text{Equation 33}$$

This ensures $U_2(r) \leq U_1(r)$, where r is the location of the product attractor, the U_2 minimum. According to Equation 33, the product's attractor is allowed to lie on the reactant's diabatic curve, but it is not contained by the reactant's diabatic curve. When both force constants are independently varied through the range k, s ϵ [0.1; 20], the product's zero-point energy, t, is kept fixed. As the product's zero-point energy is scanned as $0 \leq t \leq 50$, the product's force constant, s, is either fixed or a multiple of the reactant's force constant, k. The range for the reactant's force constant is increased to [0.1; 100] to compensate for the reduced parameter space when scanning t. Similar steps were taken when the field coupling intensity was varied. Typical examples of k, s, t, r values are illustrated in Figure 2.

A: Dissociative model

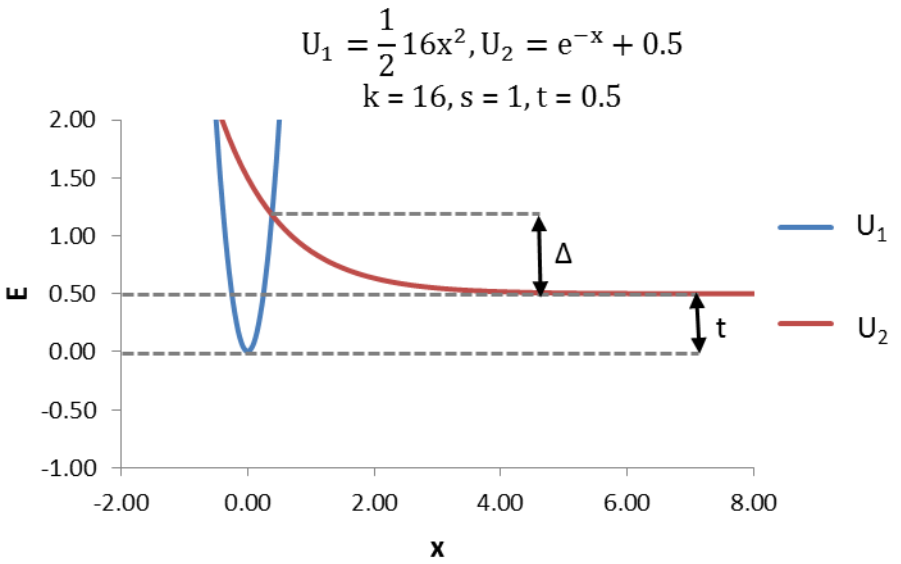

B: Isomerization model

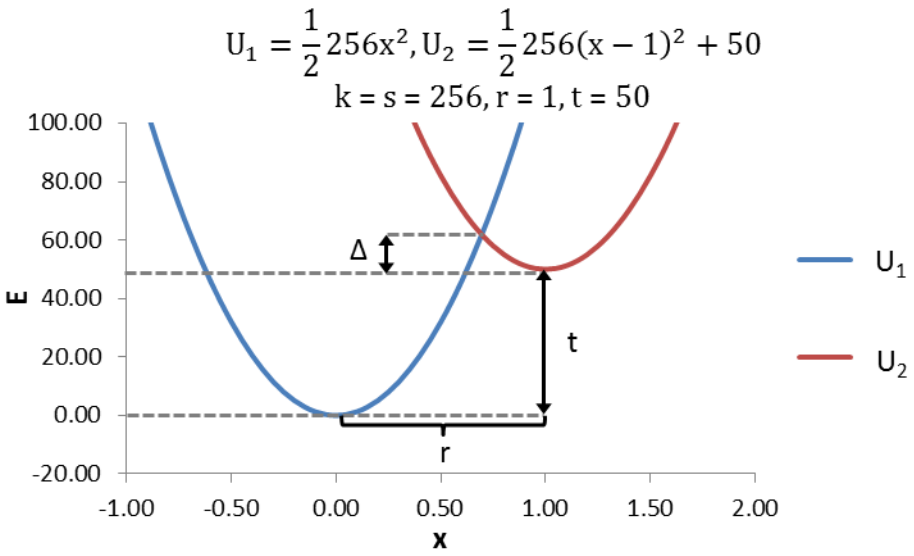

Figure 2. Semi-classical model parameters

U_1 and U_2 represent the reactant and product's uncoupled diabatic potential energy curves respectively. Δ is the pseudo-barrier of the reaction, the value of the reaction barrier in the limit of zero field. The parameter t is the product's zero-point energy and r is the distance along the nuclear coordinate x between the two diabatic eigenfunctions.

3.2 Modeling the external coupling

Considering the ever-growing number of experiments demonstrating how reactions can be controlled via tuning of a laser [4,8,53], it is thus desirable to explore several different types of external field couplings. For example, a constant field coupling can be related to field produced by a catalyst's flat surface (see Equation 34.1). We may expand upon this analogy to include surface defects by making the V_{12} coupling a discontinuous (Equation 34.5) or a non-smooth function (Equation 34.6). The discontinuous field coupling can also represent a different crystallographic plane (or facet) found on a surface.[54,55]

The function describing the field coupling, V_{12}, will also depend on the molecule's orientation in the field. For example, if a diatomic's dissociation occurs parallel to the catalyst's surface, the field coupling is constant. (The assumptions are that the bond-breaking leads to adsorbed species, each remaining at the same distance from the surface as for the reactant species, hence leading to a uniform V_{12} value for both states involved.) If, however, the dissociation occurs perpendicularly to the surface, within a certain range, the field coupling may be approximated as linear (see Equation 34.2, Figure 3).

Other functional representations for V_{12} are also worth considering. Scanning tunneling microscope (STM) tips have been found to accelerate adsorption onto surfaces.[56] The field coupling produced by an STM tip is locally strong, falling rapidly to zero away from the tip and may thus be modelled by a Lorentzian function (Equation 34.4). An inverse Lorentzian function (Equation 34.3), which is locally weak and nearly constant everywhere else, can describe a flat capacitor with a small hole or defect. In summary, these are the model V_{12} couplings that we will test and explore in this thesis:

$$V_{12} = \begin{cases} a & \text{Equation 34.1} \\ ax + b & \text{Equation 34.2} \\ \dfrac{a(x-c)^2}{b + (x-c)^2} & \text{Equation 34.3} \\ \dfrac{a}{1 + b(x-c)^2} & \text{Equation 34.4} \\ a_1\ (x \leq x^*), a_2\ (x > x^*) & \text{Equation 34.5} \\ a_1 x + b_1\ (x \leq x^*), a_2 x + b_2\ (x > x^*) | (a_1 - a_2)x^* = b_2 - b_1 & \text{Equation 34.6} \end{cases}$$

We shall refer to the external field coupling parameter 'a' as the *external field coupling intensity*.

We do not explicitly explore external field couplings of degree larger than two in nuclear coordinates, x. We can deduce, however, from Equation 28, that the effective reactive potential converging with the lowest uncoupled diabatic potential curve – as the nuclear coordinate goes to infinity – is now uncertain. This is due to the asymptotic limit of the term $(\frac{V_{12}}{\Delta U_{12}})$ not reaching zero if V_{12} is of degree larger than two. By examining external field couplings of order less than two, we further restrict ourselves to E_{full} potential energy curves where the reaction is bound, that is trapped as a single minimum at very high field intensities.

A. Linear V_{12}

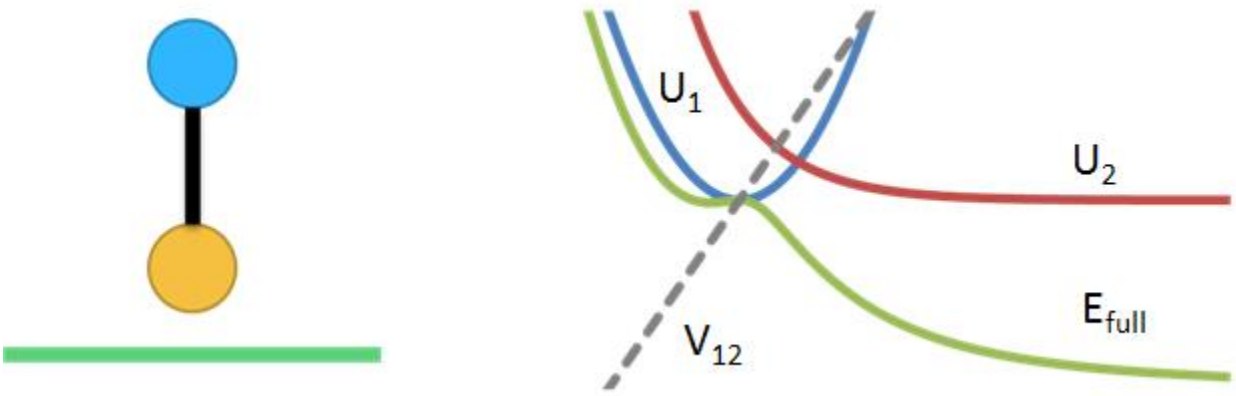

B. Constant V_{12}

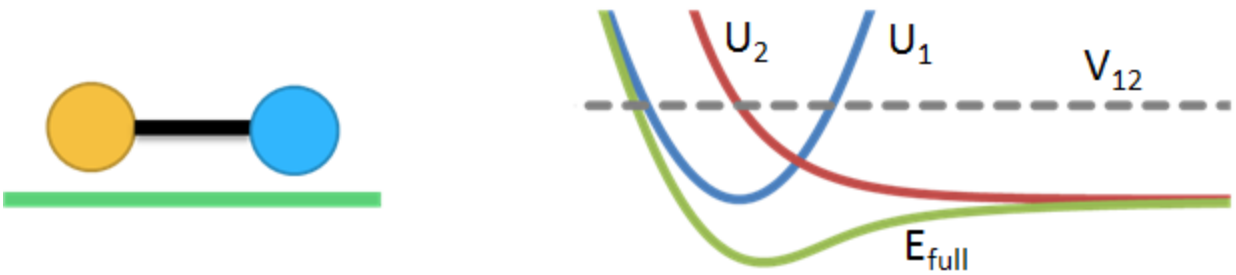

Figure 3. Molecular orientation and shape of external field coupling

The external field strength of a supporting surface is inversely proportional to the distance from that surface. The field coupling potential is represented by the dashed grey line. In A, the active bond is perpendicular to the surface, then, for a certain range of nuclear coordinates, we can approximate the field strength and the field coupling potential as a linear function. In B, however, the nuclear motion is parallel to the surface, the dissociation occurs in a field of constant strength, and in turn the field coupling potential V_{12} is constant as well.

3.3 Characterizing the potential energy surfaces: a simple topological phase diagram

The basic information conveyed by critical point topology, or "Morse theory", is the total number of maxima and minima found on the potential energy surface [57]. This topological index serves as rough guide on whether, with such system and field parameters, a reaction is feasible. We shall denote the topological index that is the number of non-trivial extrema as μ, that is excluding the asymptotic extrema for $x \rightarrow \pm\infty$. We may extend this idea to a manifold of models to create "phase" diagrams, or simple topology maps in a two parameter space. Initially we chose the reactant's force constant, k (Equation 29), and the pseudo-barrier, Δ, as the two parameters. In other words, the (Δ,k)-plane is partitioned into regions, or phases, where the manifold of two-state models gives rise to effective potential energy functions E_{full} with the same topological characteristics, that is the same μ-index. In some practical applications, however, it is more important to understand how the potential energy surface changes with a field intensity parameter. In these cases, topology maps in the (a,k)-plane, corresponding to the reactant's force constant and the field intensity, were also created.

In terms of extracting the topological information using the derivative of the equation for the effective potential energy surface, the simplicity of the model diabatic potential energy curves is deceptive. Excepting those models with some symmetrical feature and a linear or constant external field coupling, finding the number and type of critical points becomes a numerical approximate procedure for an already approximate model.

Numerical methods to determine the number of extrema using the derivative of Equation 28 require a range or a starting point; whether the method converges to a particular value is not always guaranteed. Evaluating the derivative of the effective potential energy curve analytically is only helpful in determining the number of extrema in the most symmetrical cases. Numerically, a critical point is obtained by analyzing the slope of two consecutive points and comparing it to that of a previous pair of points. In other words, a local critical point is located numerically if the following conditions are found (see Figure 4):

A: Dissociative model

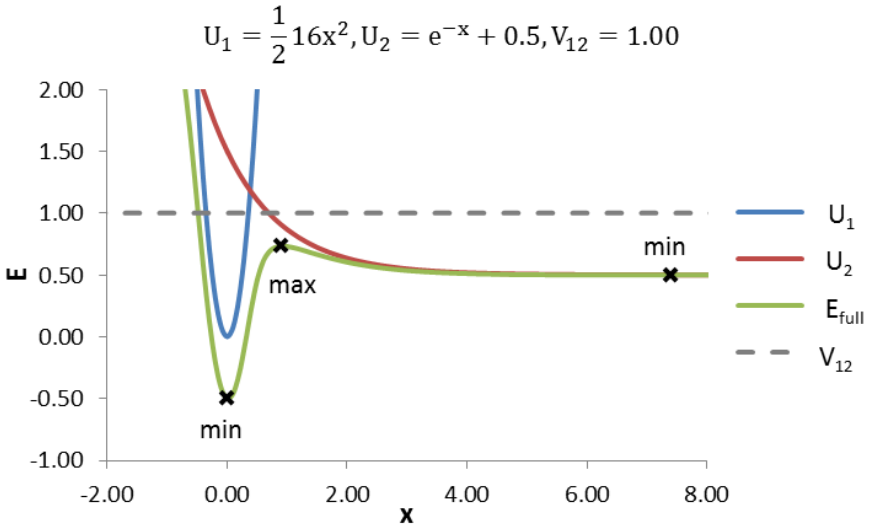

B: Isomerization model

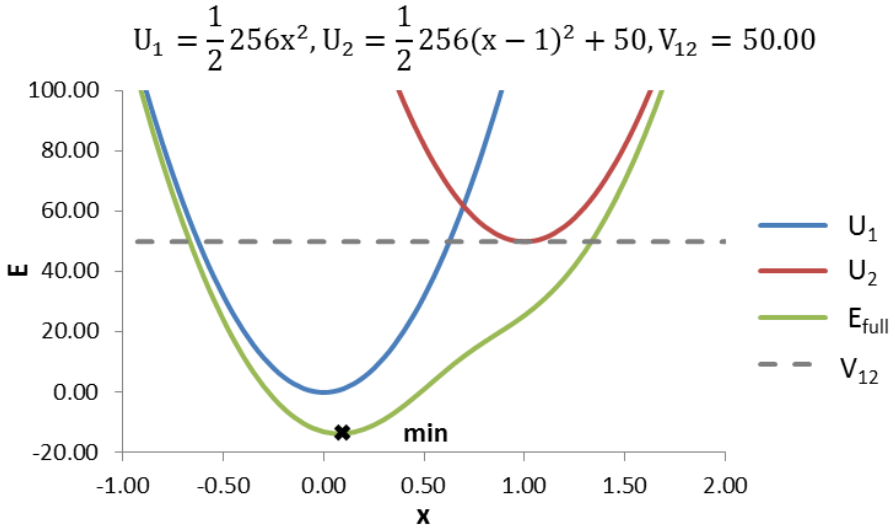

Figure 4. Applying an external field coupling and extracting topological features

This figure illustrates the E_{full} potential energy surfaces generated by applying a constant external field leading to V_{12} = 1 (A) and 50 (B) to the systems shown in Figure 2. The resulting E_{full} curve A has two minima and a maximum corresponding to an effective reaction barrier. In contrast, the E_{full} curve B shows a single minimum. All local extrema are indicated by bold crosses. Our topological classification then assigns them the codes $\mu = 3$ and $\mu = 1$, respectively. Trivial (asymptotic) extrema are not counted in the classification. The next task is to obtain this classification by an efficient computational algorithm.

$E_{full}(x_i) \leq E_{full}(x_i + \Delta x)$ and $E_{full}(x_j) \geq E_{full}(x_j + \Delta x), j > i$ (a maximum) Equation 35 .1

$E_{full}(x_i) \geq E_{full}(x_i + \Delta x)$ and $E_{full}(x_j) \leq E_{full}(x_j + \Delta x), j > i$ (a minimum) Equation 35 .2

Each topological map is drawn with at least 40 000 model effective curves (see Figure 5). It is not necessary, however, to show all 40 000 models as points on the topological map. We need only the set of models that determine the border of a topological phase. The manifold of models is scanned along two parameters; whenever a model gives a topology that is different from the previous model, that model is recorded.

The increasing roughness of the borders between topological phases at low force constants can be corrected by lowering the force constant increment, Δk, in that region of the phase diagram. On the other hand, roughness at higher force constants is due to the potential energy curve scanning increment not being small enough. Especially for the dissociative model, as the force constant increases, relevant topological features (the location and number of critical points) become so compressed in space that they are no longer detected by a certain Δx. While this can lead to miscategorising the topology of a model under a particular field, one might also present the argument that the overlooked features correspond to models with extreme k, Δ values that are not physically relevant.

All effective potential energy curves, E_{full}, and topological maps in the (Δ,k) and (a,k) spaces were made using a Fortran programme the author designed. The code for the programme can be found in appendix A1.

Figure 5 shows a typical example of the (Δ,k) plane for a collection of two-state models of isomerization with the range of $k \leq 100$ and $t \leq \frac{kr^2}{2}$. In this case, the external field coupling is linear in the elongation variable: $V_{12} = 10x$. The top diagram gives the location of three illustrative examples of E_{full}, having different topological μ-labels. The bottom diagram shows the final phase regions, where we can recognize the location of the three E_{full} curves highlighted before. The topological phases are simply labelled by the total number of critical points, μ.

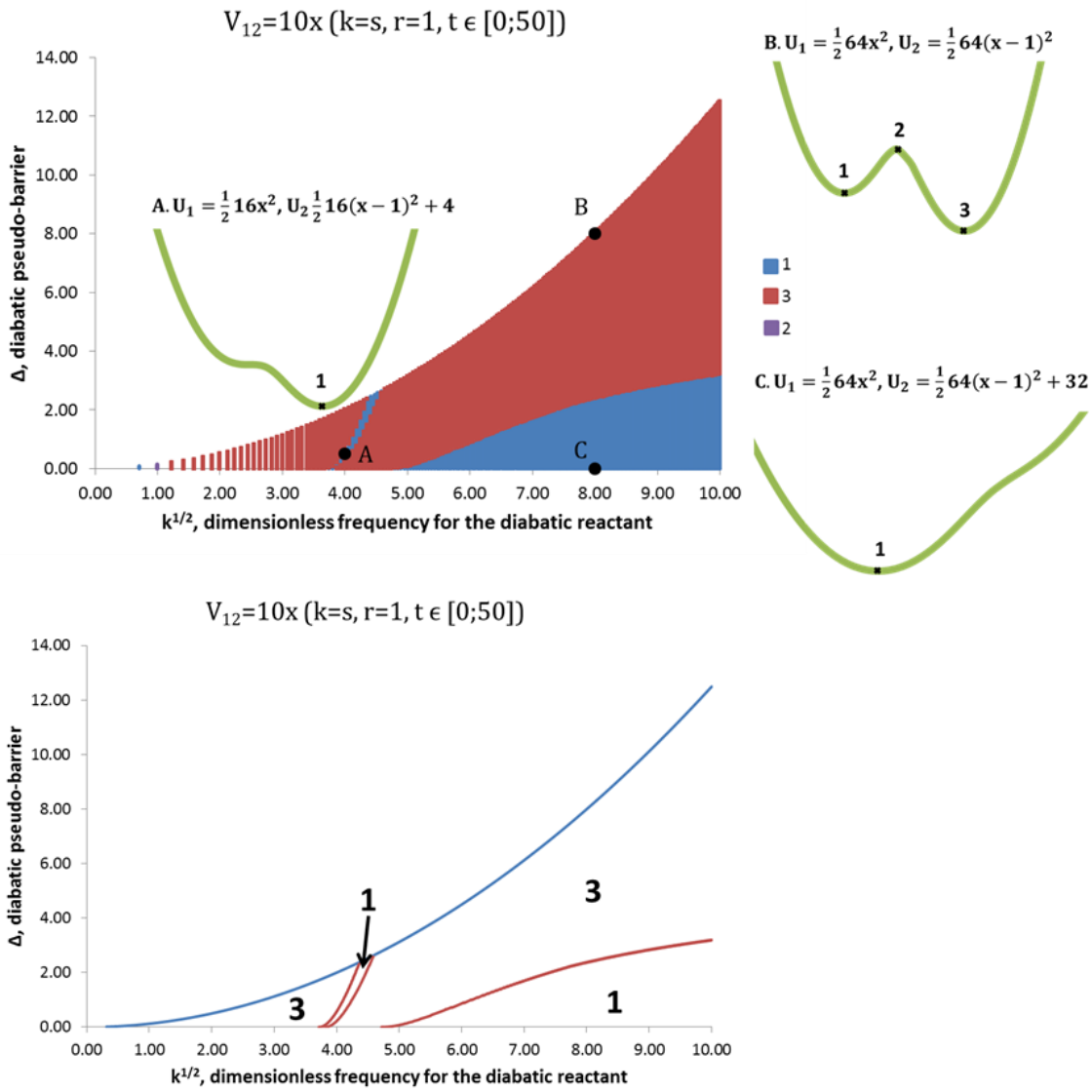

Figure 5. Constructing phase diagrams

The top diagram gives the parameter space studied and three examples of E_{full} curves. The number of local extrema on the effective potential energy surface determines which phase the model belongs to. The bottom diagram gives the partitioning of the (Λ,k) space into three topological phases, using the topological index, μ, previously defined as the total number of non-trivial critical points. A regularized scan of model parameters is done first in order to determine how many different or separate phases there are. We use a finer scan to identify the phase borders. For example there appears to be a small region at low $k^{1/2}$ where μ = 1 and μ = 2, these are artifacts due to the local minima lying outside the range of x scanned

4. Results and discussion: semi-classical models

According to Equation 28, for a dissociative model under a field that reaches a constant value at infinite distance, the effective potential energy, E_{full}, converges with the product's attractor (see Figure 4A). For the isomerization model (Equation 30, Figure 4B), the effective potential converges with the lowest diabatic potential. The situation differs when the field coupling does not reach a constant, in a linear V_{12} coupling for example. As can be seen in Figure 6, the dissociative model does not converge with the product's attractor in the limit of infinite distance. Rather, the effective potential energy, E_{full}, converges to a new value (see Equation 36) which also depends on the field coupling's intensity and the reactant's force constant:

$$\lim_{x\to\infty} E_{full} = t - \frac{2a^2}{k}, \text{where } t = \lim_{x\to\infty} U_2 \qquad \text{Equation 36}$$

A similar adjustment to the isomerization's effective potential can be given as

$$\lim_{x\to\infty} E_{full} = \min\{U_1, U_2\} - \frac{2a^2}{|k-s|} \qquad \text{Equation 37}$$

The following equation rearranges the derivative of the effective potential energy in order to locate its roots:

$$V_{12}^2(U_2' + U_1')^2 - 2V_{12}V_{12}'(U_2' - U_1')(U_2 - U_1) - 4V_{12}^2V_{12}'^2 + U_2'U_1'(U_2 - U_1)^2 = 0 \qquad \text{Equation 38}$$

The largest power in Equation 38 determines the number of roots, thereby giving the number of extrema on the effective potential energy curve. Looking first at the dissociative model (Equation 30), we can only comment on the topological behaviour in the limits of the field intensity, since the number of critical points must be obtained numerically. Inserting the exponential form of Equation 30 into Equation 38, we have the following:

$$a^2(kx - se^{-x})^2 - 4ksxe^{-x}\left(se^{-x} + t - \frac{1}{2}kx^2\right)^2 = 0 \qquad \text{Equation 39}$$

In Equation 39, we recover the attractors and the diabatic crossing in the limit of zero field ($V_{12}\to 0$). At the opposing limit of infinite field, we are faced with another transcendental

equation which, if we approximate the exponential as a truncated Taylor series, gives the position of the single minimum as

$$x = k + s \pm \sqrt{k^2 + 2ks + s^2}, \quad \text{if } k \geq -s + s\sqrt{2} \qquad \text{Equation 40}$$

While we cannot perform the same analysis for the Lennard-Jones type diabatic potential energy function U_2 for the product, we can content ourselves in the knowledge that the trends are similar to the exponential version of U_2.

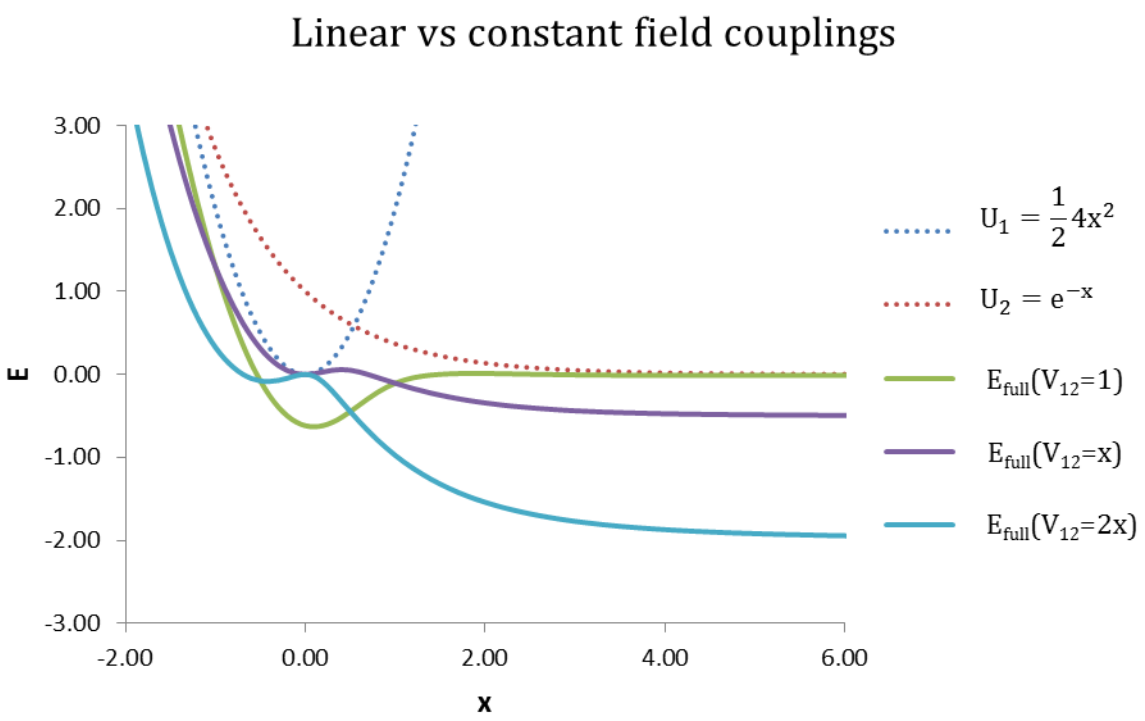

Figure 6. Linear vs constant coupling: dissociative model potential energy curves

In Figure 6, U_1 is given by $\frac{1}{2}4x^2$, and U_2 is given by e^{-x}. Unlike the effective potential energy surface under a constant field coupling, the effective potential energy E_{full} under a linear field coupling does not converge with the dissociated product's attractor, t. Instead it converges to a lower value that depends both on the reactant's force constant and the field intensity 'a' of the external field coupling (see Equation 36).

4.1 Two-state dissociative model

4.1.1 Constant field coupling

Figure 7 demonstrates that since the pseudo-barrier, Δ, is higher for larger force constants, a higher field intensity is necessary to suppress it. According to the uncoupled diabatic potentials, the topological index, μ, for low constant field intensities should be 2, that is a local minimum and a local maximum excluding the asymptotic extrema as $x \rightarrow \pm \infty$. The topological map, given in Figure 7, shows that a topological index, $\mu = 3$ dominates the (Δ,k) space for the lowest field coupling. The case of $\mu = 2$ is still found at low intensities for the exponential model of U_2, but the applicable intensities for this μ-value are much lower (see Figure 8). The intensities required to observe a phase with $\mu = 2$ with the repulsive Lennard-Jones model for U_2 are lower still. This is a natural consequence of the lower barriers exhibited in these models. A $\mu = 3$ phase, which occurs at low to intermediate field intensities, is due to a small shallow minimum that appears a finite distance after the barrier. Whether or not this shallow minimum can 'trap' the dissociated products within a fixed distance of each other will depend on the actual nuclear dynamics for the nuclear masses.

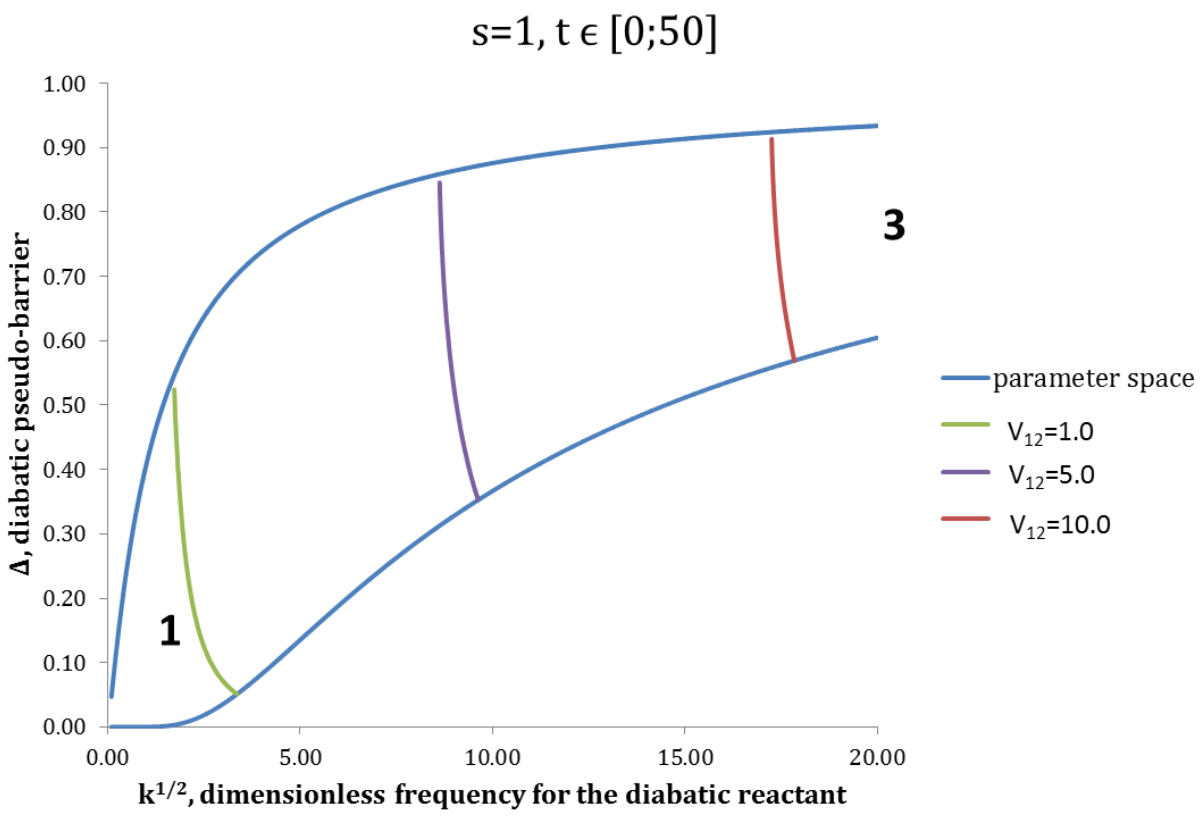

Figure 7. Effects of increasing coupling intensity: (Δ,k) space, dissociative model, $U_2 = se^{-x} + t$

In Figure 7, larger pseudo-barriers occur for larger force constants and for lower product zero-point energy. The upper border of the parameter space corresponds to t = 0 while the lower border corresponds to t = 50. The border between regions with topological indices μ = 1 and μ = 3 shifts to larger force constants as the field coupling intensity increases.

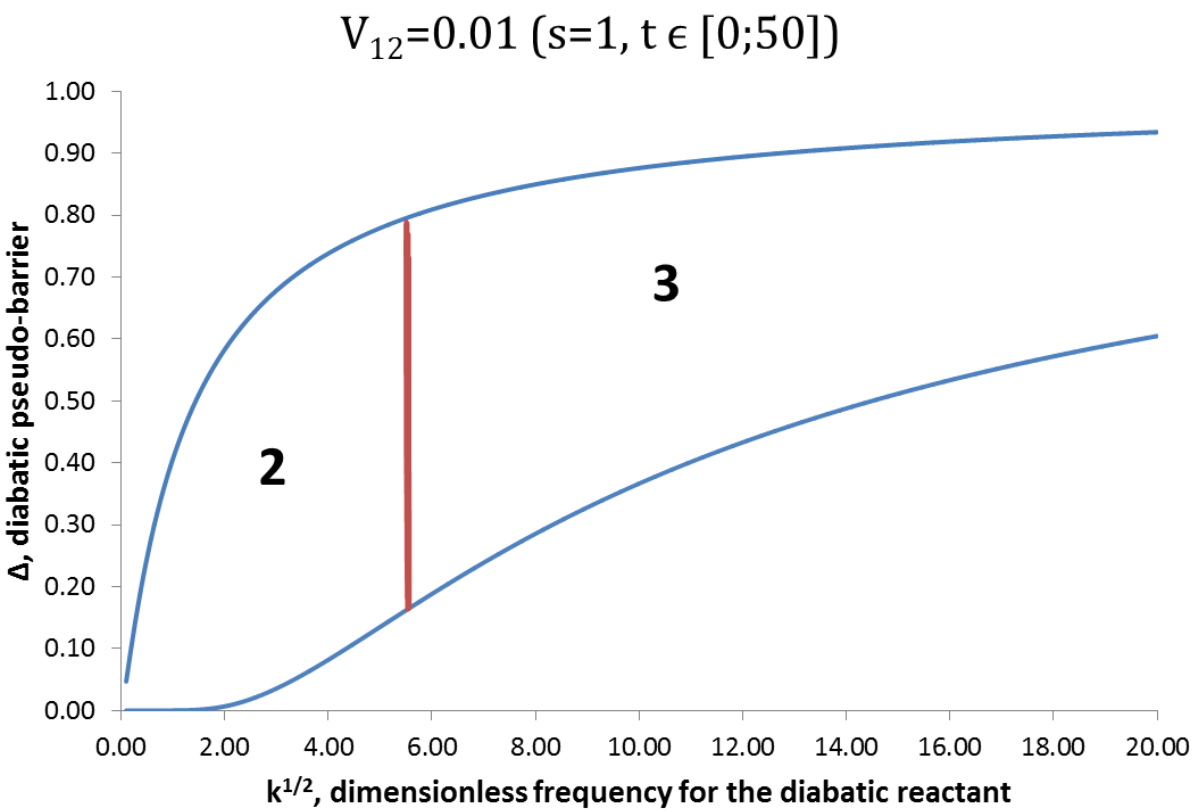

Figure 8. Topological phases at low field intensity: (Δ,k) space, dissociative model

There is a factor of two orders of magnitude between the constant field couplings necessary to see the border between the phases with μ = 2 and μ = 3 in the same region of the (Δ,k) space as the border between μ =3 and μ =1 (see Figure 7).

4.1.2 Linear field coupling

For linear field couplings, we can observe a region with $\mu = 0$, that is, with no critical points for finite x. This index implies that the reaction is spontaneous and unbound. In the (a,k) space, this new topological index occupies a narrow part between two regions of $\mu = 2$ (see Figure 9). As seen in the potential energy curves, $\mu = 0$ is the result of the reactant's attractor becoming an inflection point instead of a minimum. This inflection point appears when the nuclear coordinates for the attractor and the field coupling's intersection with the x-axis are the same. As the field intensity, a, increases, the reactant's attractor becomes a transition structure, that is to say a maximum on the potential energy curve (see Figure 9). If we turn to the (Δ,k) space where the field has a small energy intercept, a topological region of $\mu = 4$ appears (see Figure 10A). We might expect the additional extrema to appear near the reactant's attractor as a result of the field coupling's potential not quite coinciding with a diabatic attractor. This is not the case; new topological features occur on the product's side of the pseudo-reaction barrier. Again, whether or not these features correspond to certain geometries being trapped experimentally will depend on the nuclear dynamics for the nuclear masses.

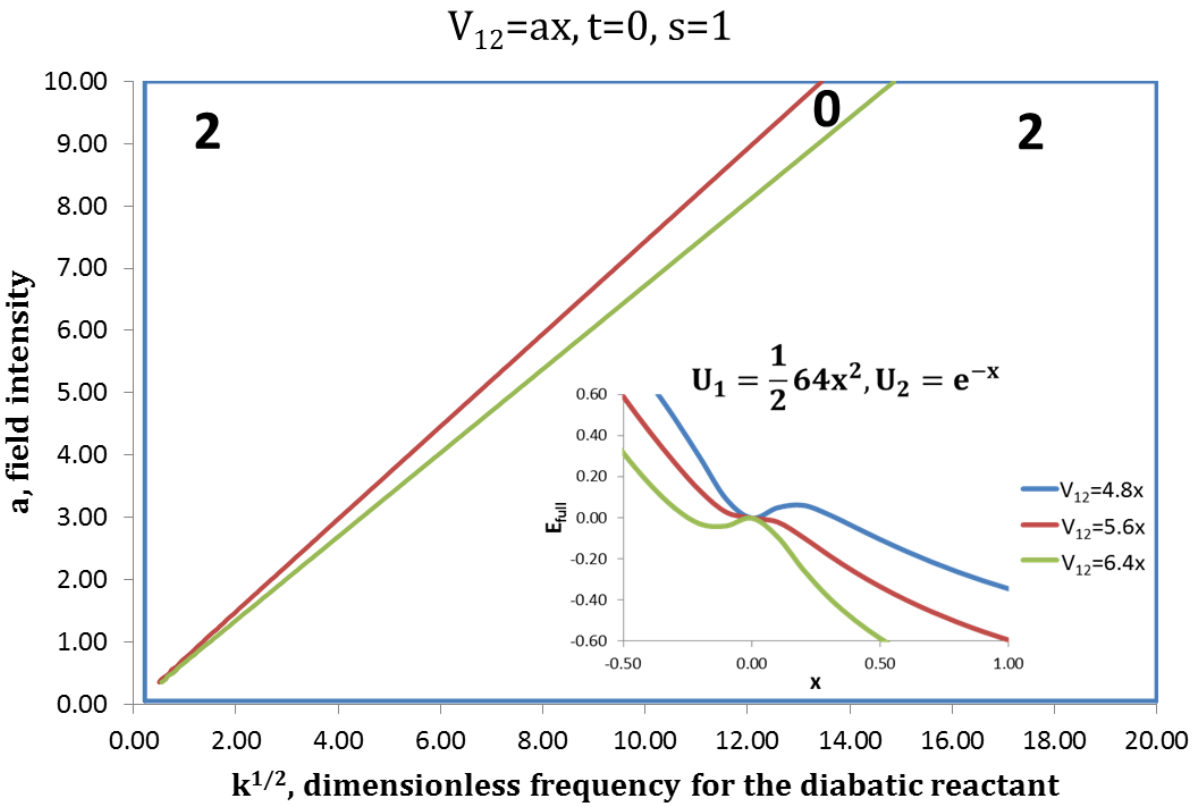

Figure 9. Increasing the V_{12} field coupling intensity, a, in the linear field coupling for the dissociative model

As the field intensity increases, the reactant configuration transitions from a minimum to an inflection point and finally to a maximum (see inset). The parameter space shows two separate phases characterized by the topological index $\mu = 2$. The corresponding minima in E_{full}, however, are quite different. The minimum on the effective potential energy curve is still situated at the reactant's attractor for low-a field couplings. Beyond a critical field intensity a_c, the minimum in E_{full} corresponds to a compressed bond, that is $x_{min} < 0$.

A

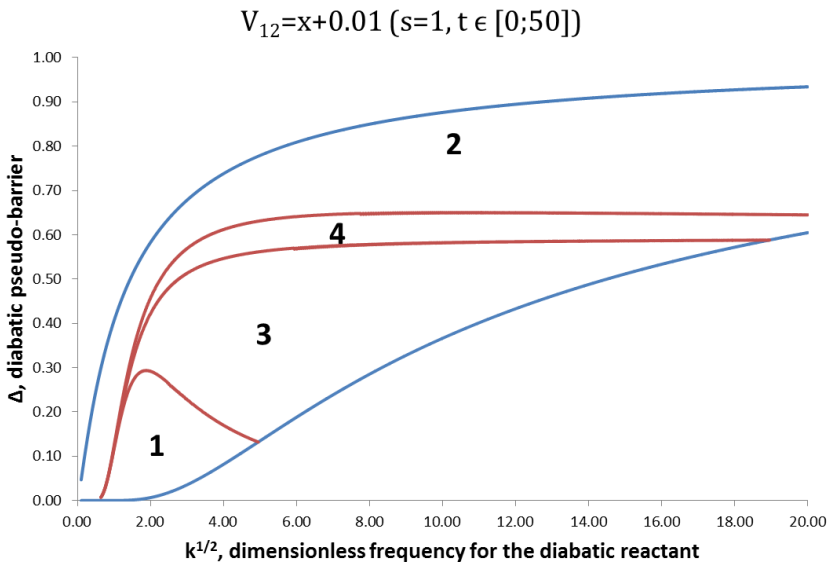

B

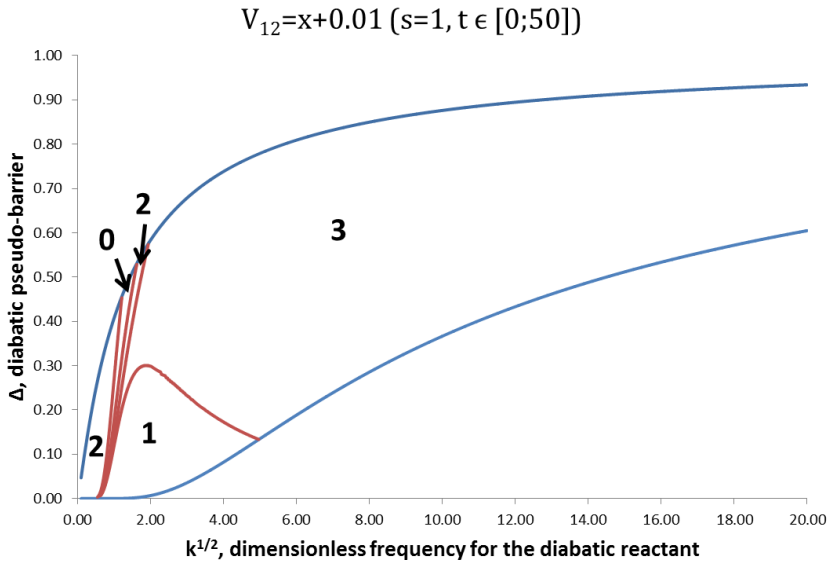

Figure 10. Effects of a small shift in the point where a linear V_{12} vanishes

Figure 10 shows dramatic changes in the topological phases and the portion of parameter space that they occupy. The absence of $\mu = 0$ for $V_{12} = x - 0.01$ (A) underlies the importance of keeping the point where $V_{12}(x) = 0$ outside the range of relevant reaction coordinates for a barrier-less reaction as present in B.

4.1.3 Inverse Lorentzian field coupling

For low intensities, the topological partitioning of (Δ,k) space for an inverse Lorentzian field coupling resembles the phase diagrams for a constant field coupling (see Figure 11). To appreciate the difference despite the similar topology maps, some example potential energy curves are also given in Figure 12. The inverse Lorentzian field coupling (see Equation 34.3) is locally weak and, since it is centred at the reactant's attractor, the diabatic reactant geometry is not as stable as under a constant field coupling. When the inverse Lorentzian field coupling's intensity increases, the differences between the topological maps and the potential energy curves become more noticeable. Since the field coupling intensity is exactly zero at a single point (x = 0) and greater than zero everywhere else, that point becomes the reaction barrier on the effective potential energy surface for a particular $a \geq a_c$ value, a critical field intensity. This particular field coupling is therefore inefficient at producing a barrier-less effective potential energy curve, E_{full}. Equation 28 involves the square of the field coupling – the absolute value of the field coupling increases on either side of the point where $V_{12} = 0$ – thereby producing E_{full} curves with $\mu = 5$ (3 minima, 2 maxima). Additional minima form on either side of the reactant attractor when the inverse Lorentzian field coupling is centred on the reactant attractor. Unlike the linear field coupling, however, the inverse Lorentzian field coupling rapidly reaches a constant intensity. Thus the dissociated products will always reach their uncoupled diabatic zero-point energy at $x \rightarrow \infty$ instead of a lower value. Scaling with the experimental data will determine whether the additional minimum at $x > 0$ will accommodate vibrational states. Even if this minimum does not allow any vibrational states, its modest energy difference will affect nuclear dynamics via quantum scattering.

A Constant field coupling

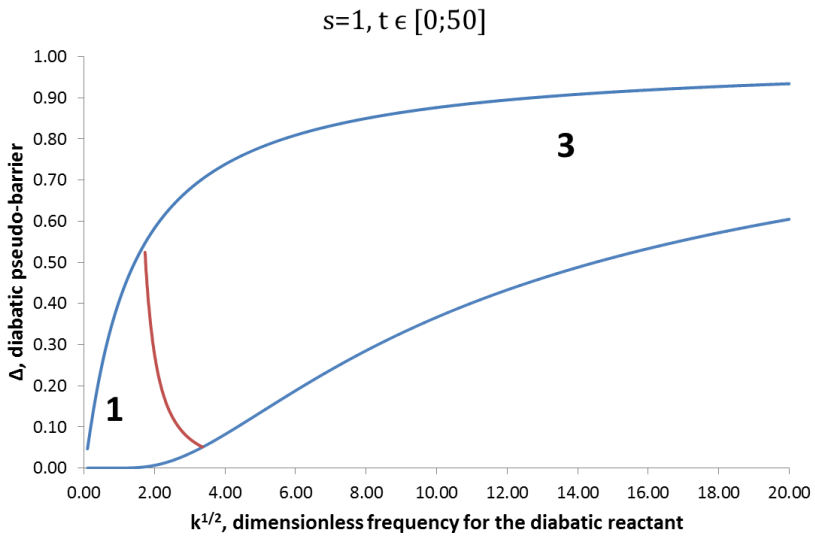

B Inverse Lorentzian field coupling

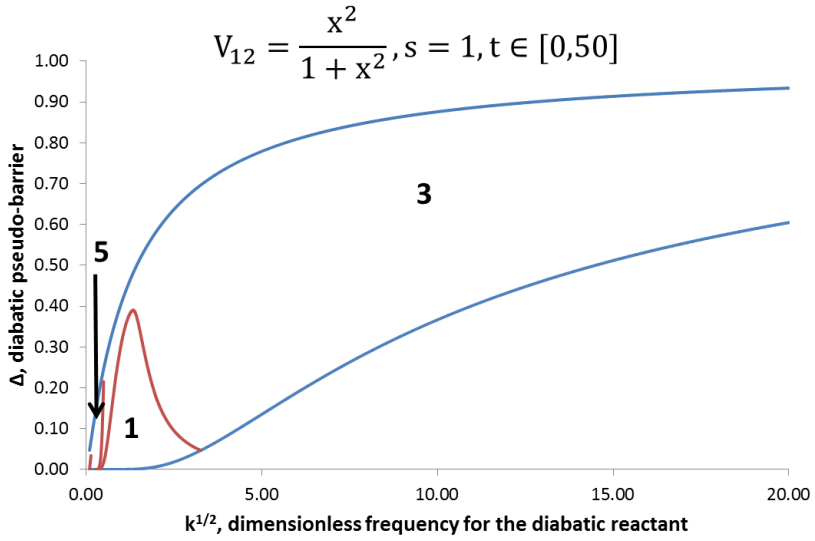

Figure 11. Constant vs inverse Lorentzian V_{12} field couplings: (Δ,k) space, dissociative model

In Figure 11, for low field intensities, the topological partitioning of the (Δ,k) space for the constant (A) and inverse Lorentzian (B) field couplings do not differ greatly. This is in part due to the small difference between the maximum and minimum values found in the inverse Lorentzian field coupling.

A

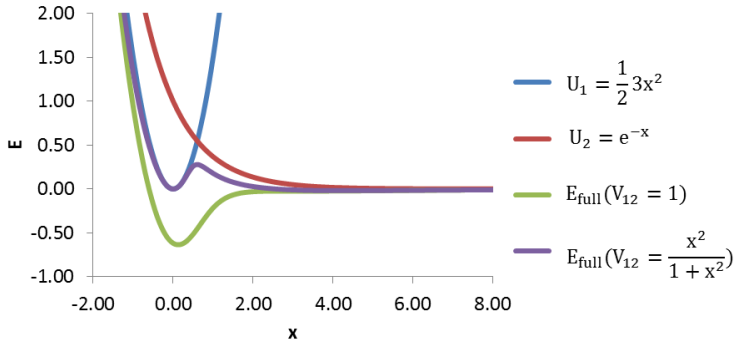

B

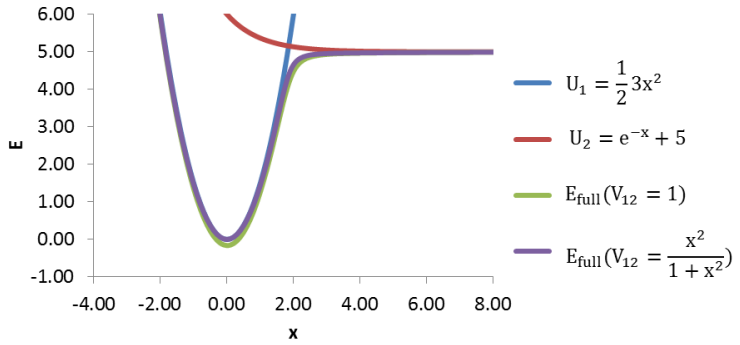

C

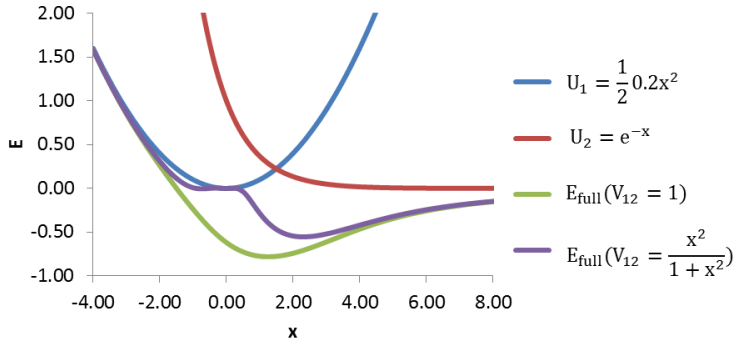

Figure 12. Constant vs inverse Lorentzian V_{12} couplings: dissociative model potential energy curves

Although the topological index for the curves in A and B remain the same ($\mu = 3$ and $\mu = 1$ respectively), it is clear that the effective potential energy curves can differ greatly depending on the $|\Delta U_{12}|$ where the inverse Lorentzian is centred. Indeed, B has a larger $|\Delta U_{12}|$ and the effective potential energy curve with the inverse Lorentzian coupling does not differ greatly from the curve produced by the constant field coupling. C exhibits $\mu = 5$ with the inverse Lorentzian V_{12} and $\mu = 1$with a constant V_{12}.

4.1.4 Lorentzian field coupling

This V_{12} coupling produces a larger effect in both of the repulsive Lennard-Jones forms of the dissociated product's diabatic potential than for the exponential form (see Equation 30). The phase diagrams with repulsive Lennard-Jones potentials have a larger barrier-less phase ($\mu = 1$) and resemble the constant field coupling phase diagrams more closely (see Figure 13). Each form of the dissociation model has in principle an infinitely broad reaction barrier. In practice, however, there is a defined distance where the chemical species are considered dissociated. Alternatively there is a distance where the energy is degenerate or nearly degenerate with the system's energy at infinite separation. The initial rate of decay in the exponential form of the product's potential simply indicates that the 'practicable' barrier for the repulsive Lennard-Jones potentials are not as broad. With the exponential form, the barrier is broader, therefore to achieve a phase diagram with a similar or larger barrier-less phase, the field intensity, 'a', must increase or the intensity must decay more slowly. If the maximum of the Lorentzian field coupling coincided with the exact location of the diabatic crossing, the barrier-less phase would be larger. For a single molecule, this may represent an energetically efficient way of stabilizing a configuration. This field coupling would also be effective for selective adsorption or desorption. If we were to adsorb several molecules onto a surface, however, the constant field coupling V_{12} represents a better choice.

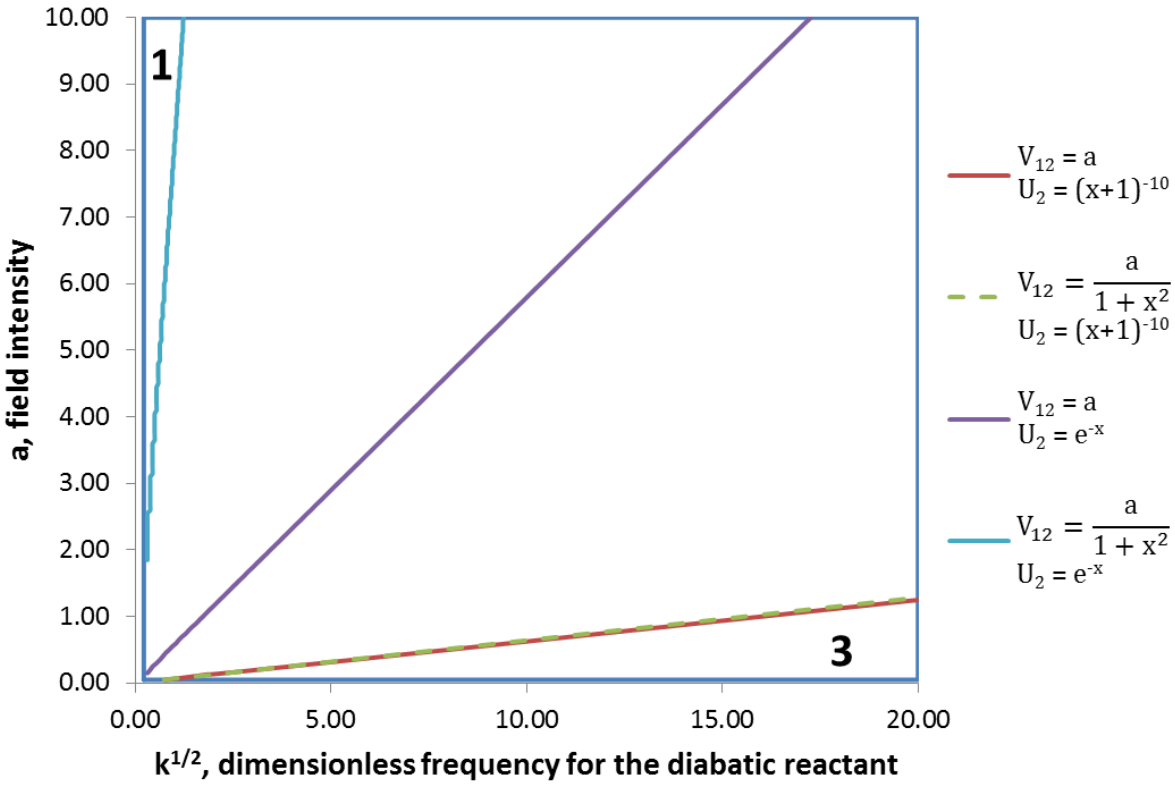

Figure 13. Comparison between phase diagrams: Lorentzian vs constant field coupling for the exponential and Lennard-Jones form of U_2.

The borders given correspond to those separating the $\mu = 1$ and $\mu = 3$ phases, where $\mu = 1$ is the region above and $\mu = 3$ is the region below any given border. For simplicity, the borders between the $\mu = 2$ and $\mu = 3$ regions that occur with the Lorentzian field coupling have been omitted (they would appear for the largest $k^{1/2}$ values and the smaller field intensity constant values). The larger difference in the phase border position with respect to the type of field coupling for the exponential form of dissociation is attributed to the larger barrier width. In comparison, the repulsive Lennard-Jones models have a much narrower barrier and a Lorentzian coupling is wide enough to be considered approximately constant everywhere. (In the case of the repulsive Lennard-Jones models, the abscissa is scanned for $x > -1$; in contrast, the exponential form of U_2 is scanned from $x = -4$.)

4.1.5 Discontinuous and non-smooth field couplings

Both the discontinuous field coupling and the Lorentzian field coupling can be locally more efficient than the constant V_{12} field coupling. There is a portion of nuclear coordinate space that can be more stable than others because the field coupling is locally stronger there. Of course, the effective reaction features, that is the number and location of local extrema, will depend on the position of the discontinuity and the intensities of each section of the $V_{12}(x)$ function. We have observed previously that a constant field coupling shifts the most stable configuration to larger positive nuclear coordinates. By placing the discontinuity at the diabatic reactant configuration, that is at $x = 0$, and letting the V_{12} section for $x \geq 0$ be greater than the section for $x < 0$, the barrier will disappear. This will only work if we find $\mu = 1$ when $a_2 = a$ where a is the intensity for a global constant field coupling; otherwise the barrier still appears although it is much reduced. Alternatively we may greatly stabilize the reactant's attractor and maintain the reaction barrier if the intensities of the sections corresponding to $x \geq 0$ and $x < 0$ are reversed. If the purpose is to keep a single stable geometry, that is to trap the quantum system in a reactant-like state, this type of coupling is worth considering. The discontinuities in the field coupling translate to discontinuities in the potential energy surface. By increasing the number of discontinuities, we can produce a potential energy surface that resembles a series of finite wells (see Figure 14). For our discontinuous field coupling, regardless of the number of discontinuities, the V_{12} function is sectionally constant, therefore the product's attractor will never be more stable than the reactants. This can be remedied if the field coupling is non-smooth and the linear section is placed over the attractor one seeks to stabilize.

By increasing the number of discontinuities, we can, in principle modify the topological index at will. In practice, however, the features on a surface that would give rise to such field couplings are larger in nuclear coordinate space than depicted in Figure 14. For a more realistic setting, we shall restrict ourselves to field couplings with only one discontinuity in their 0^{th} or their 1^{st} derivative with respect to the nuclear coordinate.

A

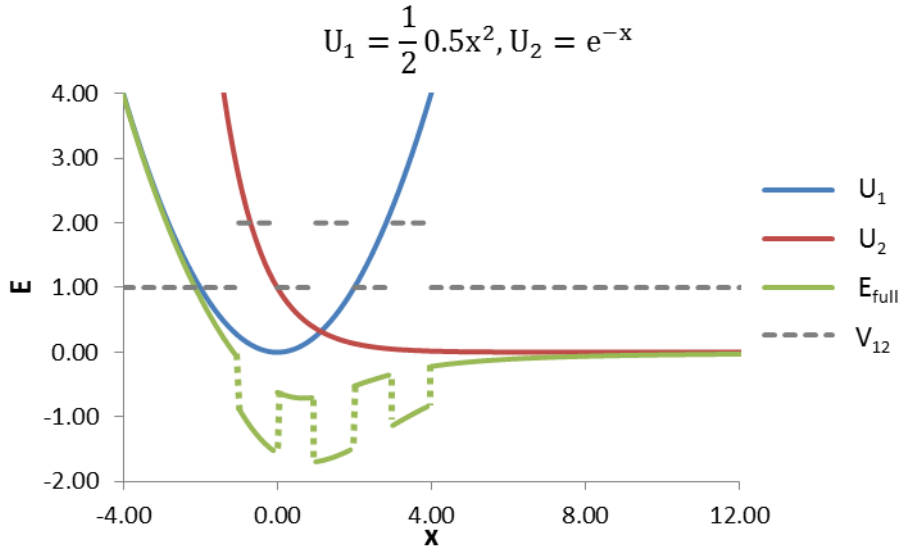

B

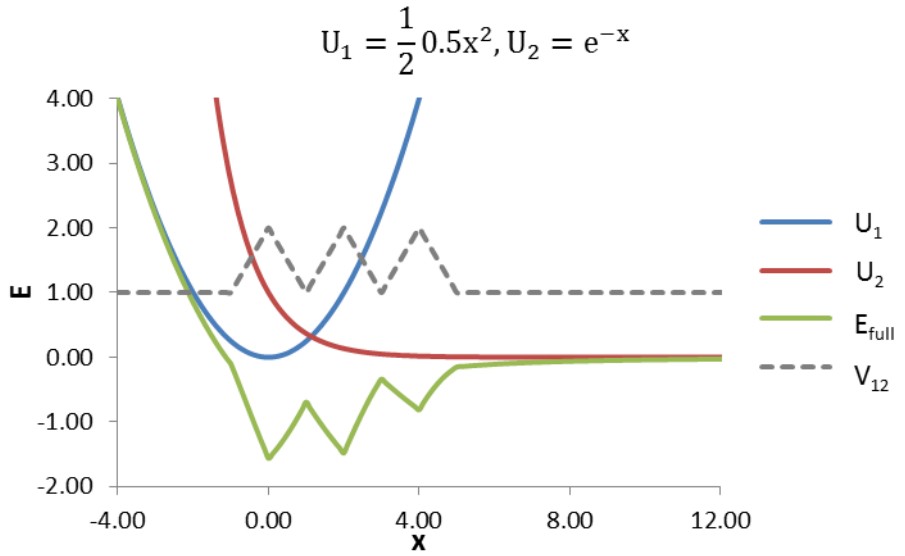

Figure 14. Effects of multiple discontinuities and non-smooth sections in the V_{12} field coupling on E_{full}

In Figure 14, the number of detectable critical points in E_{full} increases with the number of discontinuous (A) or non-smooth (B) sections in the V_{12} function for the range of coordinates where $0 \leq |\Delta U_{12}| < \infty$. Within this range, several configurations between the reactant and products can be stabilized.

All of the phase borders in the topological partitioning of the (a,k) space for a non-smooth field coupling coincide with borders found in the map with a purely linear field coupling (see Figure 15). The topological indices, μ, are naturally different and more extrema can be found on the effective potential energy surface with a linear coupling because there is a point where the coupling is exactly zero. (At the point where $V_{12} = 0$, the diabatic basis functions are uncoupled and the effective potential energy curve coincides with the lower of the two U_i functions. This may result in additional critical points.) We must also take into account the fact that the energy axis intercept for both the linear coupling and the linear section of the non-smooth coupling are the same and that the linear part starts at the reactant's attractor, in this case, $V_{12}(0) = 1$. In this case the linear section of the V_{12} field coupling is applied to the nuclear coordinates that are relevant to the reaction. Similarities between linear and non-smooth field coupling topology maps are not found without these two factors. We should note that the phase with $\mu = 0$, that is an unbound E_{full} function, extends to larger force constants as the field coupling's intensity, a, increases. Compared to the linear case, it is much simpler to obtain a region with $\mu = 0$ using a non-smooth field coupling. Any field intensity constant $a \geq a_c$ for a given section with a constant V_{12} value suffices with a non-smooth field coupling. In contrast, to get a $\mu = 0$ phase, we would be limited to single value for the linear field coupling's intensity. Another advantage of the non-smooth field coupling over the linear field coupling is that the $\mu = 0$ region in (a,k) space does not shrink much when the product's zero-point energy is increased (see Figure 16). This is not true when the section switch occurs at $x > 0$ (see Figure 17, Figure 18). For a given switch point there is a maximum force constant k for the diabatic reactant where the diabatic crossing occurs a certain distance after the switch between the constant and linear segments. For models with force constants below this maximum, the barrier is supressed and the resulting phase region is characterized by a topological index of $\mu = 1$ or $\mu = 0$. For models above this maximum k value, the reaction barrier appears before or near the switch though some may have an index $\mu = 1$. This phase corresponds to sections with low intensity linear $V_{12}(x)$ couplings. The effective minimum energy configuration resembles the reactant more closely than the models below the maximum k whose stable configurations are much more relaxed. Despite these reservations, out of all the field couplings analyzed, the non-smooth field coupling is the most effective in promoting dissociation, that is, in generating an effective product-like minimum energy configuration.

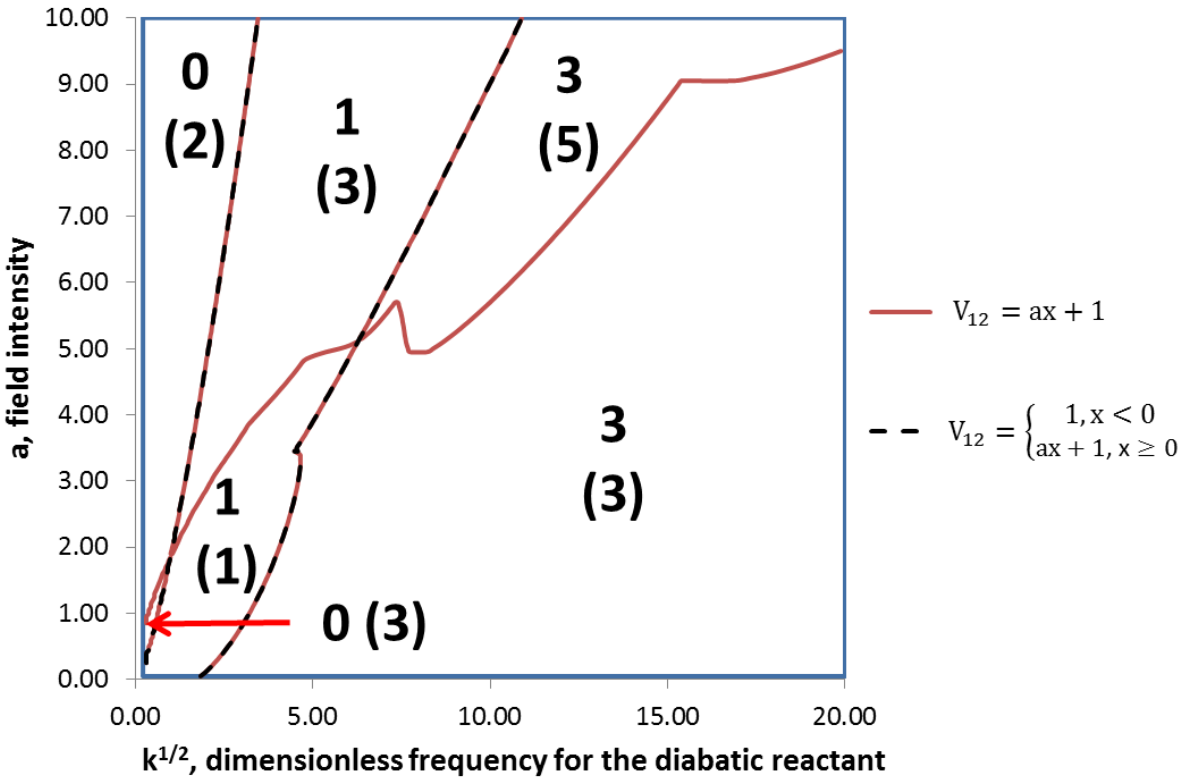

Figure 15. Effects of the linear and non-smooth $V_{12}(x)$ field coupling in the (a,k) space for the dissociative model

In Figure 15, the topological partitioning of the (a,k) space for a linear $V_{12}(x)$ coupling shares some phase regions with the non-smooth $V_{12}(x)$ function, which is overlaid in the same graph. The values for the topological index, μ, for the linear field coupling are indicated in parentheses. The different μ values and phase borders can be attributed to the fact that the external field coupling reaches zero for a linear coupling. In other words, the differences are due to the field couplings being represented by different functions for $x < 0$.

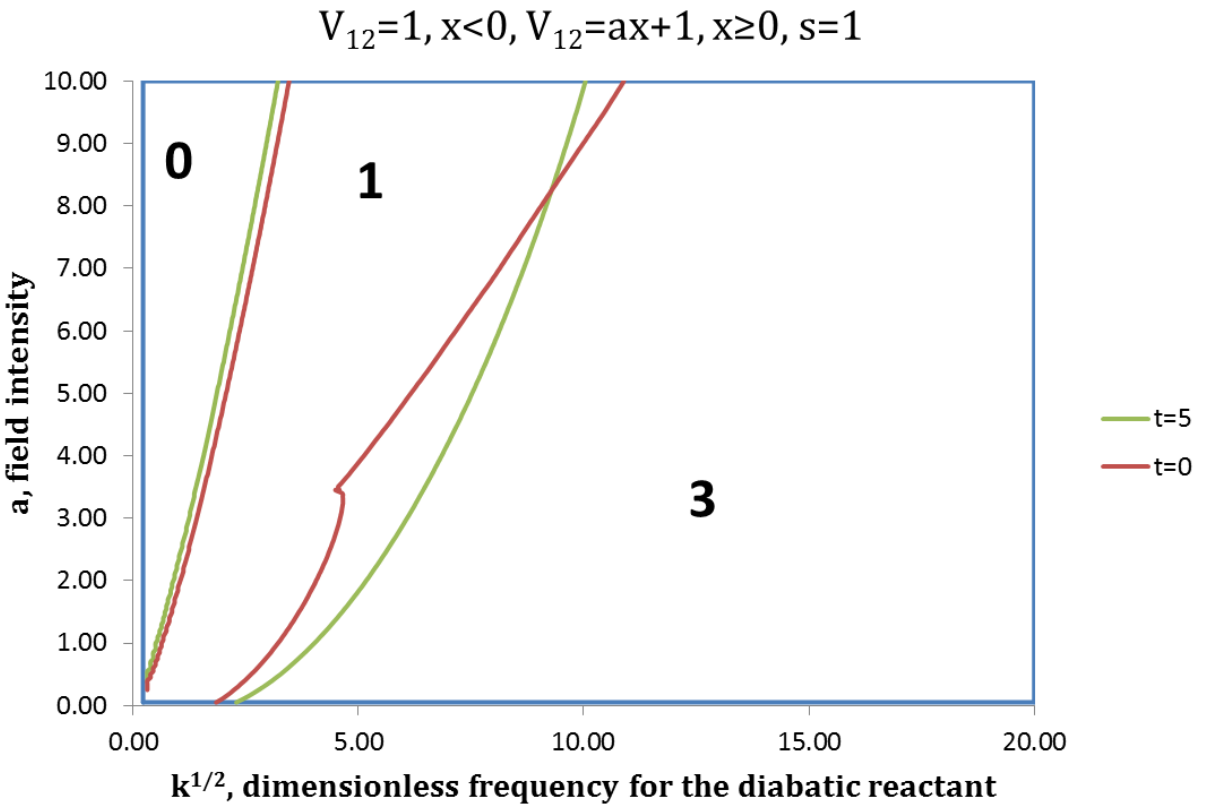

Figure 16. Topological partitioning of (a,k) space for models with different t values for the zero-point energies: case of the non-smooth V_{12} coupling and the dissociative model

In Figure 16, the region with topological index $\mu = 0$ for higher product zero-point energies (here, $t = 5$) shrinks because the diabatic reactant potential energy function U_1 is comparatively deeper. This leads to effective potential energy curves with $\mu > 0$. The models with larger t values require, therefore, larger field intensity a-values in the linear section of $V_{12}(x)$ to lower the portion corresponding to the unbound state. The intersection of the borders for the $\mu = 1$ and $\mu = 3$ regions is due to the interplay of the height of the pseudo-reaction barrier, Δ, and the field coupling's intensity, a. Field couplings with linear segments at low field intensity a-values give topological maps similar to those for a global constant coupling; with larger product zero-point energies, t, for the same force constant, the barrier is easily suppressed.

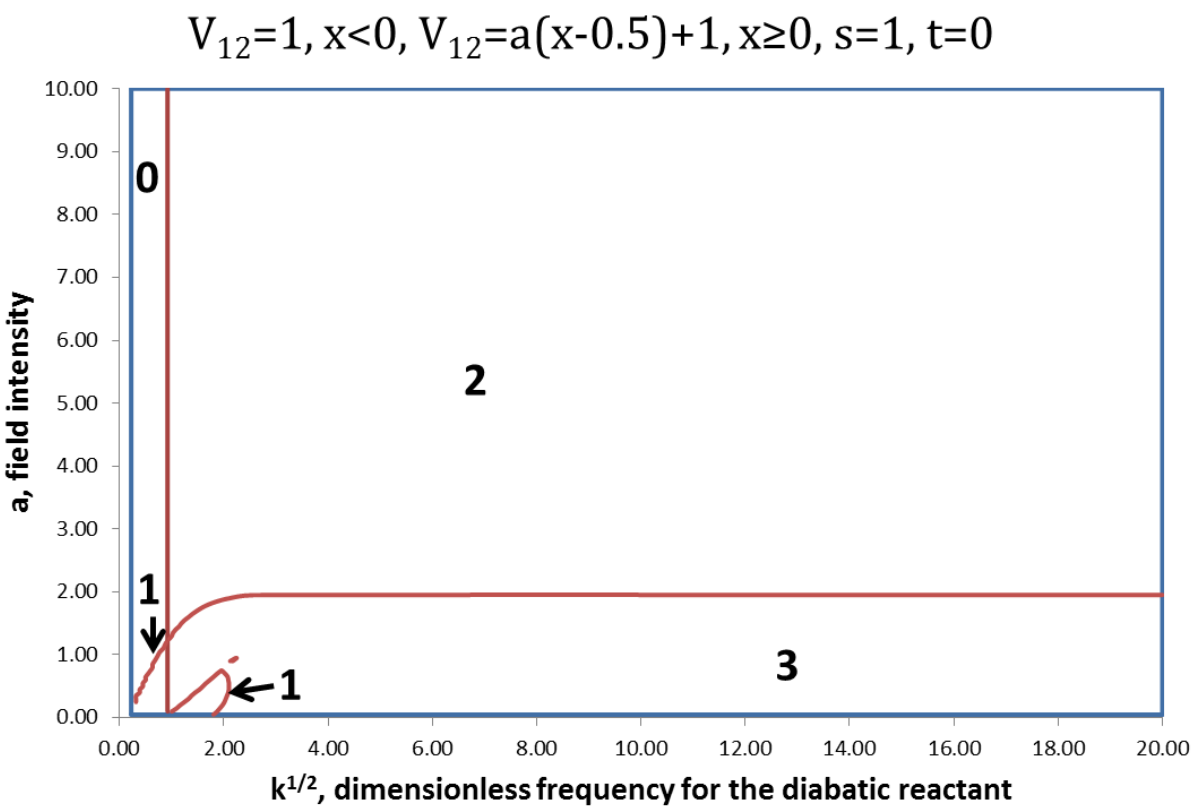

Figure 17. Topological partitioning of the (a,k) space for a non-smooth field coupling with a switch from constant to linear behaviour not centred at one the diabatic attractors

The larger number of phases in Figure 17, compared to Figure 16, is an effect of displacing the switch from critical geometries in the uncoupled diabatic potentials, that is, the uncoupled attractors, and the pseudo-barrier. We find that, for a given switch point for increasing the a-values for the field intensity, a critical force constant is reached for the transition between the phases characterized by the topological indices $\mu = 2$ and $\mu = 0$. Likewise, by increasing the force constant, k for the diabatic reactant, a critical value for the intensity is achieved ($a = a_c$) that divides the phase (a,k) space into regions with $\mu = 2$ and $\mu = 3$.

A

$$U_1 = \frac{1}{2}0.5x^2, U_2 = e^{-x}, V_{12} = 1, x < 0.5, 0.4(x - 0.5) + 1, x \geq 0.5$$

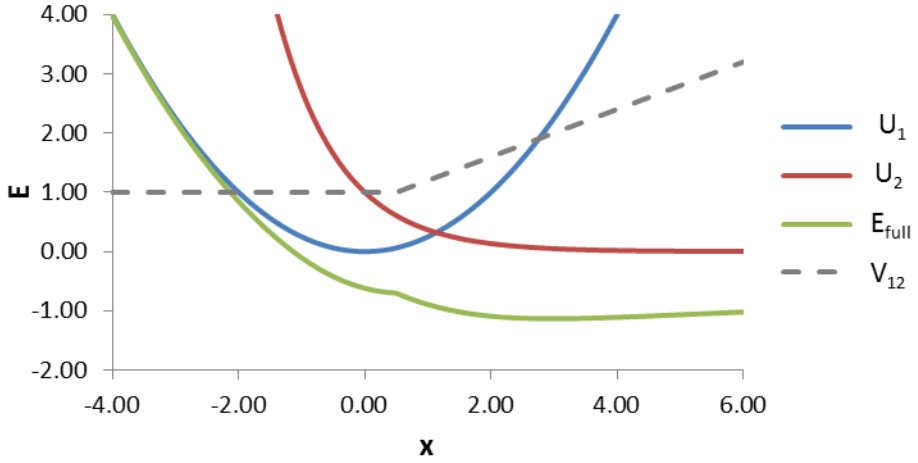

B

$$U_1 = \frac{1}{2}4x^2, U_2 = e^{-x}, V_{12} = 1, x < 0.5, 0.4(x - 0.5) + 1, x \geq 0.5$$

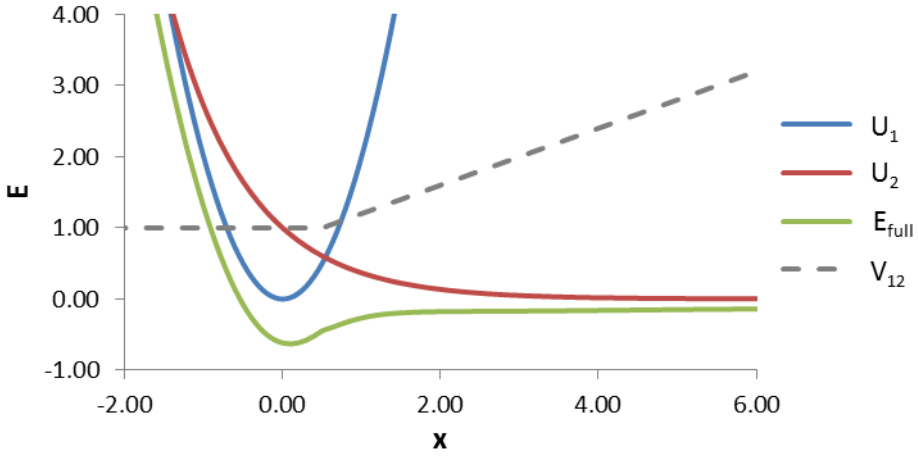

Figure 18. Effects of non-smooth field coupling V_{12} with a switch not centred at a diabatic attractor

For smaller force constants (A), the single minimum is significantly displaced from the uncoupled reactant attractor (here, $\min(E_{full}) \approx -1.1327$, at $x \approx 3.0$). The single minimum in models with larger force constants (B) does not shift significantly from the uncoupled reactant attractor (here, $\min(E_{full}) \approx -0.6318$ at $x \approx 0.1$).

4.2 Two-state isomerization model

4.2.1 Constant field coupling

For the isomerization model (Equation 30), the highest order term in Equation 38 is of order six in the reaction coordinate, x, therefore there should be at most six non-trivial extrema. Let us consider first a symmetrical model, where the reactant and product force constants and zero-point energies are equal, that is k = s and t = 0. Under a constant external field we obtain the following:

$$0 = \left(x - \frac{1}{2}r\right)^2 \left(a^2 + k^2 r^2 x\left(x - \frac{1}{2}r\right)\right) \qquad \text{Equation 41}$$

Clearly x=r/2 is a doubly degenerate critical point, invariant with respect to the field intensity. The other extrema must vary with the field as:

$$x = \frac{r \pm \sqrt{r^2 - 16\left(\frac{a^2}{k^2 r^2}\right)}}{2} \qquad \text{Equation 42}$$

We can see that when the field is zero, we recover the extrema on the uncoupled diabatic potential energy surface, x = 0 and x = r for the diabatic reactant and product attractor respectively. The doubly degenerate root x = r/2 is the coordinate value for the diabatic curve crossing. It is apparent that the non-degenerate extrema are field-modified reactant and product configurations. We may discern a critical field intensity, a_c, when the topological index switches from $\mu = 3$ to $\mu = 1$. All four roots become degenerate when

$$a_c = \frac{1}{4}kr^2 \qquad \text{Equation 43}$$

(see Figure 19).

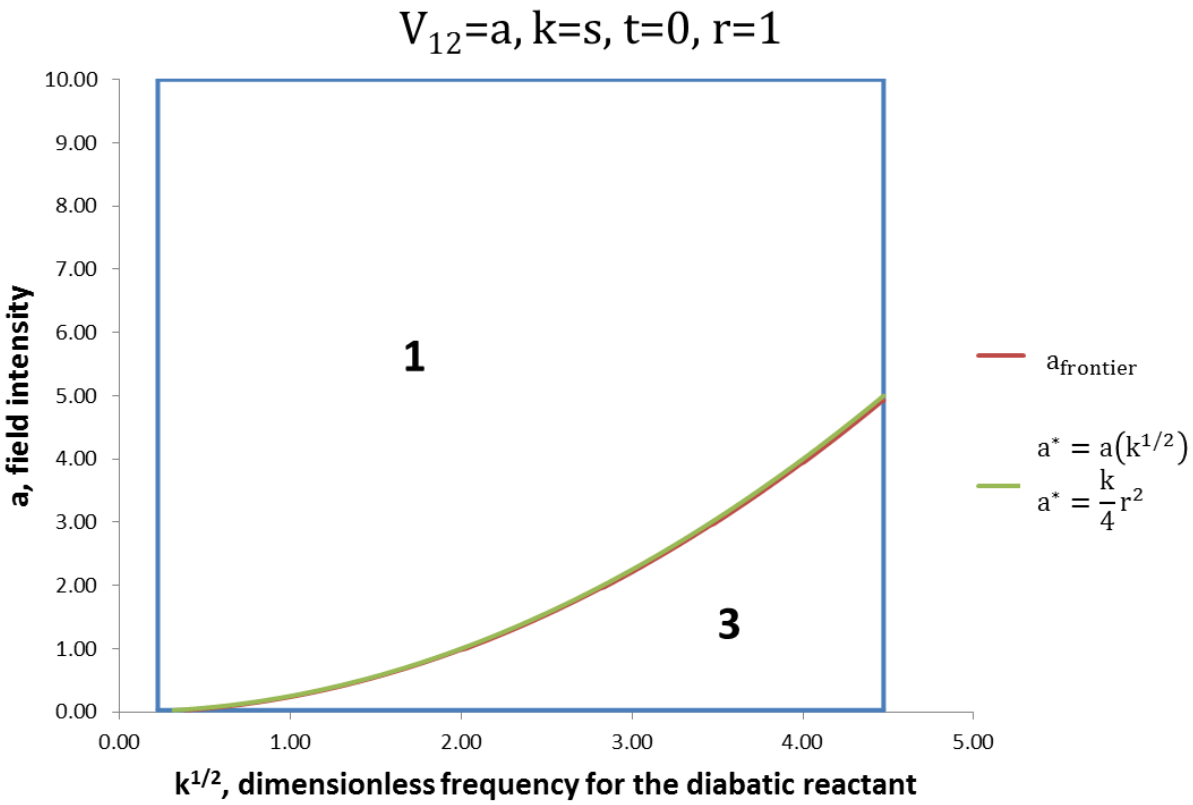

Figure 19. Constant coupling phase transition: analytic solution vs parameter scan

In Figure 19, any point along the line $a = a_c = \frac{1}{4}kr^2$ is at a critical field intensity where the topological index, μ, changes. This is corroborated by the line produced as the topological classification of each curve is analyzed using the numerical method to detect critical points discussed in section 3. The small discrepancy at higher force constant values can be attributed to the numerical limitations in our procedure to scan for critical points on E_{full} which are discussed in the section 3.2.

At field intensities greater than or equal to the critical intensity, ($a \geq a_c = \frac{1}{4}kr^2$) the transition structure between the reactant and product diabatic states, found at x = r/2, is energetically the most stable configuration. Such closed form solutions are not possible if the symmetry is broken either through different force constants or different zero-point energies. We can, however, predict the position of the single minimum in asymmetric models ($k \neq s$ or $t \neq 0$) when the field coupling reaches infinite intensities:

$$x_{min} = \frac{sr}{s + k} \qquad \text{Equation 44}$$

At infinitely large field couplings, if the product's force constant is larger than the reactant's, that is s > k, the stable configuration will resemble the product's attractor (see Figure 20). This convenient result is true regardless of the zero-point energies.

It is interesting to note that the line corresponding to the equality of the force constants acts as a line of symmetry in the topological partitioning of (Δ,k) space. This aspect appears only when the external field coupling is symmetrical with respect to all curve crossings in the manifold of diabatic potentials, $\{U_i\}$, examined. One might argue that representing such a set of parameters is redundant since they can be obtained by a reflection about the crossing point and a translation. Without considering the external field this is, of course, mathematically true. When the field is not symmetrical with respect to all the crossing point in the manifold, however, symmetries in the topological phases are not found in the same (Δ,k) space. To illustrate this point, we extend the idea of a symmetrical effect to discontinuous field couplings. The difference in this case is that the symmetry is between a pair of topological phase diagrams instead of within a single map. For example, the topological regions for a field coupling $V_{12} = 1$ for $x < x^*$ and $V_{12} = 2$ for $x \geq x^*$ where $x^* = 0.5$ are mirrored in the map where the sections' field intensities are switched (Figure 21B, Figure 21C). This is a natural consequence of $x^* = 0.5$ also being the position of the totally symmetric diabatic potential energy curve crossing (k = s, t =0). This effect continues even if the discontinuity in V_{12} does not coincide with the symmetrical model's diabatic crossing. This fact is best exemplified by the phase diagrams with the same intensities but where the discontinuities are placed at x = 0.25 and 0.75 respectively (Figure 22).

A

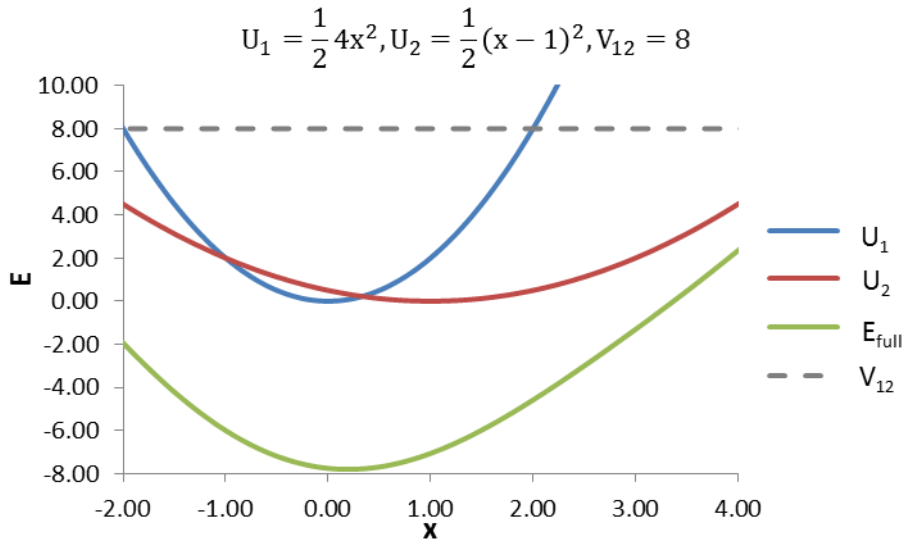

B

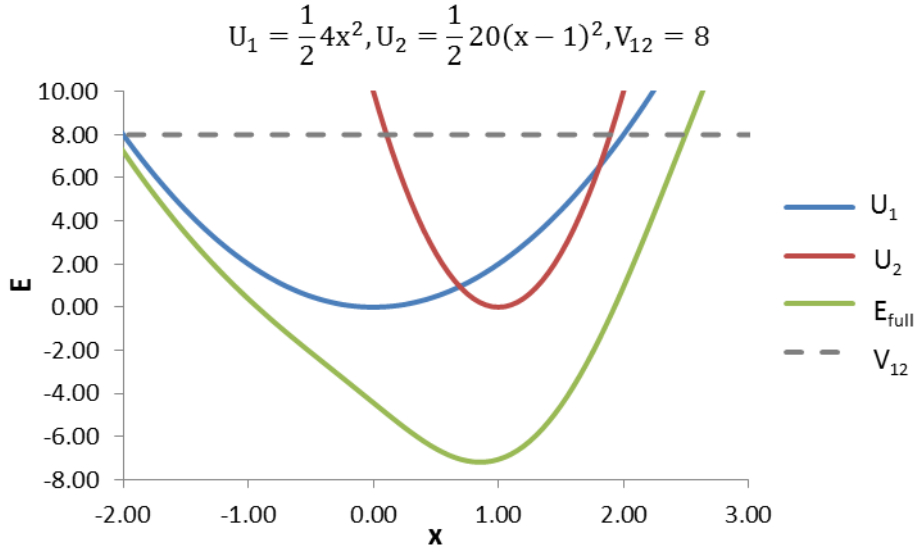

Figure 20. Stable configurations in asymmetric models with large constant field coupling

For identical or approximately identical zero-point energies, in the limit of infinite field coupling intensity, the larger force constant determines the identity of the most stable configuration. In A, a reactant-like structure is stable with k > s, while in B, a product-like structure is more stable with k < s.

A

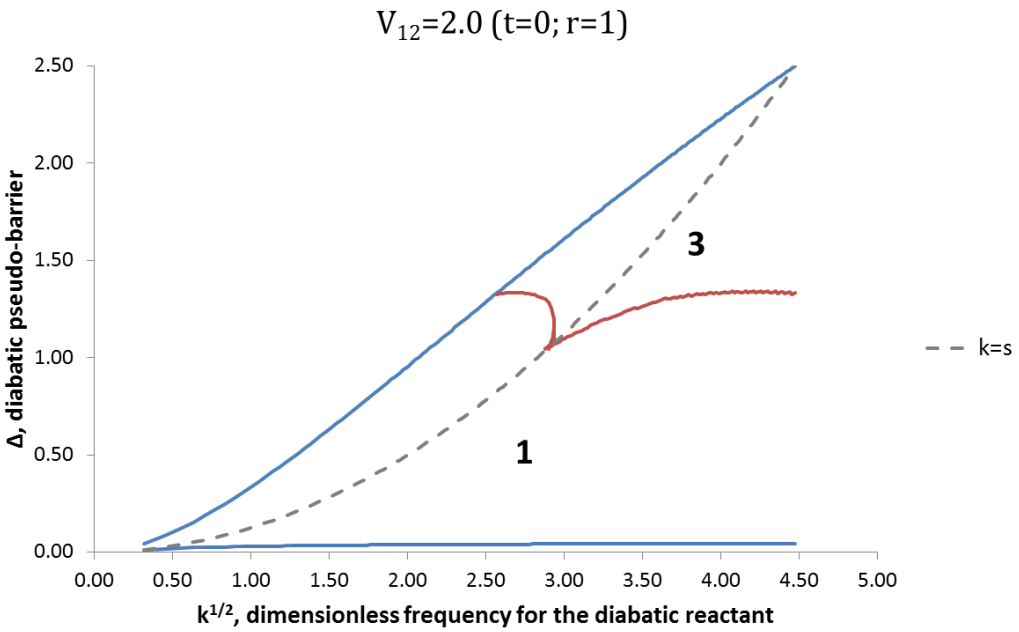

B

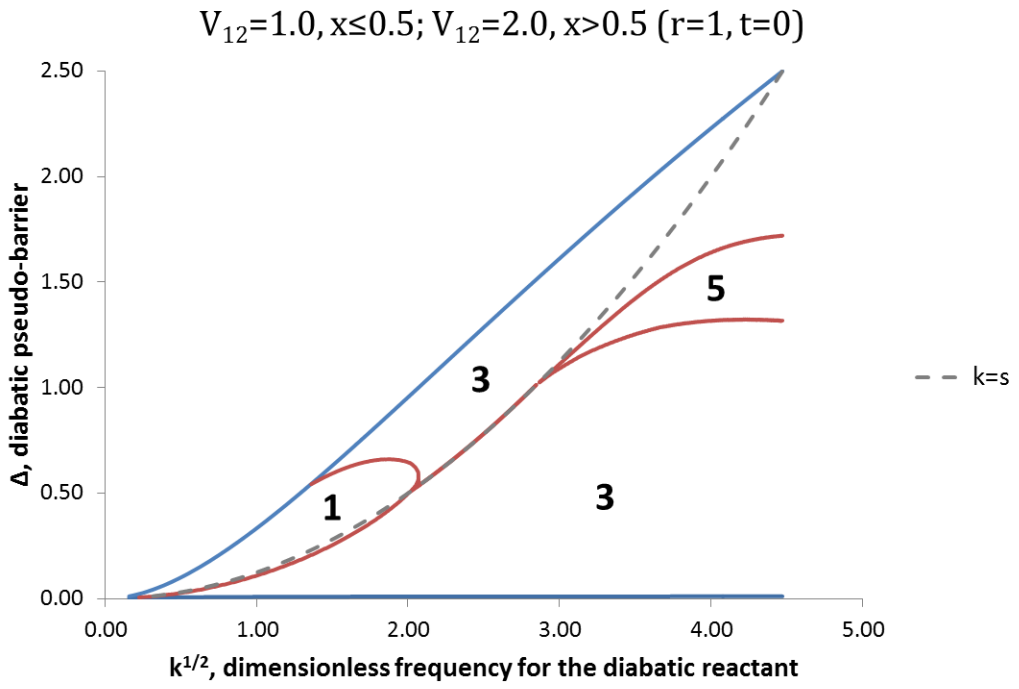

Continued on following page

Continued from previous page

C

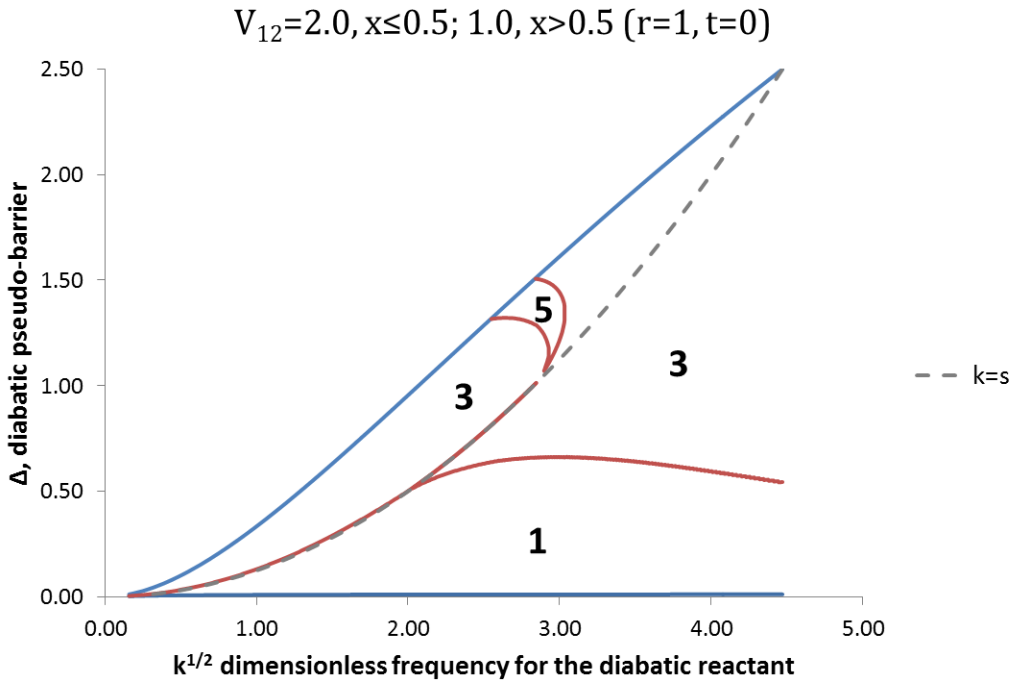

Figure 21. Topological phases mirrored about k = s for constant (A) and discontinuous (B, C) V_{12} couplings in the (Δ,k) space for an isomerization with the product's zero-point energy t = 0. In graph A, all the topological phases on one side of line Δ(k) for k = s are "reflected" on the other side of the line for a constant field. In graph B, the field is discontinuous at the diabatic crossing for the set of symmetric models. The topological features in one map are mirrored in the other about the line Δ(k) for k = s (dashed line), when the field intensities constants are reversed around the switching point as seen in graph C.

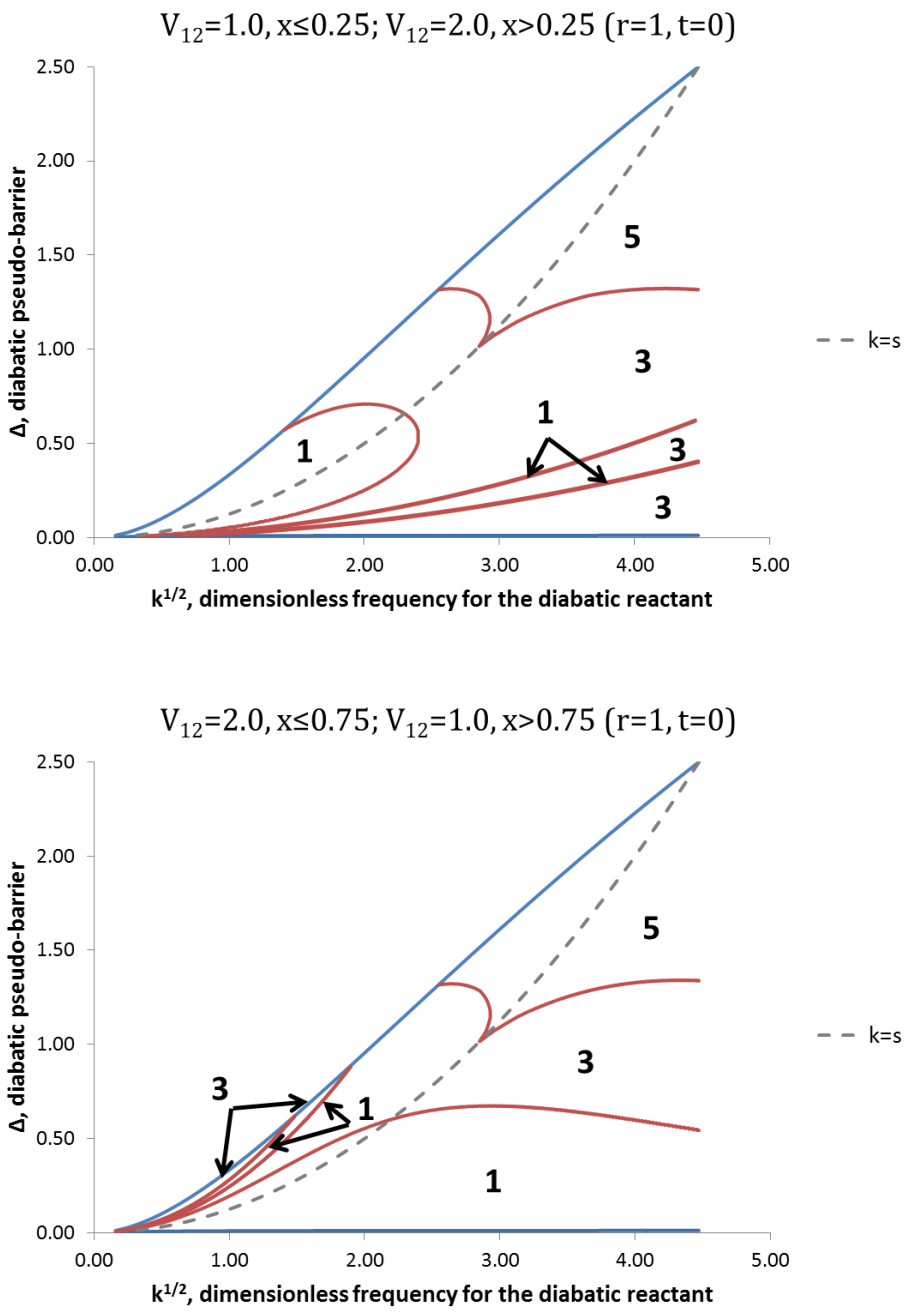

Figure 22. Symmetry in phase diagrams for discontinuous field couplings

In Figure 22, despite the discontinuity in the V_{12} coupling not being placed at the diabatic pseudo-barrier for the symmetric model (k =s and t = 0), the 'mirror image' topological map A can be found by switching the V_{12} values of each section of the discontinuous coupling and shifting the discontinuity an equal amount to the other side of x = r/2 as shown in B.

4.2.2 Linear field coupling

We can extend the notion of symmetry in the topological partitioning of (Δ,k) parameter space to the linear field couplings as well. The (Δ,k) phase diagrams for the following field couplings are identical although the potential energy curves that produce them are not (Figure 23):

$$V_{12} = ax \qquad \text{Equation 45.1}$$

$$V_{12} = a(x - r) \qquad \text{Equation 45.2}$$

These findings are the result of both zero-point energies being identical, that is $\min U_1 = \min U_2$. No such symmetry is found, however, in the maps where the product diabatic potential is raised to t=1.

Inserting either form of Equation 45 into Equation 38 guarantees a root for the derivative of the effective potential where the field coupling satisfies $V_{12} = 0$. For $V_{12} = ax$, the root at x = 0 is doubly degenerate if the following is true:

$$a^2 = \frac{1}{2}k\left(\frac{1}{2}sr^2 + t\right) \qquad \text{Equation 46}$$

Alternatively, we find a root at x = r if $a^2 = \frac{1}{2}kt$. Incidentally, for a completely symmetric model, when the field coupling's intersection with the nuclear coordinate axis coincides with the diabatic curve crossing, the positions of all three extrema are known. The root at x = r/2 is doubly degenerate and is a maximum. This comes as no surprise as it corresponds to the apex of the reaction barrier. Since the external field coupling is zero at that point, there is nothing to reduce the barrier. The position of nuclear configurations corresponding to the minima, however, are given as

$$x = \frac{\frac{1}{2}kr(a^2 + 2r^2) \pm \sqrt{\frac{1}{4}k^2r^2(a^2 + 2r^2)^2 + a^2(a^2 + r^2)\left(\frac{1}{4}k^2r^2 + a^2\right)}}{k(a^2 + r^2)} \qquad \text{Equation 47}$$

Admittedly, this is not as impressive a result when one deduces that all models where both the product and reactant share the same zero-point energy also have a topological index μ = 3 (2

minima, 1 maximum). This is easily understandable when one considers that although the field coupling may not be exactly zero at the diabatic crossing, it is very small. As the field intensity increases, we may then anticipate that the maxima will shift from the diabatic crossing to where the field coupling vanishes (dashed line in Figure 25). The minima will also shift from the attractor geometries away from position where $V_{12} = 0$. Both species are stabilized by the field at slightly different geometries. If the zero-point energies are equal, then determining which species is the most stable depends on where the field coupling is greatest. Such a simple conclusion is not possible when the zero-point energies are unequal ($t > 0$, Figure 26).

In the topological phase diagrams, there is only a narrow part of (Δ,k) parameter space with an index $\mu = 1$. In fact, with infinite precision, the narrow wedge would reduce to a line: this phase occurs when the point where the field coupling is zero becomes an inflection point in E_{full}. As the field intensity increases, the inflection point becomes an unstable transition structure (Figure 27). The stability of a configuration over another is linked to the strength of the field coupling at that configuration; the linear field coupling provides an excellent example. Whichever uncoupled attractor, say the reactant, is lower in energy will define the most stable configuration for a low intensity linear field coupling. This is true even if the field coupling vanishes at the diabatic reactant attractor. If we increase the field coupling's intensity, however, the nuclear configuration corresponding to the product becomes the most stable even if it is not for the uncoupled diabatic states. In this case, the field strength over the product's attractor is significantly larger than over the reactant's attractor. This effect matches the experimental situation where the external field stabilizes a structure that would be unstable at zero field.[8]

A

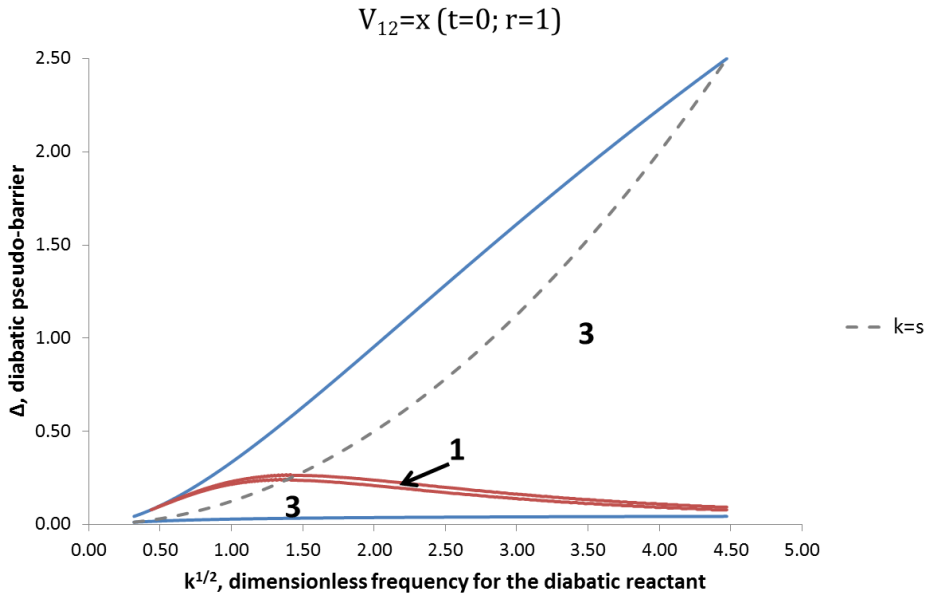

B

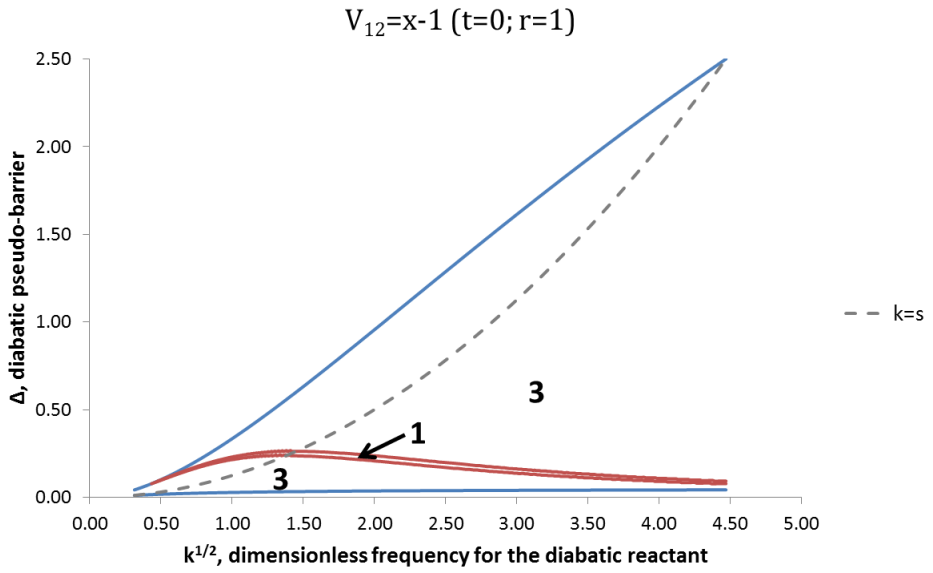

Figure 23. Identical topological partionings of (Δ,k) space for linear couplings that vanish at either diabatic attractor where each has the same zero point energy

Figure 23 shows how the topology maps for linear field couplings V_{12} that vanish at either attractor, at x = 0 (A) or x = r (B), are the same although the potential energy curves are not (see Equation 45 and Figure 24).

A

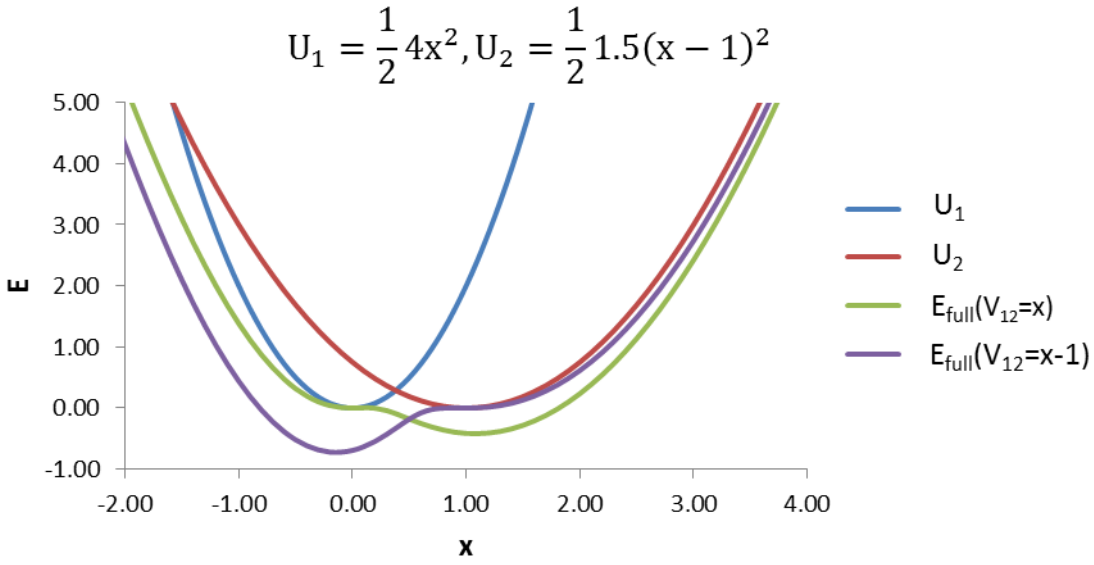

B

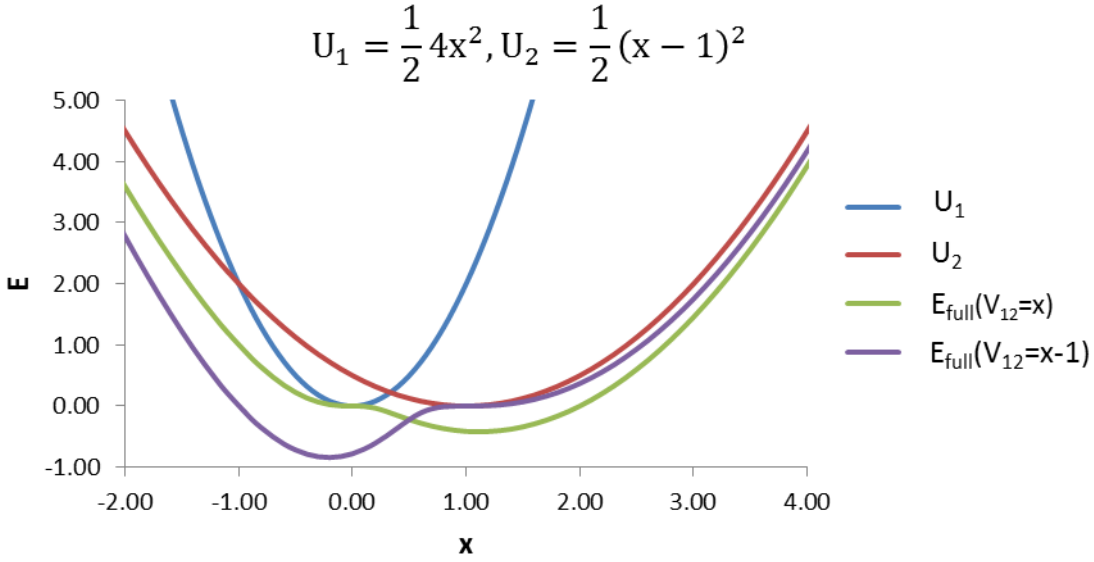

Figure 24. Samples of diabatic models with t = 0 and a linear V_{12} that vanishes at a diabatic attractor configuration.

The field coupling V_{12} vanishes at the reactant attractor when $V_{12} = x$ and at the product attractor when $V_{12} = x - 1$. Although the effective potential energy curves produce the same topological index, both E_{full} curves in A have $\mu = 3$ and those in B have $\mu = 1$, the minimum energy configuration is not the same.

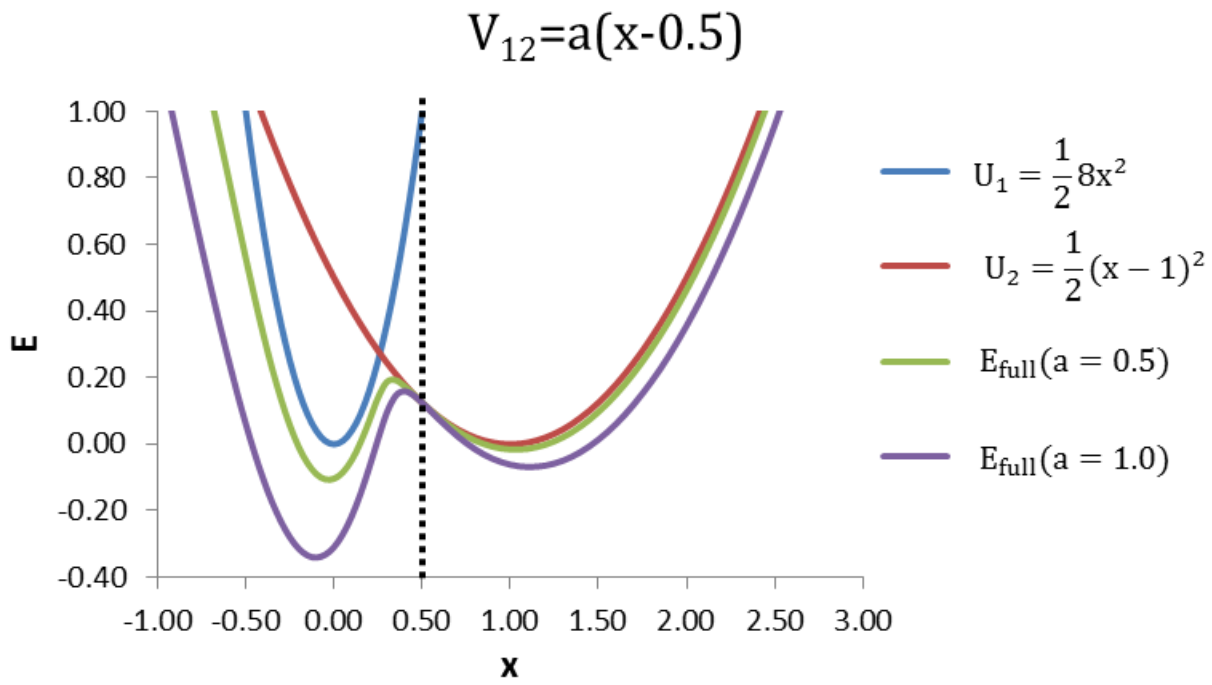

Figure 25. Effect of increasing the field intensity when using V_{12} linear couplings on the effective isomerization potential energy curve

In Figure 25, though all curves exhibit the same topological index ($\mu = 3$), the maximum's position shifts towards the location where the field coupling vanishes (marked by the dotted line). The most stable reactant configuration is compressed (the product's configuration is relaxed) as demonstrated by the minima shifting to increasingly negative (positive) values.

A

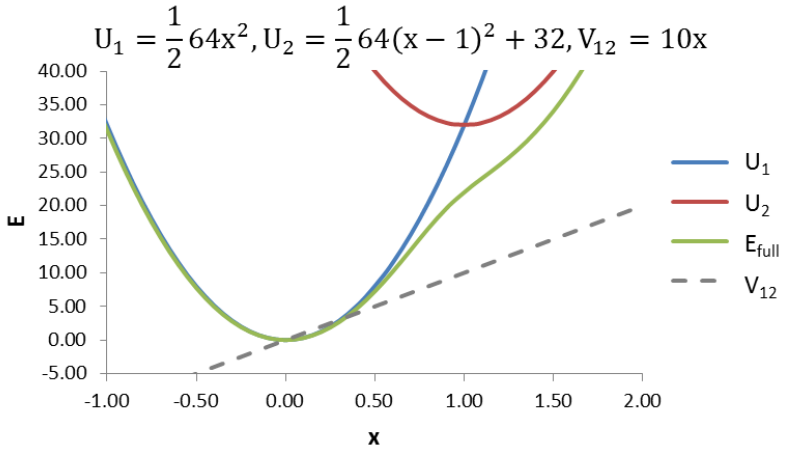

B

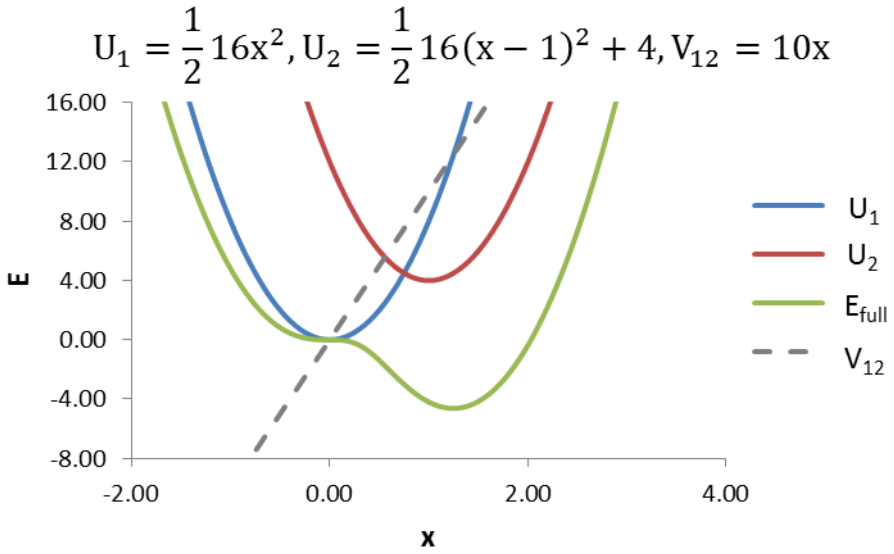

Figure 26. Effects due to the field intensity and the ΔU_{12} functions on the effective potential energy surface E_{full}

In Figure 26, although the field coupling is stronger over the product's attractor than over the reactant's attractor ($V_{12}(r) > V_{12}(0)$), the product may not be the most stable configuration if the zero-point energies are unequal ($t > 0$). Comparing graphs A and B, we can deduce the existence of a critical field intensity, $a=a_c$, when a minimum corresponding to a product configuration will have at most the same energy as a reactant configuration. A closed form equation for the critical field intensity, a_c, can be obtained from the roots of quartic equation derived from Equation 38.

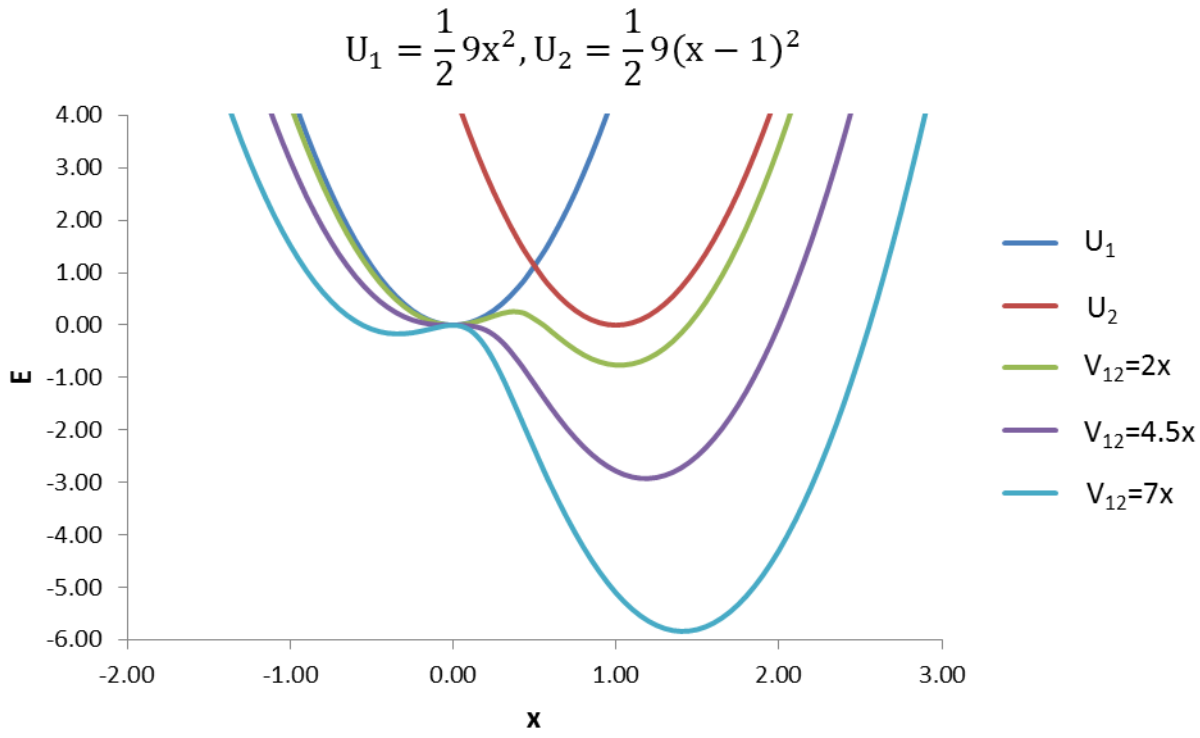

Figure 27. Occurrence and shift of stable configuration in E_{full} when using linear V_{12} field couplings

In Figure 27, as the field coupling's intensity, a, increases, the reactant's attractor shifts from a minimum at V_{12}=2x to an inflection point at V_{12}=4.5x and finally a transition structure or maximum at V_{12}=7x. The isomerization to the product at V_{12}=4.5x is spontaneous and exothermic as the reaction barrier is completely supressed and the product is energetically lower than the reactant on the effective potential energy surface. Increasing the field intensity to a = 7, however, re-establishes a barrier, but the stable reactant geometry is now compressed, that is, $x_{min} < 0$.

4.2.3 Inverse Lorentzian field coupling

Similar observations can be made for an inverse Lorentzian field coupling (Equation 34.3). However, in the vicinity of the field coupling's minimum, the field strength increases more slowly than in the case of a linear field (refer to Equation 34.2, Equation 34.3). The slower field increase creates a third phase with the topological index $\mu = 5$ (3 minima, 2 maxima) as shown in Figure 28A. This phase may only be observed if the field is correctly 'tuned'. For example, if the inverse Lorentzian field coupling is centred at the reactant's attractor ($x = 0$) and we find $\mu = 5$, the reactant's attractor is a weakly stable geometry. The other minima correspond to a 'compressed' reactant geometry and a relaxed product-like configuration. As with the phase $\mu = 1$ in the linear V_{12} coupling, this present $\mu = 5$ phase also occupies a narrow strip of parameter space (Figure 28). At low field intensity, the fact that the point for uncoupling ($V_{12} = 0$) coincides with an attractor's geometry has little effect on the effective potential energy. As the intensity increases, however, that geometry becomes weakly stable and eventually a transition structure (Figure 29).

A

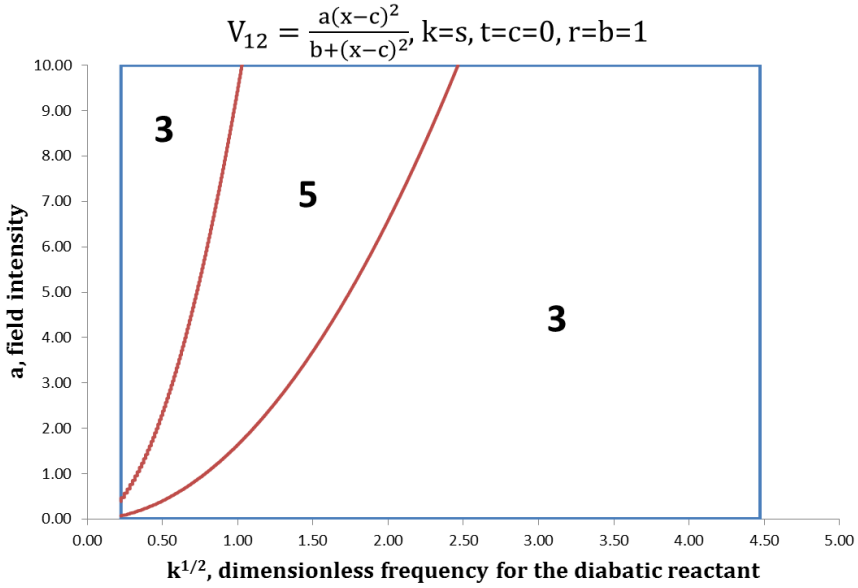

B

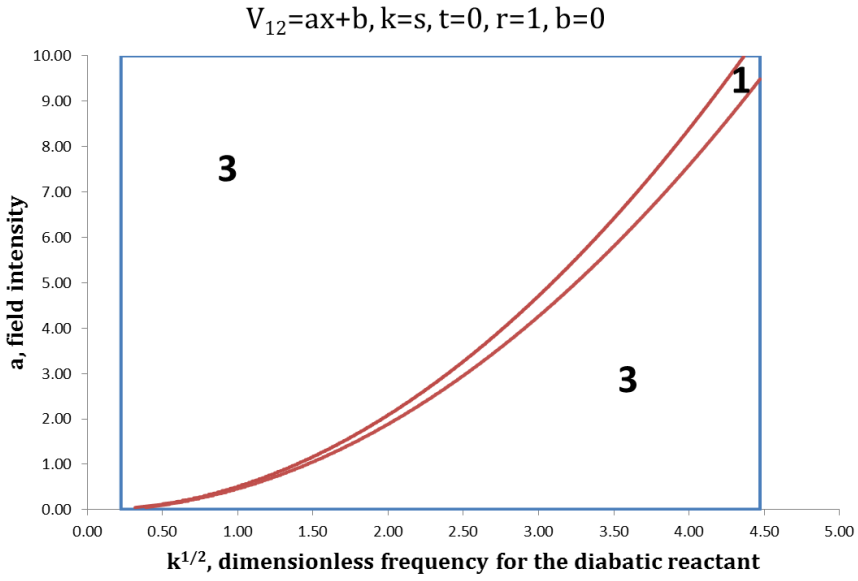

Figure 28. Topological phase diagrams in (a,k) space for the isomerization model using an inverse Lorentzian V_{12} coupling

The region with topological index μ = 5 in A plays a similar role as the region with μ = 1 in B. Both occupy a narrow portion of the (a,k) parameter space. Unlike the linear field coupling, however, the inverse Lorentzian coupling will not reduce this phase region to a single line with infinite surface scanning precision (refer to section 4.2.2).

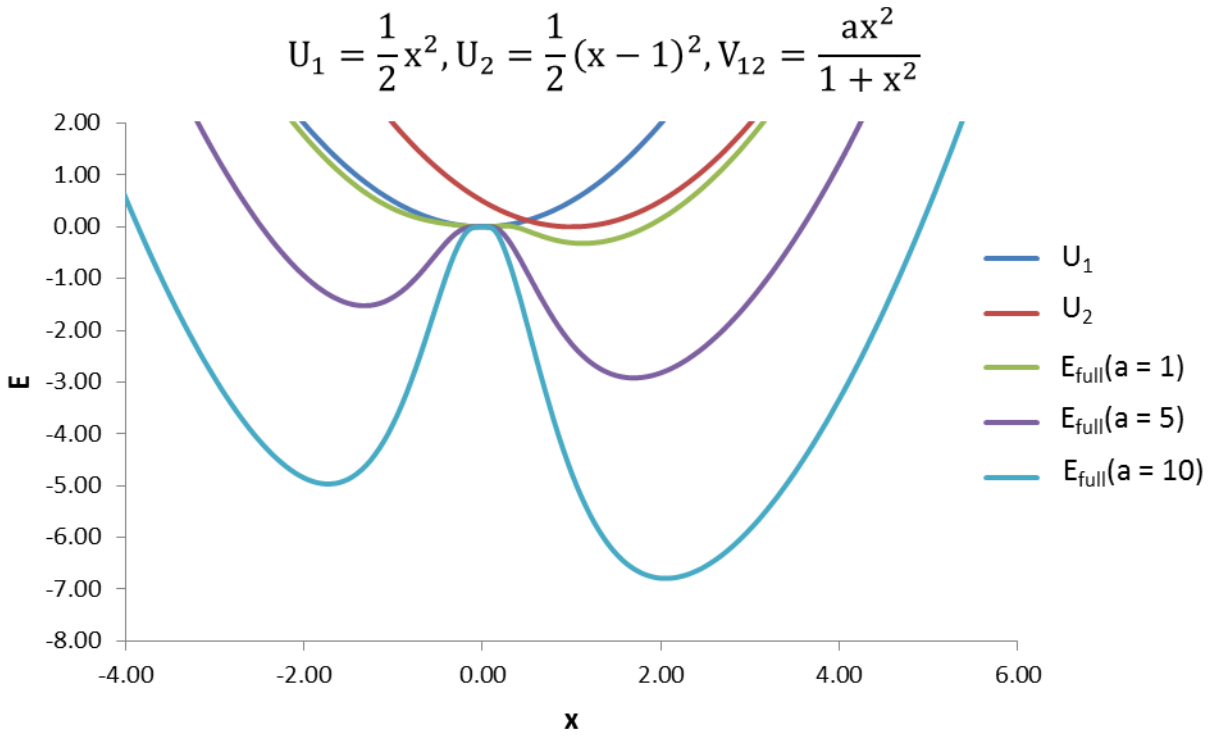

Figure 29. Effects of increasing the inverse Lorentzian coupling intensity, a, on potential energy curves

In Figure 29, by increasing the inverse Lorentzian field coupling's intensity a, the stability of the reactant's configuration decreases until it becomes a transition structure. As the a-value increases, the most stable configurations are increasingly compressed reactants and relaxed products as shown by the minima's shift.

4.2.4 Lorentzian field coupling

The Lorentzian field coupling (Equation 34.4) has quite the opposite effect on the potential energy curves compared to the inverse Lorentzian coupling. The phase diagrams in (a,k) parameter space for the Lorentzian V_{12} coupling resemble those produced by a constant field coupling as shown by the green and red lines respectively in Figure 30. The maps' resemblance in (Δ,k) space is less noticeable because the Lorentzian field coupling is not symmetrical with respect to all the diabatic crossings in the manifold of models examined. The similarity in (a,k) space can be explained when one considers that the field strength is approximately the same over the relevant values of the reaction coordinates. Although the pseudo-barrier can be higher in the isomerization models, unlike the dissociative reaction models, the pseudo-barrier has a finite width. Since the product is not an asymptotic minimum, a local high-intensity field coupling is more effective for this reaction. Comparing the effective potential energy curves for a constant field coupling and a high-intensity Lorentzian field coupling, the latter can select an attractor over another if the position for the V_{12} minimum is chosen carefully. Also, the effective potential energy curve, E_{full}, forms a narrower well around the stable configuration; the effective reaction force constants are not only degenerate, but also greater than those required with a constant field coupling.

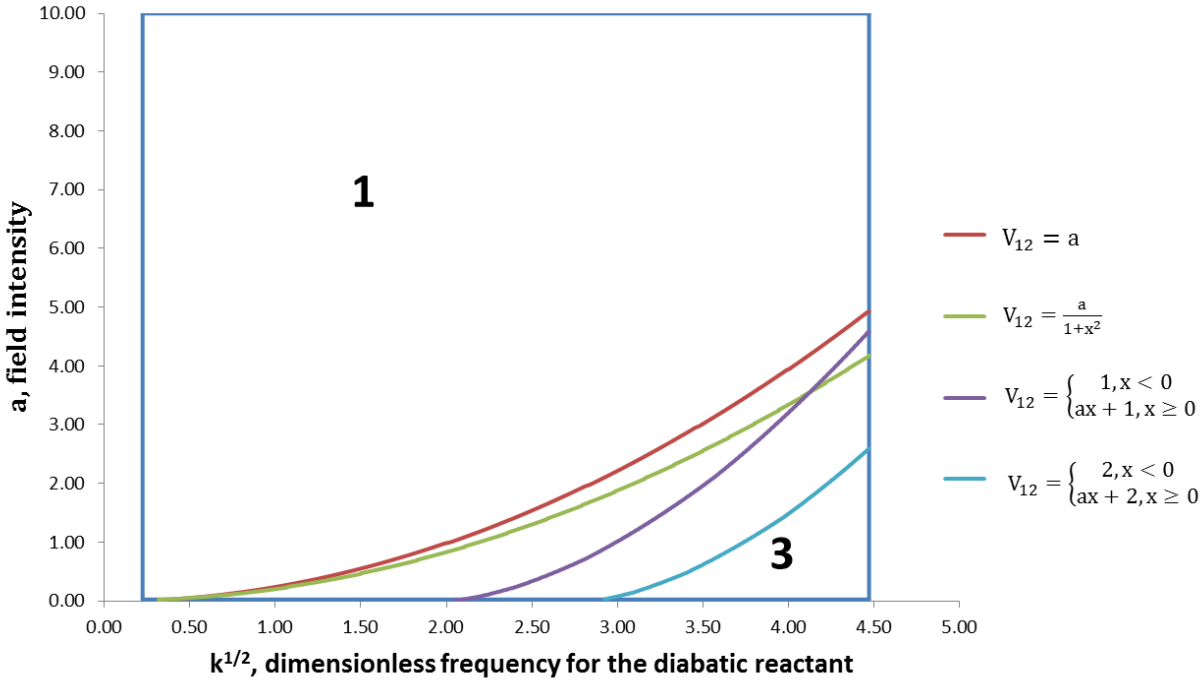

Figure 30. Comparing the borders between the μ = 3 and μ = 1 phase regions when using constant and partially constant V_{12} couplings for isomerization models

In Figure 30, while using a Lorentzian field coupling proves to be more efficient at removing the reaction's energy barrier for an isomerization model (k=s, t=0, r=1), the same cannot be said for a dissociative reaction ($U_2 = e^{-x}$, see Figure 13). The differing behaviour is not due to the height of the diabatic barrier, Δ. Indeed, the barrier height reaches a maximum of Δ = 1 in the limit of infinite force constant. Rather, the difference is due to the product attractor's position along the nuclear axis. Put another way, the barrier in the dissociative model is much wider, thereby requiring a broader field coupling to suppress it. Hence, the phase with topological index μ = 1 occurs at significantly larger values of the Lorentzian field coupling intensity a.

4.2.5 Discontinuous and non-smooth field couplings

For discontinuous field couplings applied to the radical isomerization model, if the section with the largest V_{12} value covers the range [0, r], the topological characterization is the same as if that V_{12} were applied everywhere. This field gives a conceptually simple effect: to obtain $\mu = 1$ phase, it is only necessary to have a greater intensity over the relevant reaction coordinates, for the purpose of our model: [0,r]. Additional topological features may appear when the lower intensity branch of the discontinuous V_{12} covers [0,r].

Unlike with the dissociative model, the non-smooth field coupling produces topology maps for the isomerization model that are more similar to those for a constant field coupling when the linear section covers the relevant range of the reaction coordinate. The reason is that, unlike a purely linear field, the discontinuous field coupling V_{12} never vanishes. As shown in Figure 30, for a given constant segment, the non-smooth field coupling will be more effective than a larger global field coupling for smaller force constants. As shown in previous sections, if the model parameters for each attractor are equal, then whichever attractor geometry has the greatest field coupling will the most stable geometry on the effective potential energy surface. Unlike a global constant coupling, for a totally symmetric model, the segment with linear V_{12} coupling can bias the effective potential energy curve so that a geometry closer to, say, the product's attractor geometry is favoured. For a fixed constant segment and larger force constants, the non-smooth field coupling is no longer more effective than the constant or the Lorentzian field coupling in supressing the reaction barrier. The models with larger force constants have higher pseudo-barriers therefore when beginning with a small constant V_{12} coupling the critical intensity a_c that suppresses the pseudo-barrier is much larger. The borders between the $\mu = 3$ and $\mu = 1$ phases for the constant and non-smooth field coupling will cross at much larger force constant values if the section where V_{12} is constant increases in intensity.

The topological map changes drastically if the switch between the constant and linear segments occurs between the two diabatic attractors, that is, within [0, r]. When the switch coincides with the symmetric diabatic pseudo-barrier, the border between the $\mu = 1$ and $\mu = 3$ phases is determined by Equation 43 (see Figure 31). The topology maps changes again when the switch is shifted to r (see Figure 32). Together, these maps show how the position of the switch affects this

field coupling's effectiveness in producing not only a barrier-less reaction, but also in biasing the effective potential energy surface so that the desired outcome is energetically favoured (see Figure 33).

The non-smooth field coupling can compensate for the product's larger zero-point energy, that is a larger t value. We have shown that for equal zero-point energies, the attractor with the largest field coupling will be most stable (see section 4.2.2). At what point is this true for different zero-point energies? Suppose the field coupling over the reactant's attractor is $V_{12}(0) = A$ and the field coupling over the product's attractor is $V_{12} = B$. By taking E_{full} at the attractor geometries and expanding the root in Equation 28, we have the following conditional statements:

$$t > \frac{1}{2}kr^2 \Rightarrow E_{full}(r) < E_{full}(0) \Rightarrow B^2 > \left(t - \frac{1}{2}kr^2\right)\left(\frac{A^2}{\frac{1}{2}sr^2 + t} + \frac{1}{2}kr^2\right) \qquad \text{Equation 48}$$

$$t < \frac{1}{2}kr^2 \Rightarrow E_{full}(r) < E_{full}(0) \Rightarrow B^2 > \left(\frac{1}{2}kr^2 - t\right)\left(\frac{A^2}{\frac{1}{2}sr^2 + t} + t\right)$$

These complementary equations show that square of the field coupling over the product must be proportional to the difference between the potential energy curves at r (see also Figure 34). This can only work for non-smooth couplings which can bias the effective potential energy surface so that the minima will resemble the attractor configurations. Constant and discontinuous fields, however, will tend to produce minima in accordance with Equation 44, that is to say, the stable configurations will tend to be some average between the two attractors. (Note that the implicit assumptions for Equation 48 are that the field coupling V_{12} is continuous, positive and asymmetric.

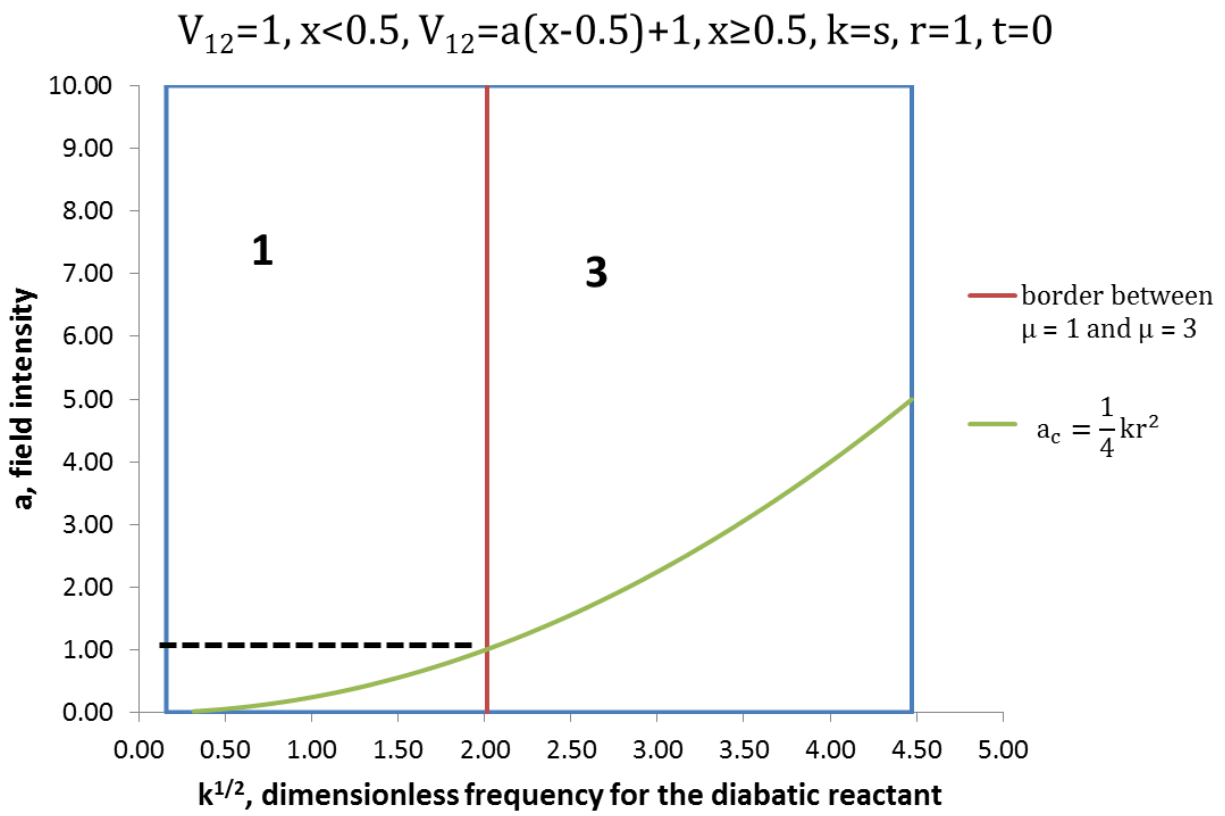

Figure 31. Borders between topological phases in (a,k) parameter space when using non-smooth coupling with switch at midway between diabatic attractors with equal zero-point energies

In Figure 31, when the non-smooth field coupling switches at the pseudo-barrier for the totally symmetric model, the border between the μ = 1 and μ = 3 phases is determined by the line corresponding to $a_c = \frac{1}{4}kr^2$, where $a_c = b_1$ and $a_1 = 0$ (see Equation 34.5). The barrier is suppressed for force constants below $b_1 = \frac{1}{4}kr^2$. The most stable configuration, however, resembles the product more than the configuration at the pseudo-barrier. For larger force constants, the barrier still exists, but the product is energetically favoured.

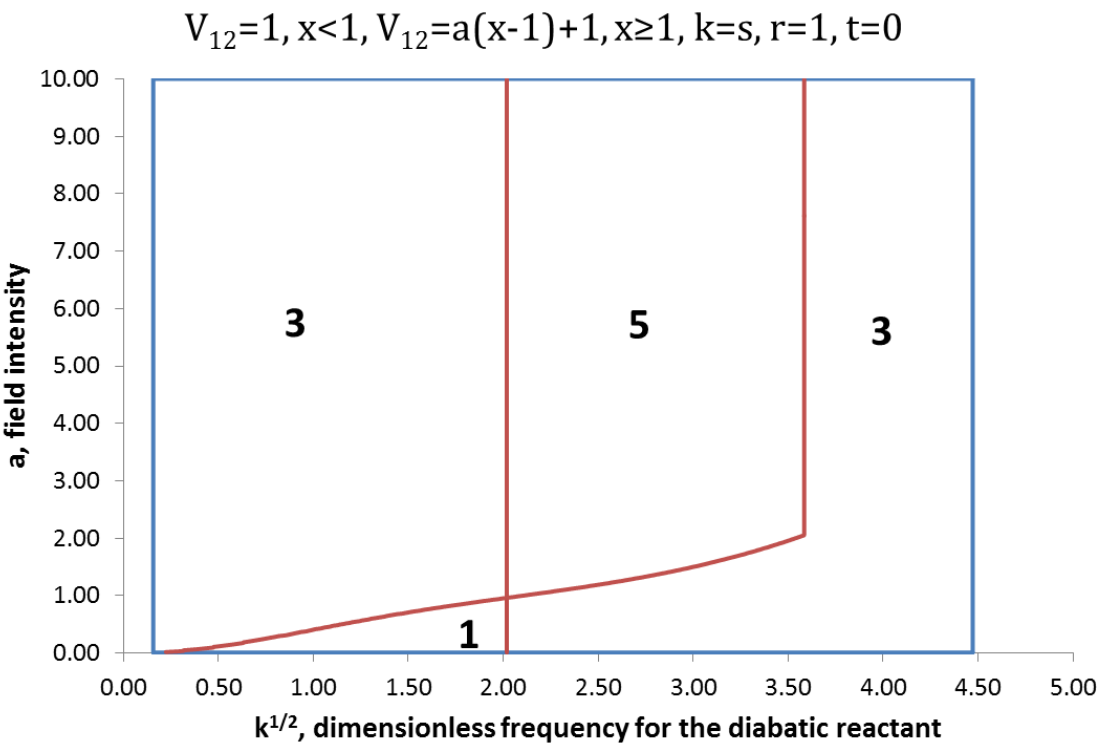

Figure 32. Borders between topological phases in (a,k) parameter space when using non-smooth coupling with switch at the position of the product attractor, x = r, for the case of equal zero-point energy, t = 0

In Figure 32, the borders between the μ = 3 and μ = 5 phases are defined by the same line giving the border between the μ = 1 and μ = 3 phases in Figure 31. As shown in Figure 20, increasing constant field will draw stable configurations together until there is a single stable configuration, that is μ = 1. Increasing the a-value of a linear field coupling, however, will push the stable configurations farther apart in nuclear configurational space (see Figure 25). Hence, we have a splitting of stable product configurations as a result of the switch coinciding with the product's attractor at x = r. The vertical part of the border between the regions defined by μ = 5 and μ =3 is a result of the constant section of the V_{12} function being too weak to cause any splitting. If V_{12}=a everywhere, the minimum around the product's attractor would not have shifted enough from x=r to be detectable. The diagonal section of the latter phase border is due to the fact that the coupling intensity, a, is too small to cause any splitting at the product's attractor. The μ = 1 topological region occurs when the linear section of the discontinuous V_{12} couplings has very low field intensity.

A

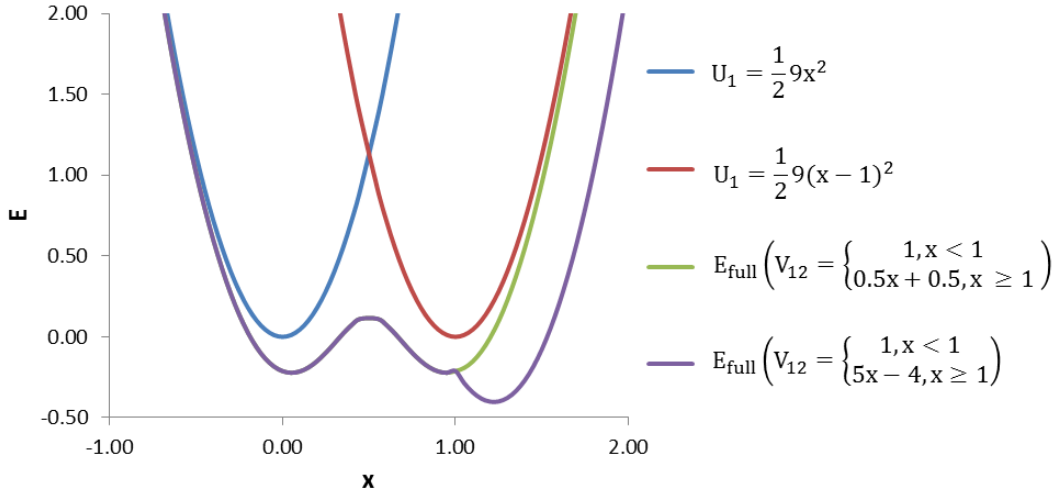

B

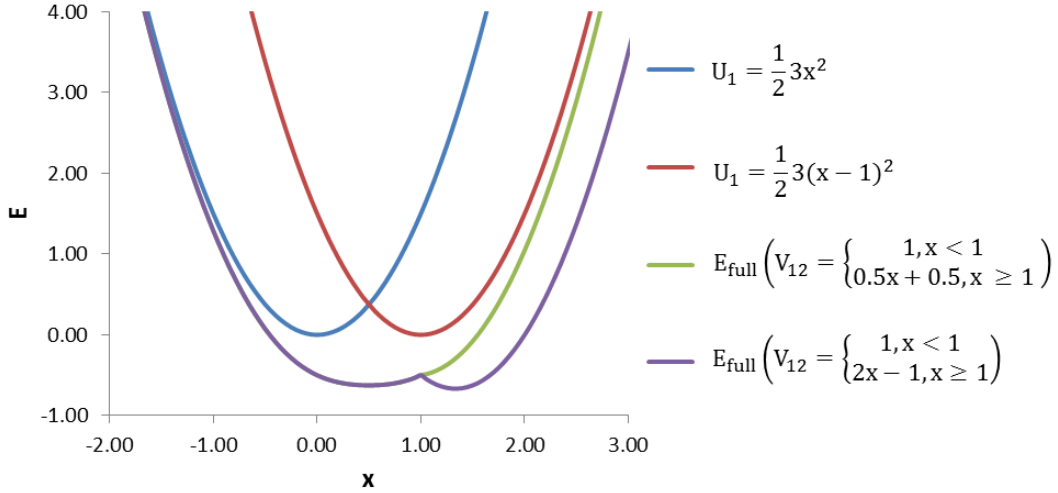

Figure 33. Examples of E_{full} for increasing intensity of non-smooth coupling with switch at the product's attractor, x = r, (r = 1)

The E_{full} produced with low field intensities resemble the E_{full} produced by a globally constant V_{12}. The majority of models with μ = 1 would have had the same topology if the V_{12} were globally constant. Increasing the field coupling intensity causes a splitting at the position of the switch, here at the product attractor. For models with larger force constants as shown in A, both a relaxed and compressed product configuration are energetically stable. For models with smaller force constants as shown in B, we observe a stable transition structure and a relaxed product configuration (x_{min} > r).

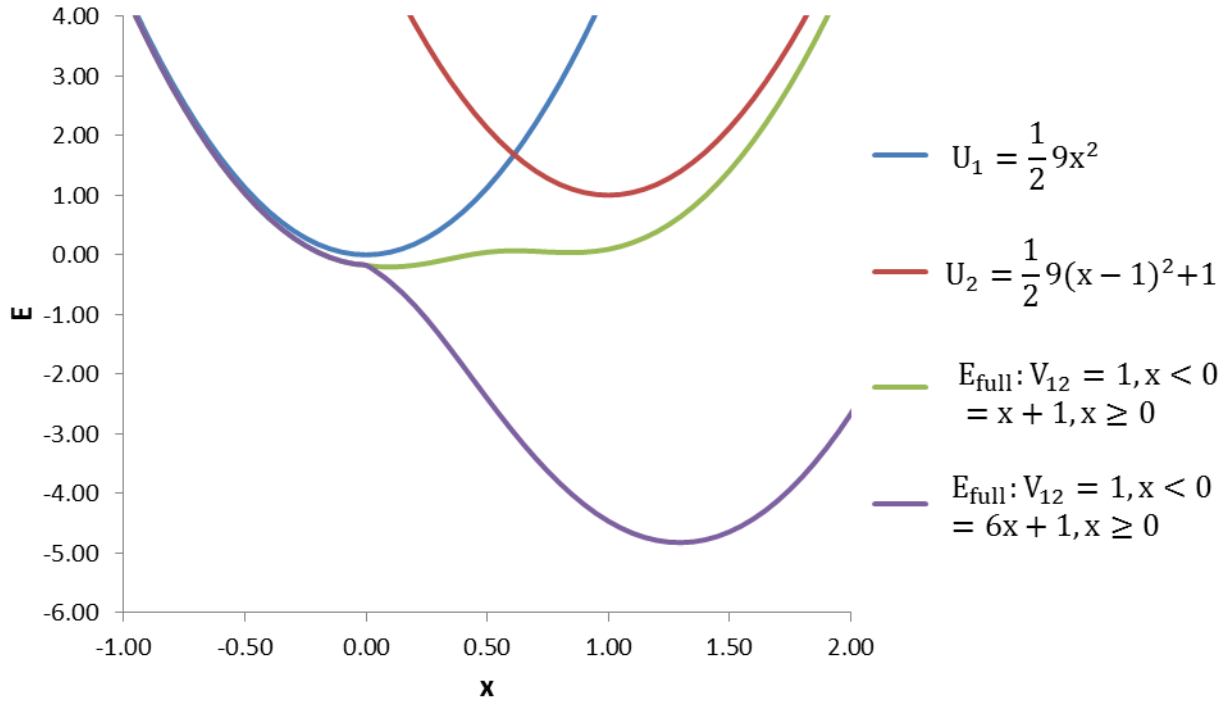

Figure 34. External field stabilization of an isomer whose diabatic attractor has a higher zero-point energy (here t = 1)

In Figure 34, we can observe use Equation 48 is as a guideline to determine the most stable attractor. For instance, we see that when a = 1, B = 2 and A = 1, we find $4 < 3.5(\frac{1}{5.5} + 1)$ thus product is not the most stable configuration. If the field intensity constant is increased to a = 6, however, the product is the most stable configuration, since B = 7 leads to $49 > 3.5(\frac{1}{5.5} + 1)$. Equation 48 only acts as a guide; it does not show which attractor the absolute minimum resembles more but which attractor geometry is more stable.

5. HBN ⇄ BNH isomerization: illustration of a fully quantum approach to using a two-state diabatic model

In the previous section, we mapped all possible potential energy curves, or E_{full}, generated in the presence of an external field for a manifold of two-state one-dimensional models of a chemical process. In this case, we have resorted to using two already built diabatic attractor potentials U_1 and U_2 modeled by simple semi-classical functions. Even though this approach is sufficient to illustrate general trends in external field effects and explore the central ideas in the GED methodology, in a fully quantum mechanical approach, these potential energy functions must be built from actual electronic diabatic functions. In this section, we show how to implement one such approach [8] using a simple isomerization process whose essential properties can be captured by a two-state system coupled in an external field. We consider the HBN ⇄ BNH isomerization (hydrogen boronitride to hydrogen boroisonitride) which involves radical species in their ground states. (As previously explained, the species need to be radicals in order to have the symmetry required to use a two-state model.) This problem has been studied in the literature using standard techniques [58] and will be presented here from the point of view of the GED approach.

5.1 Floating Gaussian orbitals

Each electronic structure is usually calculated as an optimized linear combination of basis functions; in the linear combination of atomic orbitals (LCAO) approach, these are centred on the nuclei. When atoms join to form molecules, however, the electron density is not necessarily centred on the nuclei. The same concern may be raised when a molecule is in an external field. By including polarization functions, that is, atomic orbitals with higher angular momenta, one may account for such deformations. Nevertheless, a normal basis set where atomic orbitals are centred on the nuclei will not produce a diabatic solution as these orbitals will "move" with the nuclei thereby changing the electronic function by default. As recently proposed in the literature, floating Gaussian orbitals provide a natural alternative.[8] Floating functions are centred at points in space, for example on a grid instead of at a nucleus. In other words, they provide a natural, partial decoupling between the models representing electronic and nuclear behaviours.

Over the last half century these orbitals have been used to calculate electric properties, optimize geometries and most recently for molecular dynamics.[59] More floating Gaussian orbitals may be added to a system to allow for shell separation. While these orbitals offer significant improvement, they are computationally demanding for near Hartree-Fock limits for electronic properties and energies.[60]

The quantum-mechanical implementation of the GED model uses an irregular grid of floating Gaussian orbitals.[8] Since they are not anchored on any nucleus, they provide a conceptually simple diabatization scheme. The same orbital grid must sustain all the diabatic electronic basis functions at the attractor geometries.[8,13] We may use a single grid to capture both electronic basis functions since neither species is asymptotically fragmented.[13] In other words, the optimal grid will give a minimum energy with respect to all orbitals and nuclei for all the attractors included in the model. (The grid is the same, but, of course, the floating orbitals will be combined in a different linear superposition for the reactant and product diabatic functions.) With regards to optimizing the orbital positions, the orbital symmetry should be the same as the nuclear framework corresponding to the attractors – it avoids spurious components of electronic properties.[8,60] This procedure has already been used to analyze a three-state, closed-shell isomerization.[8] In the following sections, we illustrate its implementation for a two-state system.

5.2 HBN ⇄ BNH radical isomerization

Optimizing a grid of floating Gaussian orbitals is a nonstandard, possibly lengthy process, because the available quantum mechanical computer codes are not designed to build, or use, truly diabatic basis functions. We are thus confronted with a molecular and electronic size limit for the practical and rapid computation of radical isomers. The peroxide (OOH) radical and the hydrogen boronitride (HBN) radical represent two of the smallest radical isomerization possibilities.[58,61] While both species have interesting industrial and environmental applications, we chose the hydrogen boronitride isomerization for the following practical reasons: i) it has fewer electrons thereby decreasing CPU calculation time, and ii) the isomerization is complementary to the semi-classical models discussed in section 4. The two species, HBN and BNH, have both different zero-point energies and different force constants.

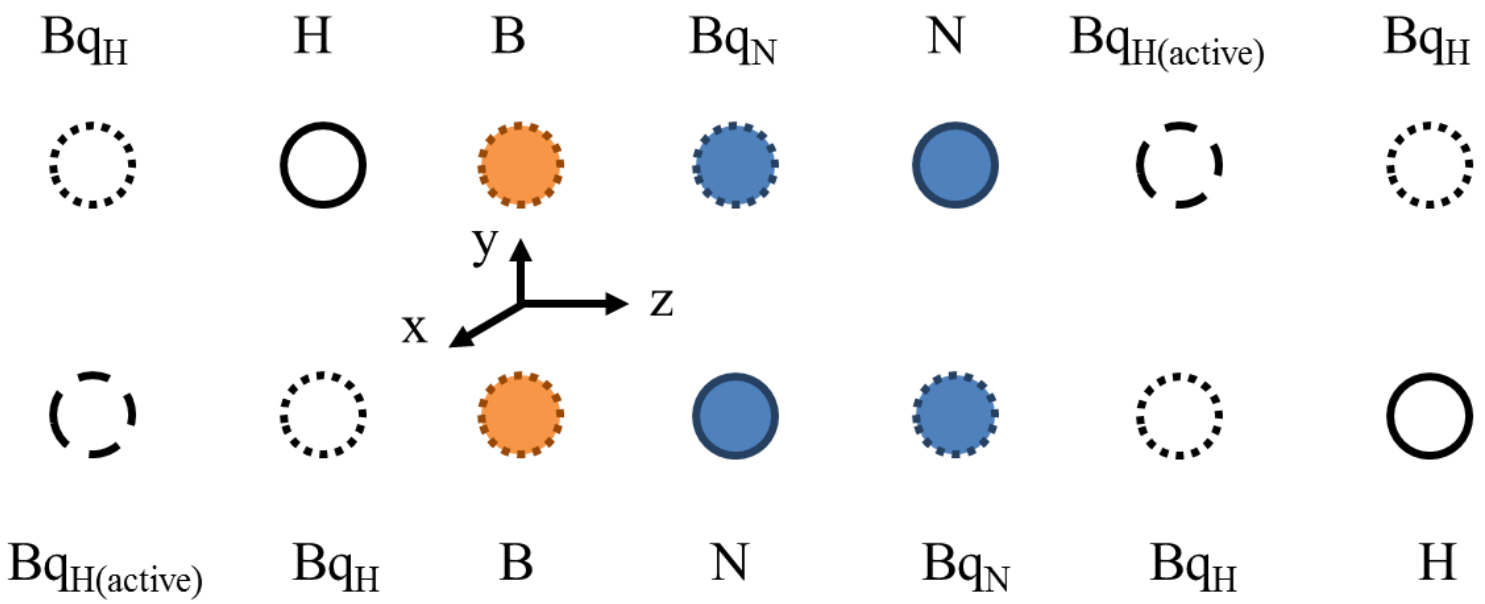

Figure 35. Linear grid for the location of the diabatic HBN and BNH attractors

In Figure 35, the nitrogen and hydrogen orbital positions along the z axis are freely optimized while the 'active' hydrogen-like ghost orbital is optimized manually. All other orbitals (dotted circles) are kept fixed. The boron atom is centred at (0.001Å; 0.0; 0.0). A degeneracy-breaking noise of 0.001Å in x and y alternates for each orbital, e.g. N, in BNH, is placed at (0.0; 0.001Å; z_N).

This system corresponds to a semi-classical model where $s \neq k$ and $t > 0$ (see Equation 29, Equation 31). The explicit construction of a grid allows us to explore different types of configurational paths and their effects on the E_{full} profile.

5.3 Creating optimal grids for the HBN ⇄ BNH isomerization

Optimizing the grid, building the diabatic potential energy curves, U_1 and U_2, and constructing the Fukui path were done using Gaussian 98.[62] In this program, floating Gaussian orbitals are also called 'ghost' orbitals and given the symbol Bq. They are not to be confused with 'dummy' atoms which are merely a point of reference to break the symmetry and no basis set is assigned to them.

For illustrative purposes, we use a linear grid (Figure 35) and the simpler 3-21+G and 6-31G basis sets to construct the electronic eigenfunctions for the HBN ⇄ BNH isomerization. (When larger basis sets are used for a grid with several floating Gaussian-type orbitals (GTOs), we often found difficulties in finding rapid convergence of self-consistent field (SCF) cycles)

The basis set's name shows how many Gaussian functions are assigned to a certain electron. In the 3-21+G basis set for example, the '3' means the orbital for a pair of core electrons is represented by a sum of 3 Gaussian functions. The dash indicates that valence electrons will be treated differently. Each valence electron is then assigned a sum with two Gaussian functions and another with one Gaussian function. A single '+' symbol shows that each atom that is not hydrogen or helium also has a single diffuse function. Two '+' indicate that all atoms have a diffuse function. The purpose of the diffuse function is to describe regions farther away from the nucleus with low, yet non-negligible, electron densities; this is achieved by using GTOs with smaller exponents. As explained below, the optimization of a fixed grid is a time consuming effort, even when using these simple basis sets. More complex basis sets may be necessary for more complex or nonlinear molecules, but there are preliminary indications that some of the corresponding calculations may exhibit convergence problems at the Hartree-Fock SCF level. Note that, even though the construction of the diabatic functions on a floating grid is time consuming, once built, they are not modified while building the diabatic potential energy

functions along desired configurational paths. The only dependence on the nuclear coordinates will be via the coefficients of the coherent superposition of diabatic basis functions.

5.3.1 Linear grid

Although both isomers are linear, the grids were built with small alternating noise in the directions orthogonal to the isomers' axis (refer to Table 1). The noise breaks the symmetry and lifts the degeneracy that occurred between the sixth and seventh eigenvalues for the α ("spin up") electrons which appeared to impede the convergence in some of the unrestricted Hartree-Fock (UHF) calculations.

The algorithm to create the grid is as follows: the initial geometries for the linear grid were taken by overlapping two grids of four orbitals, that is H-B-N-Bq and Bq-B-N-H where the boron orbitals coincide and the Bq corresponds to a 'ghost' orbital. Four orbitals, however, are not sufficient to describe the isomerization because the isomers have different BN bond lengths. Also, the optimal position for the ghost orbital, Bq, in one isomer is too different from the position of the hydrogen nucleus in the other. In order to accommodate the differences between the isomers, the number of orbitals in the grid is augmented to seven (refer to Figure 35). In this case, the atomic orbitals of one isomer become the ghost orbitals around the other isomer.

In our case, we choose to centre the boron nucleus on the location of the same floating orbital for the single grid that describes both isomers. (In other words, only for boron we find a grid orbital that coincides with always with a traditional atomic orbital.) In this way, the boron atom serves not only as a point of reference between the two isomers, but it also reduces the number of variational parameters. (The approach would be the same had the nitrogen been the reference orbital.) Upon finding a minimum energy configuration for an isomer, say HBN, we fix the positions of the hydrogen, nitrogen and the additional ghost orbitals needed to accommodate the other attractor, that is they are not "floated". These orbitals become in turn floating Gaussian orbitals when we switch to optimized BNH. The switching between isomers continues iteratively until the orbital positions on the grid converge to the stable positions for the respective isomer attractors (see Figure 35 for details in the structure of the grid).

5.3.2 Extended grids

A background classical charge without a nearby ghost orbital (loosely speaking, a ‘bare’ nucleus) greatly increases the electronuclear energy thereby artificially increasing the diabatic pseudo-barrier for the reaction. Since the linear grid has no floating orbitals along the minimum energy (Fukui) path, that is, a trajectory for the H nucleus off the HBN or BNH internuclear line, an exaggerated energy barrier is expected. In order to avoid this grid artifact, we first try a pair of off-linear floating Gaussian orbitals for the H nucleus. A pair is used, since there is an equal probability for the isomerization path from above and below the isomer’s axis (the z-axis, see Figure 36). Both off-linear orbitals are equally distanced for the isomer’s axis, forming a cross-shaped grid. We took the linear grid and kept the orbitals that remained ghost orbitals for both isomers fixed and optimized the position of the off-linear orbitals manually. The hydrogen and nitrogen orbitals were allowed to freely optimize along the z axis. A coarse scan for the off-linear orbitals in either isomer shows several minima, some of which seem to coincide for both isomers (see Figure 37). Absolute minima appear to fall in a region that requires a large number of SCF cycles, that is outside the region shown in Figure 37. Convergence within three decimal places for the orbital positions as achieved with the linear grid was not possible for any of the local minima. The position of the off-linear orbitals along the z axis would alternate between the isomers – which is perhaps unsurprising as neither isomer is symmetric along the z axis. In contrast with the linear grid, the cross grid had no floating orbital in the added dimension that related to the other isomer. In view of these considerations, a second pair of off-linear floating Gaussian orbitals was added.

In order to determine whether or not the act of simply adding another pair of off-linear orbitals would solve the lack of convergence to a single stable grid for both attractors, the same optimization procedure as the cross grid was used. Since convergence in the y-axis was achieved within 0.01 Å in the cross grid, this parameter was initially fixed in the new grid which we shall call the ‘line-box’ grid (Figure 38). The separation between the pairs of off-linear orbitals was initially fixed at 1.000Å and the y coordinate was set to ±1.000Å. For each isomer, the position of the box formed by the off-linear orbitals along the z axis was varied. Unfortunately, this procedure also does not produce a convergent optimization.

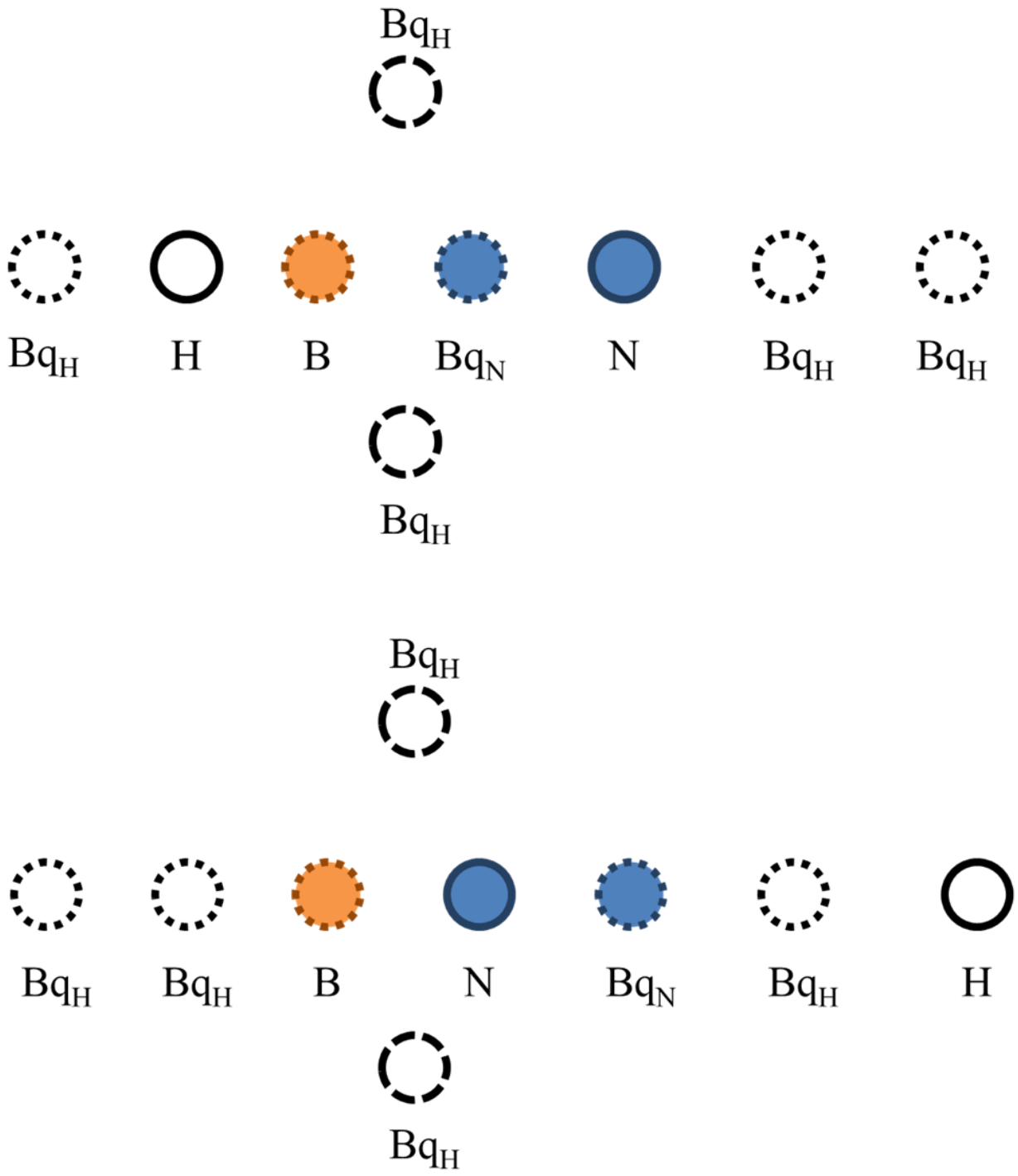

Figure 36. Cross grid for the location of the diabatic HBN and BNH attractors

The first adjustment to the linear grid was to add a pair of off-linear ghost orbitals in order to avoid artificially large reaction barriers for typical curved Fukui paths for the H nucleus. For this grid, the only active ghost orbitals are the off-linear ghost orbitals.

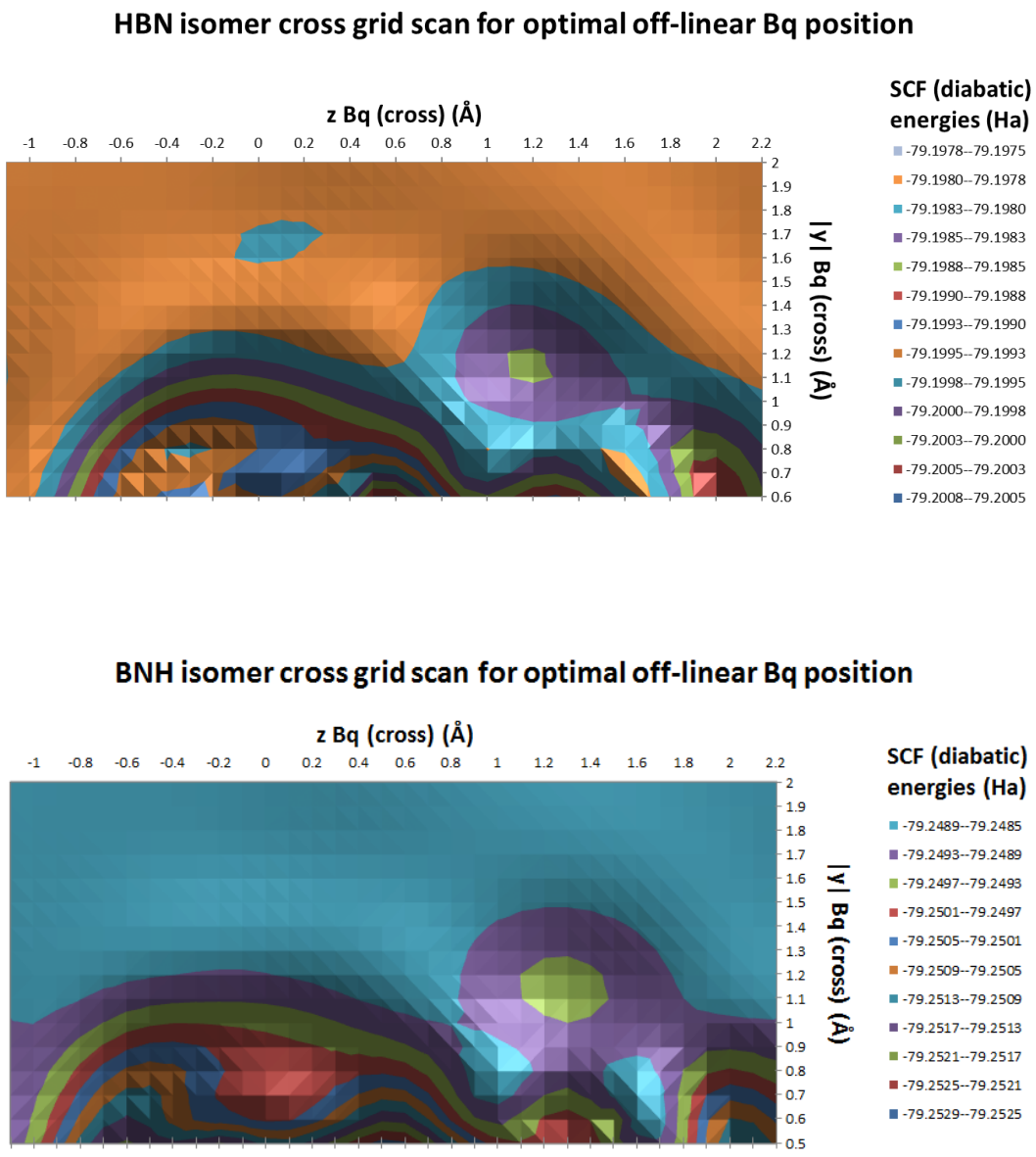

Figure 37. Cross grid coarse scans for optimal off-linear Bq position (see Figure 36)

In Figure 37, the initial scans for the optimal position of a single pair of off-linear ghost orbitals. No optimal geometry could be found for $|y| < 0.6$ Å as these geometries did not converge within the maximum number of SCF cycles given. It was conjectured that the off-linear orbitals would converge near the local minima shown here for HBN ([0.1; 1.7], [1.2; 1.1]) and for BNH ([0.0; 1.6], [1.4; 1.1]), but this did not occur. All grid position are in Å.

To completely discard the possibility that non-convergence was due to an insufficient number of variational parameters, we optimized the box's width and z coordinate. Convergence to within 0.001Å as in the linear grid was not achieved for either parameter. The convergence of the box's z coordinate, however, improved to be within 0.1Å, a factor 2 improvement on the previous optimization scheme's convergence limit. Nevertheless, this factor is too low to suggest that the convergence limit desired would be reached by simultaneously optimizing the box's width, height, and z coordinate. The lack of an anchoring set of floating Gaussian orbitals in the added dimension then appears as the cause of the non-convergence. A pair of off-linear floating Gaussian orbitals was then assigned to each isomer (Figure 38). The z coordinate and the absolute value of the y coordinate for the 'active' pair were finally optimized while the coordinates for the other pair remained fixed until the next isomer iteration.

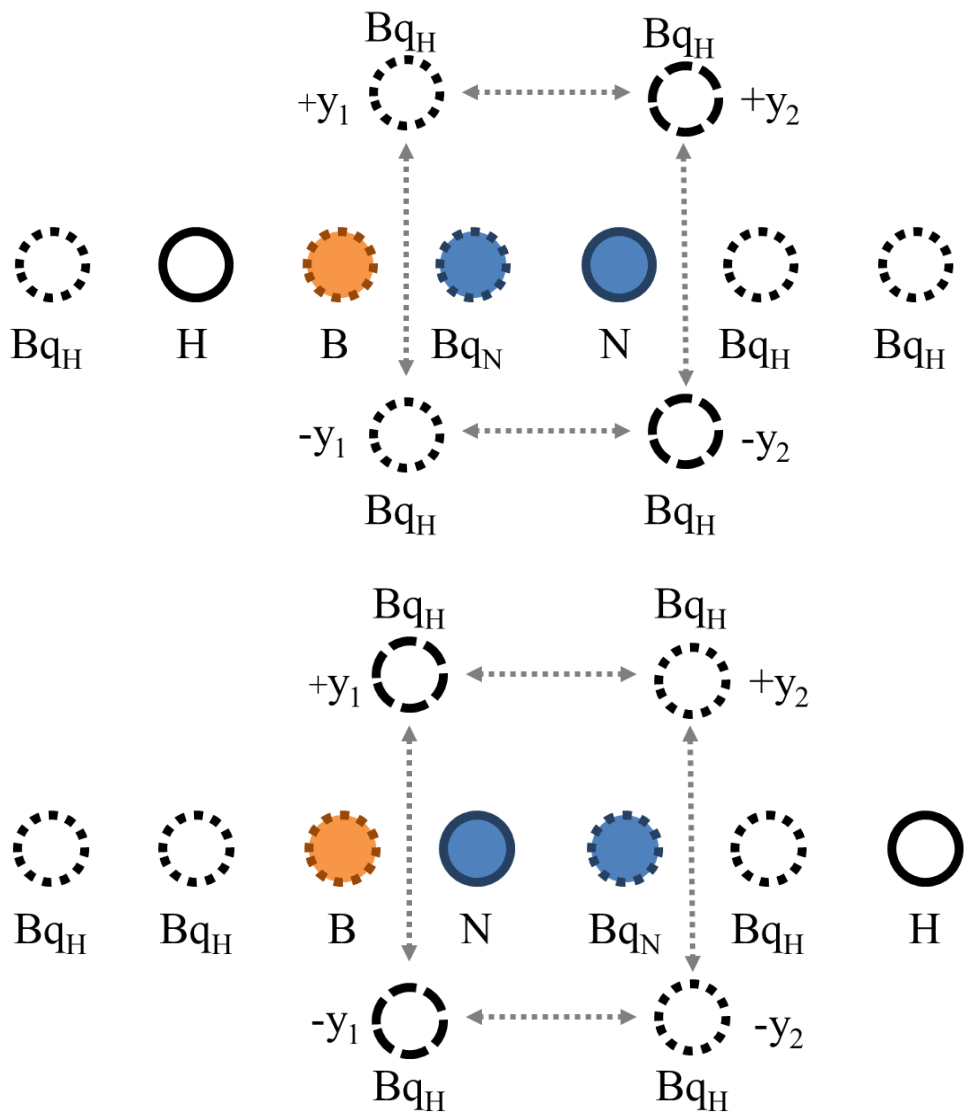

Figure 38. 'line-box' grid for the location of the diabatic HBN and BNH attractors

In Figure 38, the nitrogen and hydrogen positions in each isomer are allowed to freely optimize their z coordinate. Initially $y_1 = y_2$ and the width between the pairs of floating Gaussian orbitals is fixed. It was determined that the lack of an anchor in the second dimension hampered convergence. The off-linear Bq_H orbitals with orbitals $y = \pm y_2$ were assigned to HBN where they were manually optimized in that isomer's iteration. The $\pm y_1$ Bq_H orbitals which were assigned to BNH were manually optimized in the BNH iteration. All other ghost orbitals are kept fixed.

5.4 Mapping possible paths for the reactions coordinates

Three different tentative trajectories and their variations were used to create the uncoupled potential energy curves for the 'path' followed by the H-nucleus in the HBN ⇄ BNH isomerization. We used the largest smooth part of the Fukui path produced with the 3-21+G basis set. The Fukui trajectory was obtained by fixing the bond angle and letting the bond lengths freely optimize by using the standard Born-Oppenheimer adiabatic approach. (The BO approximation was only used for the sake of creating a reasonable "reaction path" to build the diabatic $\{U_i\}$ potential energy functions and then monitor the E_{full} function in an external field. The BO wave function was, of course, not used in the GED approach)

Following this procedure, a small jump discontinuity in the energy profile is observed when the HBN bond angle is between 151^o and 152^o. Similar and more frequent discontinuities were observed with the 6-31G basis set (see Figure 39). At higher angles, coefficients for orbitals along the x and y axes including the s orbitals are zero, while those along the z axis are non-zero. The reverse occurs at lower angles. It is significant that we do not observe similar discontinuities when the BNH bond angle is near 150^o. Since Li and co-workers found no discontinuity in the Fukui path observed when using a cc-pVQZ basis set [58], we may attribute such features to the size of basis set we use. In particular, this demonstrates the inability of our basis sets to properly capture the nature of the BH bond at non-equilibrium bond angles.

The Fukui path involves changing the BN bond length outside the range prescribed by the distance between the boron and nitrogen-like orbitals in the grid. Allowing the nitrogen nucleus to move along this path creates an unphysical barrier between the two attractors (see Figure 40). When the nitrogen nucleus is fixed on its starting orbital, however, or when its position is linearly interpolated between those for the two orbitals, the barrier disappears. This demonstrates that the exaggerated barrier is an artifact of the grid (Figure 40).

We also used an interpolating parabola on the yz plane through the transition structure as determined by the Fukui path transition structure as an initial geometry. The parabolic trajectory offers a natural extension outside the reaction coordinates so that we may observe that the attractor is indeed a minimum on the uncoupled diabatic potential energy surface. An unphysical

barrier was observed as the nitrogen moved along the Fukui path. An unphysical barrier was also observed when its trajectory was parabolically interpolated. This is not unexpected in a grid that is strongly biased for linear structures and thus not well adapted for a hydrogen path that significantly deviates from the line of grid orbitals.

The creation and analysis of the Gaussian input and output respectively, was done with a Fortran programme the author created. The code can be found in the appendix. The results that follow are presented only as an illustrative prototype of how to build the U_1 and U_2 diabatic curves quantum-mechanically with a grid of floating orbitals. A more accurate description of the HBN⇄BNH isomerization will certainly require a much denser (not quasi-linear) planar grid. The present grid is probably better adapted for a donor-acceptor reaction between radical species (for example D–H ⋯A ⇄ D ⋯ H–A).

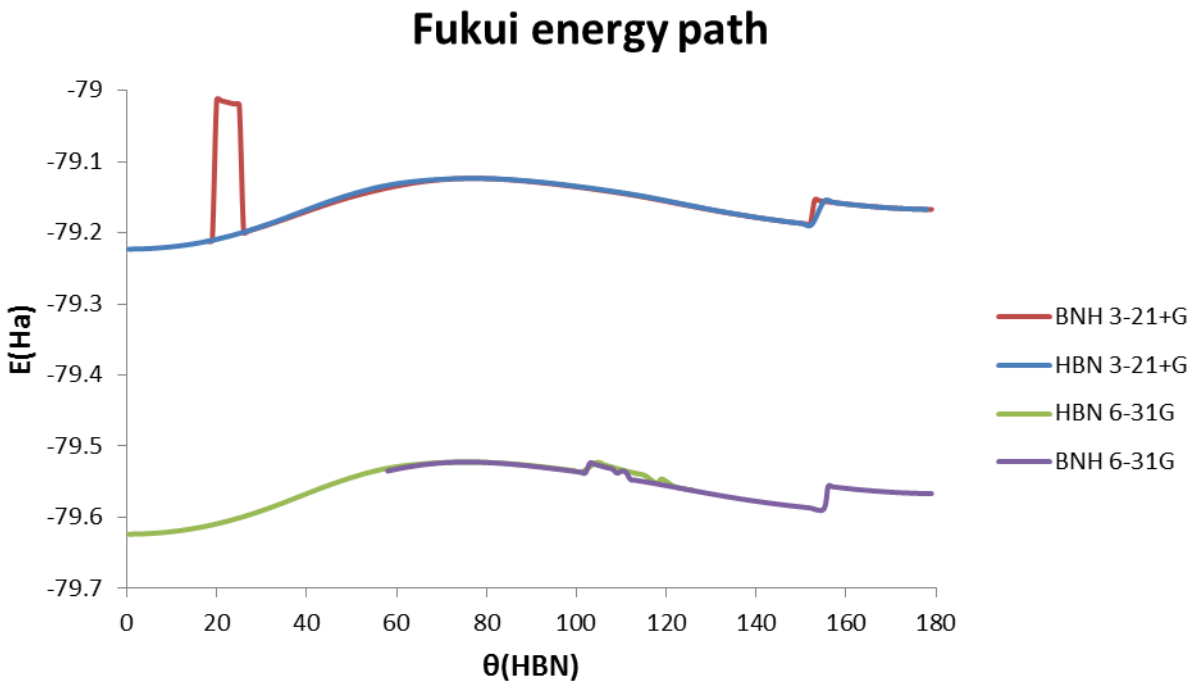

Figure 39. HBN ⇄ BNH Fukui path for the H transfer in terms of the HBN bond angle

The apparent discontinuities in the Fukui paths shown in Figure 39 are associated with a significant jump in the BN bond length. The fact that these features are not observed with a much larger basis set shows that the cause is likely the inability of the smaller basis sets to capture the electronic behaviour of the radical species in the BO approach.

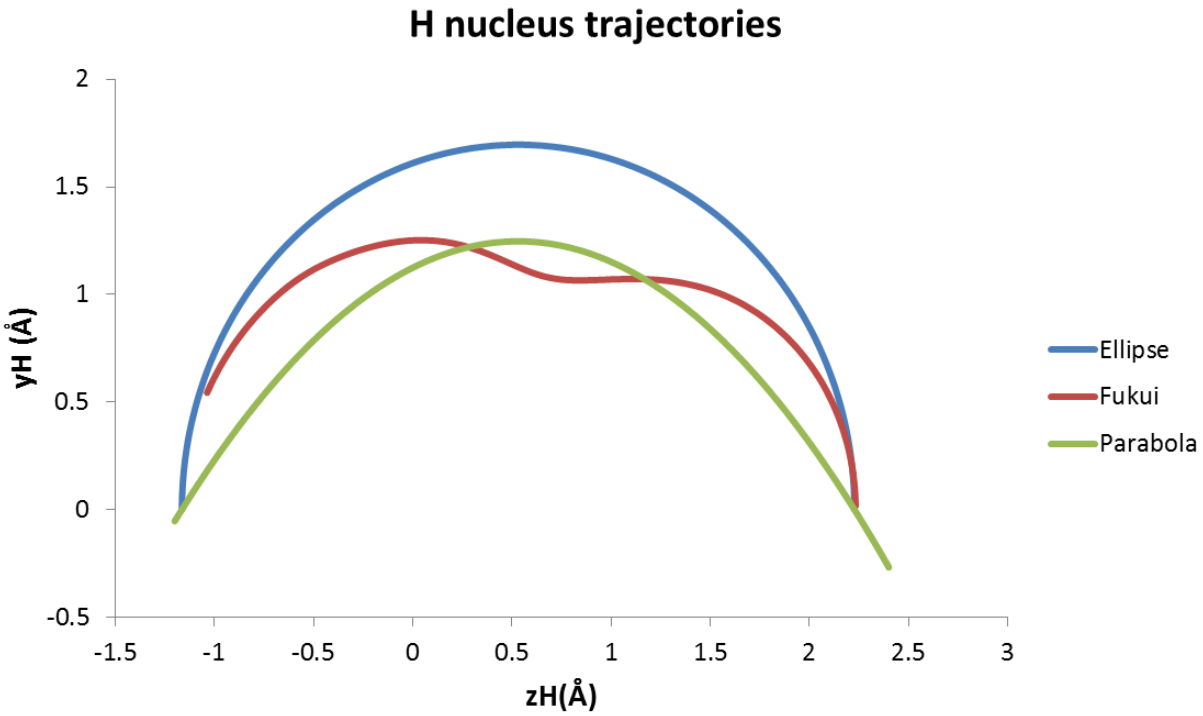

Figure 40. Tentative hydrogen nucleus paths on the yz plane to build the diabatic $\{U_i\}$ potential energy functions

The hydrogen nucleus follows the trajectories in Figure 40 for 3-21+G linear grid (see Figure 35) on a plane perpendicular to the internuclear x axis for HBN and BNH. For the HBN and BNH attractors, the hydrogen nucleus will move on the planes described by x=0.001Å and x=0.000 respectively. The Fukui path remains the same for all grids. The parabolic and circular trajectories are slightly modified for the other grids: so, the nucleus passes through the appropriate ghost orbital when it lands (approximately) on the z axis.

6. Results and discussion: fully quantum two-state model using grid-based diabatic electronic functions

6.1 HBN ⇄ BNH isomerization optimal grids

The optimal 3-21+G linear grid was confirmed within five isomer optimizations, whereas the optimal 6-31G linear grid was achieved in six. Qualitatively, the manually optimized ghost orbitals occupy the same positions with respect to the other orbitals in the grid. This suggests the grid's structure is moderately invariant with respect to the basis set used.

Table 1. Optimal linear grid geometries (all positions in Å)

	3-21+G			6-31G
orbital	X	Y	Z	Z
H	0.000	0.001	-1.1636	-1.1597
B	0.001	0.000	0.0000	0.0000
N	0.001	0.000	1.2603	1.2445
Bq_H	0.001	0.000	-1.206	-1.213
Bq_H	0.000	0.001	1.719	1.581
Bq_H *	0.001	0.000	2.2266	2.2099
Bq_N *	0.000	0.001	1.2440	1.2309

* These orbitals become H and N for the BNH geometry.

The largest difference between the two linear grids is the position of the H-like ghost orbital situated between the N and H in the BNH isomer.

Convergence for the off-linear Bq orbital positions in the line-box was achieved within six isomer optimizations. The grid is only partially optimized since the atomic orbitals on the line

have shifted but the Bq orbitals have not. The largest shift occurs with the H and N orbitals for the BNH isomer.

Table 2. Optimal ‘line-box’ grid geometry for the 3-21G basis set (all positions in Å)

Orbital	X	Y	Z
H	0.000	0.001	-1.1637
B	0.001	0.000	0.000
N	0.001	0.000	1.2601
Bq_H	0.001	0.000	-1.206
Bq_H	0.000	0.001	1.719
Bq_H*	0.001	0.000	2.2281
Bq_N*	0.000	0.001	1.2452
Bq_H**	0.000	1.652	0.144
Bq_H**	0.000	-1.652	0.144
Bq_H	0.000	1.142	1.177
Bq_H	0.000	-1.142	1.177

*These orbitals become H and N for the BNH isomer.

**During the ‘anchored geometry’ optimization process, these orbitals are fixed in the HBN geometry.

The difference in energy between the 3-21+G linear grid and the augmented ‘line-box’ grid is insignificant compared to the difference between the 3-21+G linear grid and the 6-31G linear grid (see Figure 41). The average differences with the 3-21+G linear grid and the ‘line-box’ grid are 0.0051 Ha and -0.0021 Ha for the HBN and BNH trajectories, respectively. With the 6-31G linear grid, the average differences are -0.37 Ha and -0.37 Ha. The ‘line-box’ grid’s diabatic

curves are only slightly lower in energy than the linear grid's diabatic curves for intermediate hydrogen nucleus positions [0.74Å; 1.90Å]. Since the purpose of the off-linear orbitals was to reduce the energy barrier caused by a completely bare hydrogen nucleus, this effect was expected. The energy reduction, however, is not significant enough to justify the additional computations necessary to fully optimize the off-linear orbital positions. Of course, since the atomic orbitals on the line changed position during the 'line-box' optimization, it is possible that the positions for the ghost orbitals that remained invariant in the grid were no longer optimal. With this consideration, the energetic gains to be had by a 'line-box' grid may perhaps be greater if these orbitals are eventually re-optimized as well.

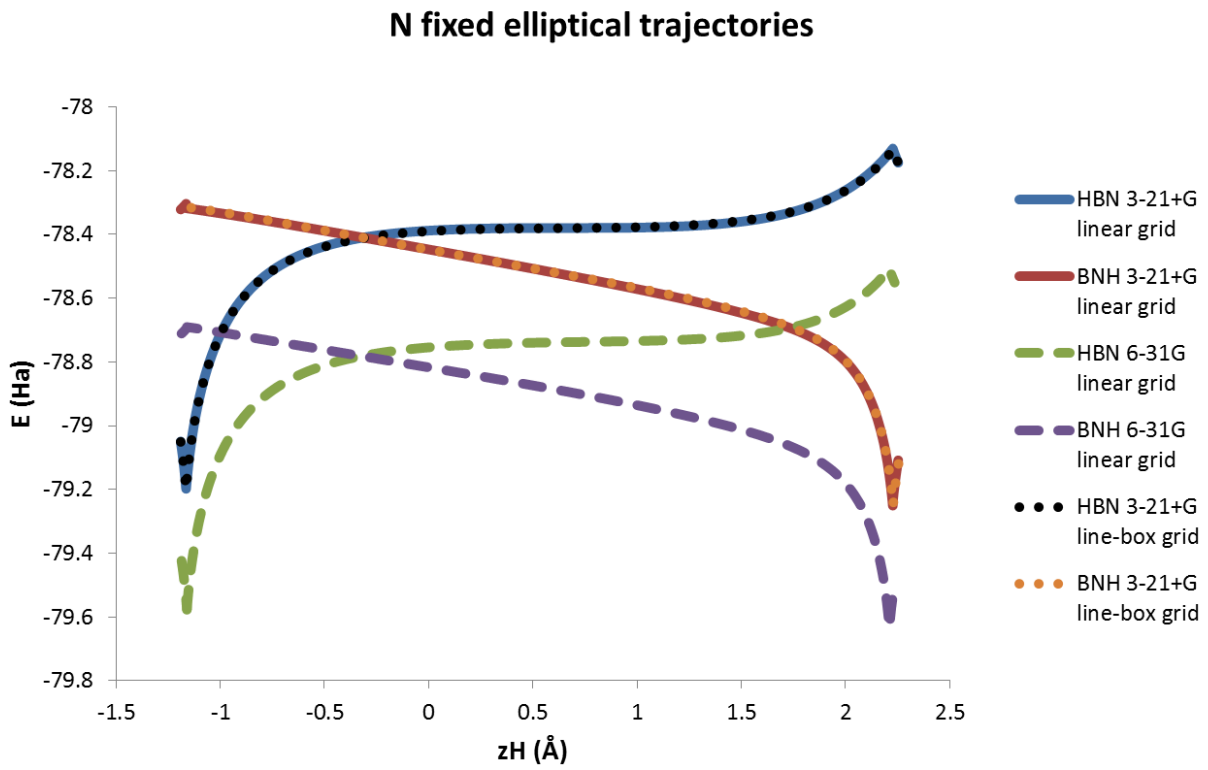

Figure 41. Diabatic potential for elliptical H-paths with N fixed

In Figure 41, where the nitrogen nucleus is fixed, a larger basis set given by 6-31G is more effective in lowering the potential energy curves than a partially optimized augmented grid. There is no significant difference between the 3-21+G linear and 'line-box' grids, indicating that the positions of the ghost orbitals in the line should have been re-optimized. Note that only the main branch of the diabatic attractors' potential energy curves is given. For $z < z_H$ (HBN) and $z > z_H$ (BNH) the curves increase rapidly, thereby completing the form of the reactant and product attractors. The resulting $\{U_i(z_H)\}$ functions are clearly anharmonic.

Table 3. Optimized nuclear configurations: comparison between the small basis set calculation with the BO approach and the present GED grid calculations. (The bottom entry corresponds to the "exact" results obtained with a post-Hartree-Fock complete-active-space calculation with a large basis set.[58])

	isomer	z_H (Å)	z_N (Å)
BO 3-21+G	HBN	-1.1582	1.2537
	BNH	2.2327	1.2471
BO 6-31G	HBN	-1.1565	1.2447
	BNH	2.2172	1.2378
Linear 3-21+G	HBN	-1.1636	1.2603
	BNH	2.2266	1.2440
Linear 6-31G	HBN	-1.1597	1.2445
	BNH	2.2099	1.2309
'line-box' 3-21+G	HBN	-1.1637	1.2601
	BNH	2.2281	1.2452
CASPT2/cc-PVQZ*	HBN	-1.1702	1.3128
	BNH	2.2304	1.2390

*from Ref. [58]

The boron is kept at $z_B = 0$ for each geometry optimization

The most significant difference observed is that between any of the present HBN geometries and the HBN geometry obtained by Li and co-workers.[58] We attribute this large difference to the different basis sets used. While the HBN geometry for the 6-31G basis set agrees with its BO homologue to within a few mÅ, the bond lengths in the BNH attractor are compressed. In fact, it

appears as though all of the grids have the same compressing effect upon the BNH attractor geometry. The HBN geometries in the 3-21+G grids are more relaxed compared to the equivalent BO geometry. Qualitatively, however, the present grid provides a reasonable description of both attractors.

6.2 Diabatic potentials for HBN and BNH using different paths for the H transfer

From Figure 42, we can see that following a parabolic or a Fukui path produces diabatic potential energy curves, U_1 and U_2, that seemingly contradict the notion of a single pair of attractors. There are several possible reasons for this odd behaviour. The BO transition structure has a much larger BN bond length than that in either attractor, thus for intermediate z_H values, the nitrogen nuclear charge does not coincide with either of the two Bq_N in all of our grids. A 'bare' nitrogen nucleus (with charge q = 7) will artificially raise the potential energy for those configurations thereby creating unphysical reaction barriers. On the HBN diabatic potential energy surface, U_1, both the hydrogen and nitrogen nuclei are no longer bare when in the BNH configurations, thus producing a minimum for the Fukui and parabolic trajectories. We should also be mindful that the calculated Fukui paths also depend on the basis set used. Indeed, if we look at the BN bond length in the transition structure Li and co-workers calculated at the CASPT2/cc-PVQZ level, it is between the BN bond lengths for their optimized BNH and HBN geometries. Apart from emphasizing our basis sets' inability to properly describe the BN bond, this comparison justifies dropping these trajectories for the nitrogen nucleus in favour of a linear interpolation between their positions at the respective attractor geometries. In order to correct the artificially high potential energies at intermediate z_H values, one could use a larger basis set, include polarization functions or add another nitrogen-like ghost orbital to the grid.

Although the diabatic crossing for trajectories where N is linearly interpolated occurs at larger z_H, all types of trajectories appear to coincide at the crossing point (see Figure 43). For the N fixed trajectories, the crossing point occurs at much lower z_H decreasing in the following order for the paths: parabolic > Fukui > circular. The linearly interpolated nitrogen trajectories give an HBN bond angle of approximately 78^o at the crossing point. The HBN angle increases to about

102^{o} when the nitrogen nucleus is kept fixed. This angle defines the pseudo-barrier in our semi-classical models, thus for a globally low intensity in the V_{12} field coupling, the angle at this point approximates a transition structure geometry. The linearly interpolated nitrogen trajectories produce a pseudo-transition structure closer to that given by Li et co-workers, with θ(HBN) of 85.9^{o}. Intriguingly, although the circular trajectory for the hydrogen nucleus does not resemble the Fukui trajectory, they are quite similar when comparing the diabatic potential energy curves, more so when the nitrogen nucleus is linearly interpolated. A circular or elliptical path in the yz plane between the reactant and product attractors may be a better approximation for the Fukui path than a path given by a regression polynomial interpolated through a transition structure. This may perhaps be generally true for 2-state reactions, but we do not expect the same approximation to be valid for reaction requiring more states, for example a non-radical isomerization. In fact, small differences between the diabatic potentials along different trajectories remain, but they are greatly reduced since moving the nitrogen nucleus clearly has a much greater effect on the diabatic potential energy curves than the smaller charge of the hydrogen nucleus (q = 1). A similar effect was already observed by Arteca and Tapia when using the GED approach for the umbrella transition in NH_3.[8] Together, these observations highlight the crucial role of the N nucleus' position in the energetics of the isomerization. For reactions in general, our observations underline the greater importance in having floating Gaussian grid orbitals along the path of larger nuclei.

Table 4. Net isomerization enthalpies (energy differences between product and reactant attractors)

	$\Delta E_{HBN \rightleftarrows BNH}$ (mHa)
3-21+G BO	55.81
6-31G BO	56.94
3-21+G linear grid	52.77
3-21+G ‘line-box’ grid	51.02
6-31G linear grid	56.19
CASPT2//CASPT2*	35.27

* From ref. [58] (the ‘//’ symbol indicates that both the reactant and product geometries and energies are computed at the CASPT2 level)

All isomerization energies obtained from the grid attractors are lower than the corresponding BO UHF energy (1-9%), however, they are still much higher (40-60%) than the exact isomerization energies given by a CASPT2//CASPT2. This last point is not unexpected; it is a higher level of post Hartree-Fock theory which takes the contribution of higher energy states into account whereas our present analysis does not.

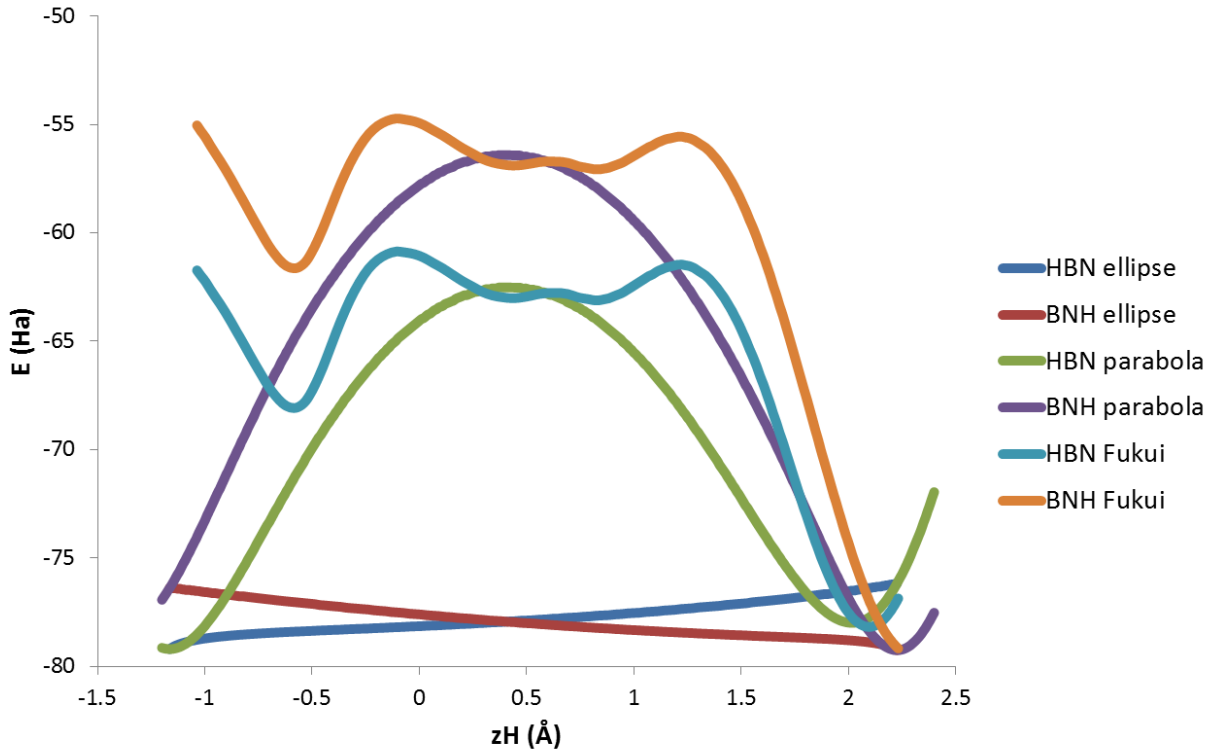

Figure 42. Effect of Fukui and parabolic interpolation H-paths on the diabatic potential energy curves $\{U_i\}$

In Figure 42, the N nucleus is interpolated linearly between the two attractors for the circular path. For the parabolic trajectory, z_N is parabolically interpolated through the transition structure. The nitrogen nucleus follows its Fukui trajectory as the hydrogen nuclear charge follows its Fukui trajectory. If the N nucleus is moved according to the 3-21G Fukui path, the diabatic crossing occurs very near a BNH geometry at $z_H \sim 2.1$Å instead of a more intermediate value between the BNH and HBN z coordinates for H. Also, the diabatic curves reach much larger energies after the crossing, than originally predicted. Note the occurrence of additional local minima when building $U_1(z_H)$ and $U_2(z_H)$ using 'trajectories' derived from the Fukui path. This behaviour is unacceptable in the context of the GED approach, thus indicating that the Fukui path can only be used in our case by substantially enlarging the off-linear components of an optimized grid of floating Gaussian functions. More acceptable $\{U_i\}$ functions are given in Figure 43.

A

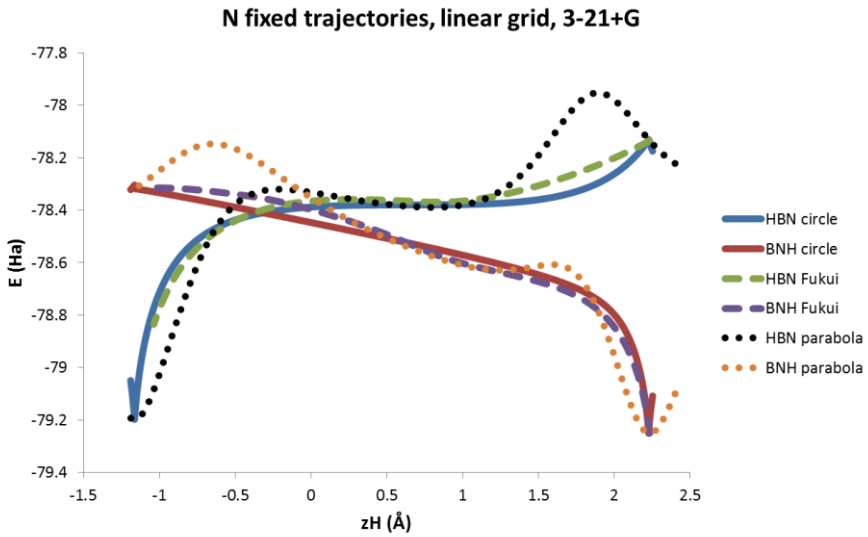

B

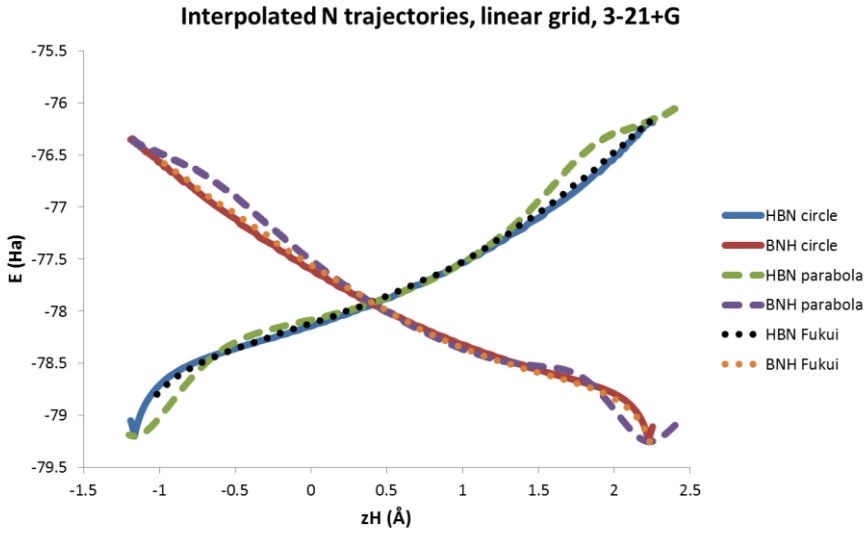

Figure 43. Diabatic potentials U_1 and U_2, built as functions of z_H for fixed and linearly interpolated N nuclear charge

In Figure 43, graph A, shallow minima appear in the potential energy curve $U_j(z_H)$ for the N fixed parabolic and Fukui trajectories. These features are contrary to the GED model and preclude the use of these functions. In contrast, graph B shows that these anomalies disappear when using the path that interpolates the N position between the two attractors. Accordingly, the $\{U_i\}$ functions in Figure 43 B are acceptable candidates for a strictly diabatic two-state model of the HBN ⇄ BNH radical isomerization.

Table 5. Comparing the energies for the reactant and product geometries when using the BO approximation and the optimized grids of floating Gaussian functions for diabatic basis functions

	HBN (mHa)	BNH (mHa)	HBN* (mHa)	BNH* (mHa)
3-21+G linear grid	-30.63	-27.58	-30.70	-27.60
3-21+G 'line-box' grid	-31.80	-27.00	-31.88	-27.03
6-31G linear grid	-10.30	-9.54	-10.30	-9.62

*Compared to BO energies using the grid's atomic orbital coordinates

Each attractor is energetically lower than the corresponding BO UHF optimized geometries and the BO energies at the grid's atomic orbital coordinates. In the absence of any ghost orbital, the energies obtained by the GED and the BO approach will be the same at the attractor geometry. Here, we obtain lower attractor energies due to the additional floating Gaussian orbitals that make up the grid.

The diabatic potential energy curves for HBN and BNH shown in Figures 38-40 are the quantum mechanically derived forms of U_1 and U_2 discussed in section 4. In this case, $z_H = x$ from the semi-classical equations. As discussed previously, the $\{U_i(z_H)\}$ functions in Figure 43 B are the best representation consistent with the concepts of the GED model. One can now use the quantum diabatic basis functions with various V_{12} field couplings to produce effective potential energy curves, E_{full}, as shown in section 4.

7. Conclusion

We have investigated the effects of six different external field coupling potentials on two semi-classical two-state models. Our aim has been to describe and understand qualitatively the role of this external field in modulating the interconversion of two chemical species. We associate these species to two diabatic basis functions, and the quantum states of the reaction system appear as coherent superpositions of these functions coupled with an electric field. As a result, the chemical process emerges as a quantum transition with an associated effective potential energy function E_{full} whose topological properties, for example the number and type of critical points, can be affected by manipulating the shape and intensity of the applied field. By creating "phase diagrams" for the manifolds of models in terms of the critical point topology of the E_{full} potential energy function, we have observed the gradual and drastic changes that occur as model and coupling parameters are modified. We have performed a detailed numerical analysis over a large range of two-state models. Closed form solutions for the extrema on the effective potential energy surface E_{full} are only available for the simpler totally symmetric radical isomerization models and only for the simplest field couplings.

We find that, in general, as the field intensity constant 'a' increases globally, the effective reaction barrier in E_{full} disappears. For a given isomerization model, a constant V_{12} field coupling can eliminate the effective reaction barrier, however, the most stable nuclear configuration will be a transition structure. In order to stabilize one attractor-like geometry over another, we find that a well-placed Lorentzian or a non-smooth V_{12} is preferable.

Our analysis shows that the barrier for the two-state dissociation models is infinitely broad and the effective potential energy surface simply reaches the product's zero-point energy at infinite separation. In contrast, the reactant geometries are stabilized compared to the uncoupled reactant potential. Thus, to get an electronically exothermic dissociation, a non-smooth field coupling is the best choice. On the other hand, if we wish to maintain the barrier yet stabilize each attractor, a well-placed linear field coupling would work for both two-state reactions, the bond breaking and the isomerization processes. An inverse Lorentzian V_{12} function would also work for the

radical isomerization because the finite range of reaction coordinates involved no asymptotic attractors.

We have also used a quantum mechanical approach to compute the diabatic potential energy functions for the reactant and the product. To this end, we use grids of floating Gaussian orbitals, which are a conceptually simple and natural way to build the U_1 and U_2 functions. For reasons of symmetry in the electronic coordinate space, the simplest single-grid two-state model corresponds to a radical isomerization, in our case, the HBN to BNH interconversion. Our present work has demonstrated that grids of floating Gaussian orbitals must be completely re-optimized when using a different basis set or a different grid geometry. The resulting quantum diabatic potential energy curves, U_1 and U_2, are highly dependent on the paths taken by the nuclear charges. The larger charge displaced from its attractor position will have a greater effect on the potential energy than the smaller nuclear charge. The different basis sets and grid geometries had little effect on the overall shape of the diabatic potential curves. The grid produced with a larger basis set did, however, produce significantly lower diabatic potential energy curves for both HBN and BNH. We find that the best model for the quantum diabatic potential energy functions $\{U_i\}$ uses a simple geometric path for the H nucleus and interpolates among the optimized positions for the other nuclei in the respective attractors.

Immediate future work should investigate the effective potential energy curves produced by entangling the diabatic states for HBN and BNH in an external field. Alternate and competing reaction pathways should be included for a more complete description of a reaction system. We may extend the GED model to multi-state systems that include intermediate or excited states. In particular, the model should be tested with more systems where the Born-Oppenheimer approximation is known to be inadequate. In this endeavour, we should also consider how to model more complex external fields, especially for reactions such as enzyme catalysis where the geometry and charge distribution around the active site determine the outcome of the reaction. Finally, a crucial step in advancing a generalized diabatic model as a computationally efficient alternative to Born-Oppenheimer approximation techniques would be the complete automation of the grid optimization procedure.

Bibliography

1. Engel, T. and P. Reid (2006) Physical Chemistry. (chap.27) Pearson Education Inc.: New York
2. Atkins, P. and J. de Paula (2006) Atkins' Physical Chemistry. 8th ed. (chap.11) Oxford U.P.: Oxford.
3. Butler, L.J. (1998) Annu. Rev. Phys. Chem. 49:125
4. Bandrauk A.D., E-W. S. Sedik, and C. Matta (2006) Mol. Phys. 104:95
5. Arabi, A.A. and C.F. Matta (2011) Phys. Chem. Chem. Phys. 13:13738
6. Krems, R.V. (2005) Int. Rev. Phys. Chem. 24:99
7. Král, P., I. Thanopulos, and, M. Shapiro (2007) Rev. Mod. Phys. 79:53
8. Arteca, G.A. and O. Tapia (2011) Phys. Rev. A 84:012115
9. Arteca, G.A. and O. Tapia (2004) J. Math. Chem. 35:1
10. Arteca, G.A. and O. Tapia (2004) J. Math. Chem. 35:159
11. Arteca, G.A. and O. Tapia (2005) J. Math. Chem. 37:389
12. Arteca, G.A. and O. Tapia (2008) Int. J. Quantum Chem. 108:651
13. Arteca, G.A., J.M. Aulló, and O. Tapia (2012) J. Chem. Math. 50:949
14. Arteca, G.A., J.P. Rank, and O. Tapia (2008) Int. J. Quantum Chem. 108:1810
15. Arteca, G.A., L. Laverdure, and O. Tapia (2014) J. Math. Chem. 52:2395
16. Crespo, R., M.-C. Piqueras, J.M. Aulló and O. Tapia (2011) Int. J. Quantum Chem. 111:263
17. Cederbaum, L.S. (2013). J. Chem. Phys. 138:224110
18. Cederbaum, L.S. (2004). Born-Oppenheimer approximation and beyond. In W. Domcke, D.R. Yarkony, H. Köppel (Eds.), Conical Intersections: Electronic Structure, Dynamics & Spectroscopy. Advanced Series in Physical Chemistry. (p.3) World Scientific: Singapore
19. Born, M. and K. Huang (1954) Dynamical Theory of Crystal Lattices (chap. 14 and appendix 7) Clarendon Press, Oxford
20. Sutcliffe, B. T. and R.G. Woolley (2012) J. Chem. Phys. 137:22A544
21. Born, M. and J.R. Oppenheimer (1927) Annalen der Physik. 84:457, translated by S.M. Blinder
22. Levine, R.D., and R.B. Bernstein (1974) Molecular Dynamics. Oxford U.P.: New York

23. Allen, M.P. and D.J. Tildesley (1987) Computer Simulation of Liquids. Oxford U.P.:Oxford
24. Matsika, S. and P. Krause (2011) Annu. Rev. Phys. Chem. 62:621
25. Domcke, W. and D.R. Yarkony (2012) Annu. Rev. Phys. Chem. 63:325
26. Yarkony, D.R. (2004) Conical intersections: their description and consequences. In W. Domcke, D.R. Yarkony, H. Köppel (Eds.), Conical Intersections: Electronic Structure, Dynamics & Spectroscopy. Advanced Series in Physical Chemistry. (p.41) World Scientific
27. Zhang, P., K. Morokuma, and, A.M. Wodtke (2005) J. Chem. Phys. 122:014106
28. Mozhayskiy, V.A., D. Babikov, and A,I. Krylov, (2006) J. Chem. Phys. 124:224309
29. Thompson, T.C., G. Izmirlian Jr., S.J. Lemon, D.G. Truhlar, and, C.A. Mead (1985) J. Chem. Phys. 82:5597
30. Benkovic, S.J. and S. Hammes-Schiffer (2003) Science 301:1196
31. Daniel, R.M., R.V. Dunn, J.L. Finney, and, J.C. Smith (2003) Annu. Rev. Biophys. Biomol. Struct. 32:69
32. Watney, J.B., A.V. Soudackov, K.F. Wong, and, S. Hammes-Schiffer (2006) Chem. Phys Lett. 418:268
33. Yarkony, D.R. (2001) J. Phys. Chem. A 105:6277
34. Migani, A. and M. Olivucci (2004) Conical intersections and organic reaction mechanisms. In In W. Domcke, D.R. Yarkony, H. Köppel (Eds.), Conical Intersections: Electronic Structure, Dynamics & Spectroscopy. Advanced Series in Physical Chemistry. (p.271) World Scientific: Singapore
35. Worth, G.A. and L.S. Cederbaum (2004) Annu. Rev. Phys. Chem. 55:127
36. Jahn, H.A. and E. Teller (1937) Proc. R. Soc. Lond. A 161:220
37. Berry, M.V. (1984) Proc. R. Soc. Lond. A 392:45
38. Köppel, H. (2004) Diabatic representation: methods for the construction of diabatic electronic states. In W. Domcke, D.R. Yarkony, H. Köppel (Eds.), Conical Intersections: Electronic Structure, Dynamics & Spectroscopy. Advanced Series in Physical Chemistry. (p.175) World Scientific: Singapore
39. Matsunaga, N., and D.R. Yarkony (1998) Mol. Phys. 93:79
40. Atchity, G.J. and K. Ruedenberg (1997) Theor. Chem. Acc. 97:47
41. Nakamura, H. and D.G. Truhlar (2001) J. Chem. Phys. 115:10353

42. Sadygov, R.G. and D.R. Yarkony (1998) J. Chem. Phys. 109:20
43. Thiel, A. and H. Köppel (1999) J. Chem. Phys. 110:9371
44. Nakamura, H. and D.G. Truhlar (2003) J. Chem. Phys. 118:6816
45. Mead, C.A., and D.G. Truhlar (1982) J. Chem. Phys. 77:6090
46. Puri, S.P. (2011) Classical Electrodynamics. Alpha Science International Ltd.:Oxford
47. Abrol, R. and A. Kuppermann (2002) J. Chem. Phys. 116:1035
48. Yang, K.R., X. Xu, and, D.G. Truhlar (2013) Chem. Phys. Lett. 573:84
49. García, V.M., M. Reguero, R. Caballol and J.P. Malrieu (1997) Chem. Phys. Lett. 281:161
50. Granucci, G., M. Persico, and, G. Spighi (2012) J. Chem. Phys. 137:22A501
51. Stock, G. and M. Thoss (2004) Mixed quantum-classical description of the dynamics at conical intersections In W. Domcke, D.R. Yarkony, H. Köppel (Eds.), Conical Intersections: Electronic Structure, Dynamics & Spectroscopy. Advanced Series in Physical Chemistry. (p.619) World Scientific: Singapore
52. Tully, J.C. (2012) J. Chem. Phys. 137:22A301
53. Lemeshko, M., R.V. Krems, J.M. Doyle, and S. Kais (2013) Mol. Phys. 111:1648
54. Read, C.G., E.M.P. Steinmiller, and, K-S. Choi (2009) J. Am. Chem. Soc. 131:12040
55. Hu, J., M. Tanabe, J. Sato, K. Uosaki, and, K. Ikeda (2014) J. Am. Chem. Soc. 136:10299
56. Ahmad Zebari, A. A., M. Kolmer, and, J.S. Prauzner-Bechcicki (2013) Beilstein J. Nanotechnol. 4:927
57. Milnor, J. (1969) Morse Theory. Princeton U.P.: Princeton, New Jersey
58. Li, W-Z., J-B. Cheng, Q-Z. Li, B-A. Gong, and J-Z. Sun (2011) Int. J. Quantum Chem. 111:123
59. Perlt, E., M. Brüssel, and, B. Kirchner (2014) Phys. Chem. Chem. Phys. 16:6997
60. Helgaker, T. and J. Almlöf (1988) J. Chem. Phys. 89:4889
61. Perry, J.W., R. Dawes, A.F. Wagner, and D.L. Thompson (2013) J. Chem. Phys. 139:084319
62. Gaussian 98, Revision A.9, M. J. Frisch, G. W. Trucks, H. B. Schlegel, G. E. Scuseria, M. A. Robb, J. R. Cheeseman, V. G. Zakrzewski, J. A. Montgomery, Jr., R. E. Stratmann, J. C. Burant, S. Dapprich, J. M. Millam, A. D. Daniels, K. N. Kudin, M. C. Strain, O. Farkas, J. Tomasi, V. Barone, M. Cossi, R. Cammi, B. Mennucci, C. Pomelli, C. Adamo, S. Clifford, J. Ochterski, G. A. Petersson, P. Y. Ayala, Q. Cui, K. Morokuma, D. K. Malick, A. D. Rabuck,

K. Raghavachari, J. B. Foresman, J. Cioslowski, J. V. Ortiz, A. G. Baboul, B. B. Stefanov, G. Liu, A. Liashenko, P. Piskorz, I. Komaromi, R. Gomperts, R. L. Martin, D. J. Fox, T. Keith, M. A. Al-Laham, C. Y. Peng, A. Nanayakkara, M. Challacombe, P. M. W. Gill, B. Johnson, W. Chen, M. W. Wong, J. L. Andres, C. Gonzalez, M. Head-Gordon, E. S. Replogle, and J. A. Pople, Gaussian, Inc., Pittsburgh PA, 1998

Appendix A

A1. Fortran code for the semi-classical models

```
C234567890123456789012345678901234567890123456789012345678901234567890123456789012
C This programme gives as output: potential energy curves, topology
C maps, map borders and the surfaces of parameter space

      character*30 output
      implicit real*8 (a-h,o-z)
      dimension Ef(1100,5),type(52000,19),surf(102,102)
      dimension imat(2,8),bor(1,20)

C matrix type for the topologies reduces size of output
C & makes formatting in Excel easier

      ai=0.d0
      na=0
      da=0.d0
      bi=0.d0
      nb=0
      db=0.d0
      ci=0.d0
      nc=0
      dc=0.d0
      c2i=0.d0
      nc2=0
      dc2=0.d0
      gi=0.d0
      ng=0
      dg=0.d0
      si=0.d0
      ns=0
      ds=0.d0
      ti=0.d0
      nt=0
      dt=0.d0
      ri=0.d0
      nr=0
      dr=0.d0
      xi=0.d0
      nx=0
      dx=0.d0
      pg=1.d0
      ins10=3
      par=0.d0

      write(6,*)'Give output file.'
      read(5,*)output
      open(20,file=output,status='unknown')

300   write(6,*)'1.Ecurves 2.types 3.surfaces 4.borders'
```

```
      read(5,*)ins1
      if((ins1.LT.1).OR.(ins1.GT.4))GO TO 300

      if(ins1.EQ.3)then
310   write(6,*)'1.k vs t 2.k vs s 3.k vs r *only 100 steps'
      read(5,*)ins2
      if((ins2.LT.1).OR.(ins2.GT.3))GO TO 310
      endif

      if(ins1.EQ.4)then
320   write(6,*)'1.top&bottom 2.top 3.bottom 4.neither'
      read(5,*)ins3
      DO i=1,2
      DO j=1,6
      imat(i,j)=0
      ENDDO
      ENDDO
      if((ins3.LT.1).OR.(ins3.GT.4))GO TO 320
      endif

      if(ins1.NE.3)then

330   write(6,*)'V12= 1.a 2.ax+b 3.a(x+c)^2/(b+(x+c)^2)'
      write(6,*)'4.a/(1+b(x+c)^2) 5.x<x*,c1,x>=x*,c2 6.c_ax+b_c2'
      read(5,*)ins4
      if((ins4.LT.1).OR.(ins4.GT.6))GO TO 330

      if(ins4.EQ.1)then
400   write(6,*)'1.dE vs SQRTk 2.a vs SQRTk'
      read(5,*)ins9
      if((ins9.LT.1).OR.(ins9.GT.2))GO TO 400
      write(6,*)'Give initial V12, steps, increment.'
      read(5,*)ai,na,da

      else if(ins4.EQ.2)then
410   write(6,*)'1.dE vs SQRTk 2.a vs SQRTk 3.b vs SQRTk'
      read(5,*)ins9
      if((ins9.LT.1).OR.(ins9.GT.3))GO TO 410
      write(6,*)'Give initial a, steps, increment.'
      read(5,*)ai,na,da
      write(6,*)'Give initial b, steps, increment.'
      read(5,*)bi,nb,db

      else if((ins4.EQ.3).OR.(ins4.EQ.4))then
420   write(6,*)'1.dE vs SQRTk 2.a vs SQRTk 3.b vs SQRTk 4.c vs SQRTk'
      read(5,*)ins9
      if((ins9.LT.1).OR.(ins9.GT.4))GO TO 420
      write(6,*)'Give initial a, steps, increment.'
      read(5,*)ai,na,da
      write(6,*)'Give initial b, steps, increment.'
      read(5,*)bi,nb,db
      write(6,*)'Give initial c, steps, increment.'
      read(5,*)ci,nc,dc
```

```
      else if(ins4.EQ.5)then
430   write(6,*)'1.dE vs SQRTk 2.c1 vs SQRTk 3.c2 vs SQRTk 4.x* vs SQRTk'
      read(5,*)ins9
      if((ins9.LT.1).OR.(ins9.GT.4))GO TO 430
      write(6,*)'Give initial c1, steps, increment'
      read(5,*)ai,na,da
      write(6,*)'Give initial c2, steps, increment'
      read(5,*)bi,nb,db
      write(6,*)'Give initial x*, steps, increment'
      read(5,*)ci,nc,dc

      else if(ins4.EQ.6)then
440   write(6,*)'1.dE vs SQRTk 2.a vs SQRTk'
      write(6,*)'3.b vs SQRTk 4.c1 vs SQRTk 5.c2 vs SQRTk'
      read(5,*)ins9
      if((ins9.LT.1).OR.(ins9.GT.5))GO TO 440
            if(ins9.NE.1)then
450         write(6,*)'fix line int w/ 1.c1 2. c2 3. neither'
            read(5,*)ins10
            if((ins10.LT.1).OR.(ins10.GT.3))GO TO 450
            endif
      write(6,*)'Give initial c, steps, increment.'
      read(5,*)ci,nc,dc
      write(6,*)'Give initial a, steps, increment.'
      read(5,*)ai,na,da
            if(ins10.NE.3)then
            write(6,*)'Give initial xint, steps, increment'
            else
            write(6,*)'Give initial b, steps, increment.'
            endif
      read(5,*)bi,nb,db
      write(6,*)'Give initial c2, steps, increment.'
      read(5,*)c2i,nc2,dc2

      endif
      endif

340   write(6,*)'U2= 1.t+s*e^-x 2.t+s(x-r)^-10'
      write(6,*)'3.t+s(x-r)^-12 4.t+s/2*(x-r)^2'
      read(5,*)ins5
      if((ins5.LT.1).OR.(ins5.GT.4))GO TO 340

      write(6,*)'Give initial k, steps, increment.'
      read(5,*)gi,ng,dg

      if(ins5.EQ.4)then
      write(6,*)'keep k = cs? 1.no 2.yes'
      read(5,*)ins8
      endif

      write(6,*)'Give initial s, steps, increment.'
      read(5,*)si,ns,ds
```

```
      write(6,*)'Give initial t, steps, increment.'
      read(5,*)ti,nt,dt

      if(ins5.NE.1)then
370   write(6,*)'Give initial r, steps. increment.'
      read(5,*)ri,nr,dr
      if((ins5.NE.4).AND.(ri.GT.0.d0))GO TO 370
      endif

      if(ins1.NE.3)then
      write(6,*)'Give initial x, steps, increment.'
      read(5,*)xi,nx,dx
      endif

      if(ins5.EQ.2)then
      ie=-10
      else if(ins5.EQ.3)then
      ie=-12
      else if(ins5.EQ.4)then
      ie=2
      endif

      index=0
      index1=0
      index2=0
      index3=0
      index4=0
      index5=0
      index6=0
      index7=0
      index8=0
      index9=0
      id1=-1
      oldg=0.d0

      DO i=1,102
      DO ii=1,102
      surf(i,ii)=0.d0
      ENDDO
      ENDDO

      DO i=1,52000
      DO ii=1,19
      type(i,ii)=0.d0
      ENDDO
      ENDDO

      DO 100 ja=1,na+1
      a=ai+(ja-1.d0)*da
      DO 110 jb=1,nb+1
      b=bi+(jb-1.d0)*db
      DO 120 jc=1,nc+1
      c=ci+(jc-1.d0)*dc
```

```
      DO 130 jc2=1,nc2+1
      c2=c2i+(jc2-1.d0)*dc2
      DO 140 jg=1,ng+1
      g=gi+(jg-1.d0)*dg
      if(ins8.EQ.2)then
      pg=g
      endif
      DO 150 js=1,ns+1
      s=pg*(si+(js-1.d0)*ds)
      DO 160 jt=1,nt+1
      t=ti+(jt-1.d0)*dt
      DO 170 jr=1,nr+1
      r=ri+(jr-1.d0)*dr

C call subroutines to determine diabatic curve crossing, energy barrier

      if((ins5.NE.1).AND.(ie.EQ.2).AND.(2*t.GT.g*r*r))GO TO 170
      if(ins1.NE.1)then
      if(ins5.EQ.1)then
      CALL DELTA(g,s,t,d3)
      else
      CALL DELTA2(g,s,t,r,ie,d3)
      endif
      endif

C call subroutines for Efull and topology analysis

      if(ins1.NE.3)then
      if(ins4.EQ.1)then
            if(ins5.EQ.1)then
            CALL GEN1(g,s,t,xi,nx,dx,a,Ef,id)
            else
            CALL GEN1b(g,s,t,r,ie,xi,nx,dx,a,Ef,id)
            endif
      else if(ins4.EQ.2)then
            if(ins5.EQ.1)then
            CALL GEN2(g,s,t,xi,nx,dx,a,b,Ef,id)
            else
            CALL GEN2b(g,s,t,r,ie,xi,nx,dx,a,b,Ef,id)
            endif
      else if(ins4.EQ.3)then
            if(ins5.EQ.1)then
            CALL GEN3(g,s,t,xi,nx,dx,a,b,c,Ef,id)
            else
            CALL GEN3b(g,s,t,r,ie,xi,nx,dx,a,b,c,Ef,id)
            endif
      else if(ins4.EQ.4)then
            if(ins5.EQ.1)then
            CALL GEN4(g,s,t,xi,nx,dx,a,b,c,Ef,id)
            else
            CALL GEN4b(g,s,t,r,ie,xi,nx,dx,a,b,c,Ef,id)
            endif
      else if(ins4.EQ.5)then
```

```
            if(ins5.EQ.1)then
            CALL GEN5(g,s,t,xi,nx,dx,a,b,c,Ef,id)
            else
            CALL GEN5b(g,s,t,r,ie,xi,nx,dx,a,b,c,Ef,id)
            endif
      else if(ins4.EQ.6)then
            if(ins5.EQ.1)then
            CALL GEN6(g,s,t,xi,nx,dx,c,a,b,c2,Ef,id,ins10)
            else
            CALL GEN6b(g,s,t,r,ie,xi,nx,dx,c,a,b,c2,Ef,id,ins10)
            endif
      endif
      endif

C defining topology map phase space 'x' vs SQRT(g)

      if(ins9.EQ.1)then
      par=d3
      else if(ins9.EQ.2)then
      par=a
      else if(ins9.EQ.3)then
      par=b
      else if(ins9.EQ.4)then
      par=c
      else if(ins9.EQ.5)then
      par=c2
      endif

      if(ins1.EQ.1)then
      write(20,600)g,s,t,r,a,b,c,c2
      write(20,610)((Ef(i,ii),ii=1,5),i=1,nx+1)
      GO TO 170
      endif

C Topology sort

      if(ins1.EQ.2)then
            if(id.EQ.1)then
            index1=index1+1
            type(index1,1)=dsqrt(g)
            type(index1,2)=par
            GO TO 170
            endif

            if(id.EQ.2)then
            index2=index2+1
            type(index2,3)=dsqrt(g)
            type(index2,4)=par
            GO TO 170
            endif

            if(id.EQ.3)then
            index3=index3+1
```

```
      type(index3,5)=dsqrt(g)
      type(index3,6)=par
      GO TO 170
      endif

      if(id.EQ.4)then
      index4=index4+1
      type(index4,7)=dsqrt(g)
      type(index4,8)=par
      GO TO 170
      endif

      if(id.EQ.5)then
      index5=index5+1
      type(index5,9)=dsqrt(g)
      type(index5,10)=par
      GO TO 170
      endif

      if(id.EQ.6)then
      index6=index6+1
      type(index6,11)=dsqrt(g)
      type(index6,12)=par
      GO TO 170
      endif

      if(id.EQ.7)then
      index7=index7+1
      type(index7,13)=dsqrt(g)
      type(index7,14)=par
      GO TO 170
      endif

      if(id.EQ.8)then
      index8=index8+1
      type(index8,15)=dsqrt(g)
      type(index8,16)=par
      GO TO 170
      endif

      if((id.GT.8).OR.(id.LT.1))then
      index9=index9+1
      type(index9,17)=dsqrt(g)
      type(index9,18)=par
      type(index9,19)=id
      GO TO 170
      endif
endif

if(ins1.EQ.3)then
surf(1,jg+1)=g
      if(ins2.EQ.1)then
      surf(jt+1,1)=t
```

```
            surf(jt+1,jg+1)=d3
            GO TO 170
            else if(ins2.EQ.2)then
            surf(js+1,1)=s
            surf(js+1,jg+1)=d3
            GO TO 170
            else
            surf(jr+1,1)=r
            surf(jr+1,jg+1)=d3
            GO TO 170
            endif
      endif

C defining phase borders in topology map

      if(ins1.EQ.4)then
      DO iu=1,20
      bor(1,iu)=0.d0
      ENDDO
      if((id.NE.id1).AND.((g.EQ.oldg).OR.(par.EQ.oldpar)))then
      ju=0
            DO iu=1,8
            ju=iu
            if((id1.EQ.imat(1,iu)).AND.(id.EQ.imat(2,iu)))then
            GO TO 350
            endif
            ENDDO

            DO iu=1,8
            ju=iu
            if((imat(1,iu).EQ.0).AND.(imat(2,iu).EQ.0))then
            imat(1,iu)=id1
            imat(2,iu)=id
            GO TO 350
            endif
            ENDDO

      ju=8
350   bor(1,2*ju-1)=dsqrt(g)
      bor(1,2*ju)=par


      if((jt.EQ.1).AND.(js.EQ.1).AND.(jr.EQ.1))then
            if((ins3.EQ.1).OR.((ins3.EQ.2).AND.(nt.NE.0))
     1      .OR.((ins3.EQ.3).AND.(nt.EQ.0)))then
            bor(1,17)=dsqrt(g)
            bor(1,18)=par
            endif
      else if((jt.EQ.nt+1).AND.(js.EQ.ns+1).AND.(jr.EQ.nr+1))then
            if((ins3.EQ.1).OR.((ins3.EQ.2).AND.(nt.EQ.0))
     1      .OR.((ins3.EQ.3).AND.(nt.NE.0)))then
            bor(1,19)=dsqrt(g)
            bor(1,20)=par
```

```
            endif
          endif
          write(20,620)(bor(1,ii),ii=1,20)
          endif
          endif

          oldg=g
          oldpar=par
          id1=id

170       CONTINUE
160       CONTINUE
150       CONTINUE
140       CONTINUE
130       CONTINUE
120       CONTINUE
110       CONTINUE
100       CONTINUE

          if(ins1.EQ.2)then
          it=max(index1,index2,index3,index4,index5,index6,index7,
         1  index8,index9)
          write(20,630)((type(i,ii),ii=1,19),i=1,it)
          endif

          if(ins1.EQ.3)then
          write(20,640)((surf(i,ii),ii=1,102),i=1,102)
          endif

600       FORMAT(8(F7.3,2x))
610       FORMAT(F7.3,2x,E16.10,2x,E16.10,2x,E16.10,2x,E16.10)
620       FORMAT(20(E16.10,2x))
630       FORMAT(18(E16.10,2x),I4)
640       FORMAT(102(E16.10,2x))

          close(20)
          end

C energy barrier for U2=t+s*exp(-x)

          SUBROUTINE DELTA(g,s,t,d3)
          implicit real*8 (a-h,o-z)

          d1=0.d0
          d2=0.d0
          x=0.d0

          DO 50 j=1,19
          ai=3.d0-j
          aj=10.d0**(ai)

          DO 60 k=1,10
          ak=k
```

```
      y=x+(ak-1.d0)*aj
      z=x+ak*aj
      u1=0.5d0*g*y*y
      v1=0.5d0*g*z*z
      u2=t+s*dexp(-y)
      v2=t+s*dexp(-z)

      d1=u2-u1

      if(d1.EQ.0.d0)then
      d3=u2-t
      GO TO 40
      endif

      d2=v2-v1

      if(d2.EQ.0.d0)then
      d3=v2-t
      GO TO 40
      endif

      if((d1*d2).LT.0.d0)then
            d3=u2-t
            x=y
            GO TO 50
      endif

60    CONTINUE
50    CONTINUE
40    RETURN
      end

C energy barrier for U2=t+s(x-r)^ie

      SUBROUTINE DELTA2(g,s,t,r,ie,d3)
      implicit real*8 (a-h,o-z)

      d1=0.d0
      d2=0.d0
      x=0.d0

      if(ie.EQ.2)GO TO 360

      DO 50 j=1,19
      ai=3.d0-j
      aj=10.d0**(ai)

      DO 60 k=1,10
      ak=k
      y=x+(ak-1.d0)*aj
      z=x+ak*aj
      u1=0.5d0*g*y*y
      v1=0.5d0*g*z*z
```

```
      u2=t+s*(y-r)**(ie)
      v2=t+s*(z-r)**(ie)

      d1=u2-u1

      if(d1.EQ.0.d0)then
      d3=u2-t
      GO TO 40
      endif

      d2=v2-v1

      if(d2.EQ.0.d0)then
      d3=v2-t
      GO TO 40
      endif

      if((d1*d2).LT.0.d0)then
            d3=u2-t
            x=y
            GO TO 50
      endif

60    CONTINUE
50    CONTINUE

360   if(ie.EQ.2)then
      rd=g*s*r*r+2.d0*g*t-2.d0*s*t
            if(dabs(s-g).GT.1.d-10)then
            xc=(s*r+dsqrt(rd))/(s-g)
                  if((xc.LT.0.d0).OR.(xc.GT.r))then
                  xc=(s*r-dsqrt(rd))/(s-g)
                  endif
            else
            xc=(s*r*r+2*t)/(2*s*r)
            endif
      d3=0.5d0*g*xc*xc-t
      endif

40    RETURN
      end

C Constant V12, U2=t+s*exp(-x)

      SUBROUTINE GEN1(g,s,t,xi,nx,dx,a,Ef,id)
      implicit real*8 (a-h,o-z)
      dimension Ef(1100,5)

      islope=0
      last=0
      V12=a
      id=0
      int=0
```

```
      xj=xi

      DO 20 i=1,1100
      DO 30 j=1,5
      Ef(i,j)=0.d0
30    CONTINUE
20    CONTINUE

      DO 40 i=1,nx+1

      x=xj+(i-1.d0)*dx
      x2=xj+i*dx
      U1=0.5d0*g*x*x
      U12=0.5d0*g*x2*x2
      U2= t+s*dexp(-x)
      U22= t+s*dexp(-x2)

      delta12=U2-U1
      if(dabs(delta12).lt.1.d-10)then
      int=int+1
      GO TO 40
      endif

      adelta12=dabs(delta12)
      Efull= 1.d0 + 4.d0*(V12/delta12)*(V12/delta12)
      Efull=dsqrt(Efull)
      Efull=(delta12 - adelta12*Efull)*0.5d0
      Efull=U1+Efull

      Ef(i-int,1)=x
      Ef(i-int,2)=U1
      Ef(i-int,3)=U2
      Ef(i-int,4)=Efull
      Ef(i-int,5)=V12

      delta22=U22-U12

      if(dabs(delta22).lt.1.d-10)GO TO 40

      adelta22=dabs(delta22)
      Efull2= 1.d0 + 4.d0*(V12/delta22)*(V12/delta22)
      Efull2=dsqrt(Efull2)
      Efull2=(delta22 - adelta22*Efull2)*0.5d0
      Efull2=U12+Efull2

      if(Efull-Efull2.GT.1.d-10)then
            if((islope.EQ.2).AND.(last.NE.2))then
            islope=1
            last=2
            id=id+1
            else if(islope.EQ.0)then
            islope=1
```

```
            endif
      endif

      if(Efull2-Efull.GT.1.d-10)then
            if((islope.EQ.1).AND.(last.NE.1))then
            islope=2
            last=1
            id=id+1
            else if(islope.EQ.0)then
            islope=2
            endif
      endif

40    CONTINUE

      RETURN
      END

C Constant V12, U2=t+s*(x-r)^ie

      SUBROUTINE GEN1b(g,s,t,r,ie,xi,nx,dx,a,Ef,id)
      implicit real*8 (a-h,o-z)
      dimension Ef(1100,5)

      islope=0
      last=0
      V12=a
      id=0
      int=0

      if(ie.LT.0)then
      xj=r+dx
      it=1
      else
      xj=xi
      it=2
      endif

      DO 20 i=1,1100
      DO 30 j=1,5
      Ef(i,j)=0.d0
30    CONTINUE
20    CONTINUE

      DO 40 i=1,nx+1

      x=xj+(i-1.d0)*dx
      x2=xj+i*dx
      U1=0.5d0*g*x*x
      U12=0.5d0*g*x2*x2
      U2=t+s/it*(x-r)**(ie)
      U22=t+s/it*(x2-r)**(ie)
```

```
      delta12=U2-U1
      if(dabs(delta12).lt.1.d-10)then
      int=int+1
      GO TO 40
      endif

      adelta12=dabs(delta12)
      Efull= 1.d0 + 4.d0*(V12/delta12)*(V12/delta12)
      Efull=dsqrt(Efull)
      Efull=(delta12 - adelta12*Efull)*0.5d0
      Efull=U1+Efull

      Ef(i-int,1)=x
      Ef(i-int,2)=U1
      Ef(i-int,3)=U2
      Ef(i-int,4)=Efull
      Ef(i-int,5)=V12

      delta22=U22-U12

      if(dabs(delta22).lt.1.d-10)GO TO 40

      adelta22=dabs(delta22)
      Efull2= 1.d0 + 4.d0*(V12/delta22)*(V12/delta22)
      Efull2=dsqrt(Efull2)
      Efull2=(delta22 - adelta22*Efull2)*0.5d0
      Efull2=U12+Efull2

      if(Efull-Efull2.GT.1.d-10)then
            if((islope.EQ.2).AND.(last.NE.2))then
            islope=1
            last=2
            id=id+1
            else if(islope.EQ.0)then
            islope=1
            endif
      endif

      if(Efull2-Efull.GT.1.d-10)then
            if((islope.EQ.1).AND.(last.NE.1))then
            islope=2
            last=1
            id=id+1
            else if(islope.EQ.0)then
            islope=2
            endif
      endif

40    CONTINUE

      RETURN
      END
```

```
C Linear V12, U2=t+s*exp(-x)

      SUBROUTINE GEN2(g,s,t,xi,nx,dx,a,b,Ef,id)
      implicit real*8 (a-h,o-z)
      dimension Ef(1100,5)

      islope=0
      id=0
      int=0
      last=0

      xj=xi

      DO 20 i=1,1100
      DO 30 j=1,5
      Ef(i,j)=0.d0
30    CONTINUE
20    CONTINUE

      DO 40 i=1,nx+1

      x=xj+(i-1d0)*dx
      x2=xj+i*dx

      U1=0.5d0*g*x*x
      U12=0.5d0*g*x2*x2
      V12=a*x+b
      V122=a*x2+b
      U2= t+s*dexp(-x)
      U22= t+s*dexp(-x2)

      delta12=U2-U1

      if(dabs(delta12).lt.1.d-10)then
      int=int+1
      GO TO 40
      endif

      adelta12=dabs(delta12)
      Efull= 1.d0 + 4.d0*(V12/delta12)*(V12/delta12)
      Efull=dsqrt(Efull)
      Efull=(delta12 - adelta12*Efull)*0.5d0
      Efull=U1+Efull

      Ef(i-int,1)=x
      Ef(i-int,2)=U1
      Ef(i-int,3)=U2
      Ef(i-int,4)=Efull
      Ef(i-int,5)=V12

      delta22=U22-U12

      if(dabs(delta22).lt.1.d-10)GO TO 40
```

```
      adelta22=dabs(delta22)
      Efull2= 1.d0 + 4.d0*(V122/delta22)*(V122/delta22)
      Efull2=dsqrt(Efull2)
      Efull2=(delta22 - adelta22*Efull2)*0.5d0
      Efull2=U12+Efull2

      if(Efull-Efull2.GT.1.d-10)then
            if((islope.EQ.2).AND.(last.NE.2))then
            islope=1
            last=2
            id=id+1
            else if(islope.EQ.0)then
            islope=1
            endif
      endif

      if(Efull2-Efull.GT.1.d-10)then
            if((islope.EQ.1).AND.(last.NE.1))then
            islope=2
            last=1
            id=id+1
            else if(islope.EQ.0)then
            islope=2
            endif
      endif

40    CONTINUE

C for sm k & lg a, if only a max is found, there must be a min
C it just might be outside the scanning range

      if((id.EQ.1).AND.(islope.EQ.1))then
      id=2
      endif

      RETURN
      end

C Linear V12, U2=t+s*(x-r)^ie

      SUBROUTINE GEN2b(g,s,t,r,ie,xi,nx,dx,a,b,Ef,id)
      implicit real*8 (a-h,o-z)
      dimension Ef(1100,5)

      islope=0
      id=0
      int=0
      last=0

      if(ie.LT.0)then
      xj=r+dx
      it=1
```

```
      else
      xj=xi
      it=2
      endif

      DO 20 i=1,1100
      DO 30 j=1,5
      Ef(i,j)=0.d0
30    CONTINUE
20    CONTINUE

      DO 40 i=1,nx+1

      x=xj+(i-1d0)*dx
      x2=xj+i*dx

      U1=0.5d0*g*x*x
      U12=0.5d0*g*x2*x2
      V12=a*x+b
      V122=a*x2+b
      U2=t+s/it*(x-r)**(ie)
      U22=t+s/it*(x2-r)**(ie)

      delta12=U2-U1

      if(dabs(delta12).lt.1.d-10)then
      int=int+1
      GO TO 40
      endif

      adelta12=dabs(delta12)
      Efull= 1.d0 + 4.d0*(V12/delta12)*(V12/delta12)
      Efull=dsqrt(Efull)
      Efull=(delta12 - adelta12*Efull)*0.5d0
      Efull=U1+Efull

      Ef(i-int,1)=x
      Ef(i-int,2)=U1
      Ef(i-int,3)=U2
      Ef(i-int,4)=Efull
      Ef(i-int,5)=V12

      delta22=U22-U12

      if(dabs(delta22).lt.1.d-10)GO TO 40

      adelta22=dabs(delta22)
      Efull2= 1.d0 + 4.d0*(V122/delta22)*(V122/delta22)
      Efull2=dsqrt(Efull2)
      Efull2=(delta22 - adelta22*Efull2)*0.5d0
      Efull2=U12+Efull2

      if(Efull-Efull2.GT.1.d-10)then
```

```
            if((islope.EQ.2).AND.(last.NE.2))then
            islope=1
            last=2
            id=id+1
            else if(islope.EQ.0)then
            islope=1
            endif
      endif

      if(Efull2-Efull.GT.1.d-10)then
            if((islope.EQ.1).AND.(last.NE.1))then
            islope=2
            last=1
            id=id+1
            else if(islope.EQ.0)then
            islope=2
            endif
      endif

40    CONTINUE

C for sm k & lg a, a min can be outside the scanning range

      if(((id.EQ.1).OR.(id.EQ.2)).AND.(islope.EQ.1))then
            if(ie.EQ.2)then
            id=3
            else
            id=2
            endif
      endif

      RETURN
      end

C inverse lorentzian V12, U2=t+s*exp(-x)

      SUBROUTINE GEN3(g,s,t,xi,nx,dx,a,b,c,Ef,id)
      implicit real*8 (a-h,o-z)
      dimension Ef(1100,5)

      islope=0
      id=0
      int=0
      last=0

      xj=xi

      DO 20 i=1,1100
      DO 30 j=1,5
      Ef(i,j)=0.d0
30    CONTINUE
20    CONTINUE
```

```
DO 40 i=1,nx+1

x=xj+(i-1.d0)*dx
x2=xj+i*dx

U1=0.5d0*g*x*x
U12=0.5d0*g*x2*x2
V12=a*(x+c)**2/(b+(x+c)**2)
V122=a*(x2+c)**2/(b+(x2+c)**2)
U2= t+s*dexp(-x)
U22= t+s*dexp(-x2)

delta12=U2-U1
if(dabs(delta12).lt.1.d-10)then
int=int+1
GO TO 40
endif

adelta12=dabs(delta12)
Efull= 1.d0 + 4.d0*(V12/delta12)*(V12/delta12)
Efull=dsqrt(Efull)
Efull=(delta12 - adelta12*Efull)*0.5d0
Efull=U1+Efull

Ef(i-int,1)=x
Ef(i-int,2)=U1
Ef(i-int,3)=U2
Ef(i-int,4)=Efull
Ef(i-int,5)=V12

delta22=U22-U12

if(dabs(delta22).lt.1.d-10)GO TO 40

adelta22=dabs(delta22)
Efull2= 1.d0 + 4.d0*(V122/delta22)*(V122/delta22)
Efull2=dsqrt(Efull2)
Efull2=(delta22 - adelta22*Efull2)*0.5d0
Efull2=U12+Efull2

if(Efull-Efull2.GT.1.d-10)then
      if((islope.EQ.2).AND.(last.NE.2))then
      islope=1
      last=2
      id=id+1
      else if(islope.EQ.0)then
      islope=1
      endif
endif

if(Efull2-Efull.GT.1.d-10)then
      if((islope.EQ.1).AND.(last.NE.1))then
      islope=2
```

```
            last=1
            id=id+1
            else if(islope.EQ.0)then
            islope=2
            endif
      endif

40    CONTINUE

      RETURN
      end

C inverse lorentzian V12, U2=t+s*(x-r)^ie

      SUBROUTINE GEN3b(g,s,t,r,ie,xi,nx,dx,a,b,c,Ef,id)
      implicit real*8 (a-h,o-z)
      dimension Ef(1100,5)

      islope=0
      id=0
      int=0
      last=0

      if(ie.LT.0)then
      xj=r+dx
      it=1
      else
      xj=xi
      it=2
      endif

      DO 20 i=1,1100
      DO 30 j=1,5
      Ef(i,j)=0.d0
30    CONTINUE
20    CONTINUE

      DO 40 i=1,nx+1

      x=xj+(i-1.d0)*dx
      x2=xj+i*dx

      U1=0.5d0*g*x*x
      U12=0.5d0*g*x2*x2
      V12=a*(x+c)**2/(b+(x+c)**2)
      V122=a*(x2+c)**2/(b+(x2+c)**2)
      U2=t+s/it*(x-r)**(ie)
      U22=t+s/it*(x2-r)**(ie)

      delta12=U2-U1
      if(dabs(delta12).lt.1.d-10)then
      int=int+1
      GO TO 40
```

```
      endif

      adelta12=dabs(delta12)
      Efull= 1.d0 + 4.d0*(V12/delta12)*(V12/delta12)
      Efull=dsqrt(Efull)
      Efull=(delta12 - adelta12*Efull)*0.5d0
      Efull=U1+Efull

      Ef(i-int,1)=x
      Ef(i-int,2)=U1
      Ef(i-int,3)=U2
      Ef(i-int,4)=Efull
      Ef(i-int,5)=V12

      delta22=U22-U12

      if(dabs(delta22).lt.1.d-10)GO TO 40

      adelta22=dabs(delta22)
      Efull2= 1.d0 + 4.d0*(V122/delta22)*(V122/delta22)
      Efull2=dsqrt(Efull2)
      Efull2=(delta22 - adelta22*Efull2)*0.5d0
      Efull2=U12+Efull2

      if(Efull-Efull2.GT.1.d-10)then
            if((islope.EQ.2).AND.(last.NE.2))then
            islope=1
            last=2
            id=id+1
            else if(islope.EQ.0)then
            islope=1
            endif
      endif

      if(Efull2-Efull.GT.1.d-10)then
            if((islope.EQ.1).AND.(last.NE.1))then
            islope=2
            last=1
            id=id+1
            else if(islope.EQ.0)then
            islope=2
            endif
      endif

40    CONTINUE

      RETURN
      end

C Lorentzian V12, U2=t+s*exp(-x)

      SUBROUTINE GEN4(g,s,t,xi,nx,dx,a,b,c,Ef,id)
      implicit real*8 (a-h,o-z)
```

```
      dimension Ef(1100,5)

      islope=0
      id=0
      int=0
      last=0

      xj=xi

      DO 20 i=1,1100
      DO 30 j=1,5
      Ef(i,j)=0.d0
30    CONTINUE
20    CONTINUE

      DO 40 i=1,nx+1

      x=xj+(i-1d0)*dx
      x2=xj+i*dx

      U1=0.5d0*g*x*x
      U12=0.5d0*g*x2*x2
      V12=a/(1+b*(x+c)**2)
      V122=a/(1+b*(x2+c)**2)
      U2= t+s*dexp(-x)
      U22= t+s*dexp(-x2)

      delta12=U2-U1

      if(dabs(delta12).lt.1.d-10)then
      int=int+1
      GO TO 40
      endif

      adelta12=dabs(delta12)
      Efull= 1.d0 + 4.d0*(V12/delta12)*(V12/delta12)
      Efull=dsqrt(Efull)
      Efull=(delta12 - adelta12*Efull)*0.5d0
      Efull=U1+Efull

      Ef(i-int,1)=x
      Ef(i-int,2)=U1
      Ef(i-int,3)=U2
      Ef(i-int,4)=Efull
      Ef(i-int,5)=V12

      delta22=U22-U12

      if(dabs(delta22).lt.1.d-10)GO TO 40

      adelta22=dabs(delta22)
      Efull2= 1.d0 + 4.d0*(V122/delta22)*(V122/delta22)
      Efull2=dsqrt(Efull2)
```

```
      Efull2=(delta22 - adelta22*Efull2)*0.5d0
      Efull2=U12+Efull2

      if(Efull-Efull2.GT.1.d-10)then
            if((islope.EQ.2).AND.(last.NE.2))then
            islope=1
            last=2
            id=id+1
            else if(islope.EQ.0)then
            islope=1
            endif
      endif

      if(Efull2-Efull.GT.1.d-10)then
            if((islope.EQ.1).AND.(last.NE.1))then
            islope=2
            last=1
            id=id+1
            else if(islope.EQ.0)then
            islope=2
            endif
      endif

40    CONTINUE

      RETURN
      end

C Lorentzian V12, U2=t+s*(x-r)^ie

      SUBROUTINE GEN4b(g,s,t,r,ie,xi,nx,dx,a,b,c,Ef,id)
      implicit real*8 (a-h,o-z)
      dimension Ef(1100,5)

      islope=0
      id=0
      int=0
      last=0

      if(ie.LT.0)then
      xj=r+dx
      it=1
      else
      xj=xi
      it=2
      endif

      DO 20 i=1,1100
      DO 30 j=1,5
      Ef(i,j)=0.d0
30    CONTINUE
20    CONTINUE
```

```
DO 40 i=1,nx+1

x=xj+(i-1d0)*dx
x2=xj+i*dx

U1=0.5d0*g*x*x
U12=0.5d0*g*x2*x2
V12=a/(1+b*(x+c)**2)
V122=a/(1+b*(x2+c)**2)
U2=t+s/it*(x-r)**(ie)
U22=t+s/it*(x2-r)**(ie)

delta12=U2-U1

if(dabs(delta12).lt.1.d-10)then
int=int+1
GO TO 40
endif

adelta12=dabs(delta12)
Efull= 1.d0 + 4.d0*(V12/delta12)*(V12/delta12)
Efull=dsqrt(Efull)
Efull=(delta12 - adelta12*Efull)*0.5d0
Efull=U1+Efull

Ef(i-int,1)=x
Ef(i-int,2)=U1
Ef(i-int,3)=U2
Ef(i-int,4)=Efull
Ef(i-int,5)=V12

delta22=U22-U12

if(dabs(delta22).lt.1.d-10)GO TO 40

adelta22=dabs(delta22)
Efull2= 1.d0 + 4.d0*(V122/delta22)*(V122/delta22)
Efull2=dsqrt(Efull2)
Efull2=(delta22 - adelta22*Efull2)*0.5d0
Efull2=U12+Efull2

if(Efull-Efull2.GT.1.d-10)then
      if((islope.EQ.2).AND.(last.NE.2))then
      islope=1
      last=2
      id=id+1
      else if(islope.EQ.0)then
      islope=1
      endif
endif

if(Efull2-Efull.GT.1.d-10)then
      if((islope.EQ.1).AND.(last.NE.1))then
```

```
            islope=2
            last=1
            id=id+1
            else if(islope.EQ.0)then
            islope=2
            endif
      endif

40    CONTINUE

      RETURN
      end

C discontinuous V12(that is __--) U2=t+s*exp(-x)

      SUBROUTINE GEN5(g,s,t,xi,nx,dx,c1,c2,xint,Ef,id)
      implicit real*8 (a-h,o-z)
      dimension Ef(1100,5)

      islope=0
      id=0
      int=0
      last=0

      DO i=1,1100
      DO j=1,5
      Ef(i,j)=0.d0
      ENDDO
      ENDDO

      xj=xi

      DO 40 i=1,nx+1
      x=xj+(i-1.d0)*dx
      x2=xj+i*dx

      U1=0.5d0*g*x*x
      U12=0.5d0*g*x2*x2
      U2= t+s*dexp(-x)
      U22= t+s*dexp(-x2)

      if(x.LT.xint)then
      V12=c1
      else
      V12=c2
      endif

      if(x2.LT.xint)then
      V122=c1
      else
      V122=c2
      endif
```

```
      delta12=U2-U1

      if(dabs(delta12).lt.1.d-10)then
      int=int+1
      GO TO 40
      endif

      adelta12=dabs(delta12)
      Efull= 1.d0 + 4.d0*(V12/delta12)*(V12/delta12)
      Efull=dsqrt(Efull)
      Efull=(delta12 - adelta12*Efull)*0.5d0
      Efull=U1+Efull

      Ef(i-int,1)=x
      Ef(i-int,2)=U1
      Ef(i-int,3)=U2
      Ef(i-int,4)=Efull
      Ef(i-int,5)=V12

      delta22=U22-U12

      if(dabs(delta22).lt.1.d-10)GO TO 40

      adelta22=dabs(delta22)
      Efull2= 1.d0 + 4.d0*(V122/delta22)*(V122/delta22)
      Efull2=dsqrt(Efull2)
      Efull2=(delta22 - adelta22*Efull2)*0.5d0
      Efull2=U12+Efull2

      if(Efull-Efull2.GT.1.d-10)then
            if((islope.EQ.2).AND.(last.NE.2))then
            islope=1
            last=2
            id=id+1
            else if(islope.EQ.0)then
            islope=1
            endif
      endif

      if(Efull2-Efull.GT.1.d-10)then
            if((islope.EQ.1).AND.(last.NE.1))then
            islope=2
            last=1
            id=id+1
            else if(islope.EQ.0)then
            islope=2
            endif
      endif

40    CONTINUE

      RETURN
      END
```

```
C Discontinuous V12, U2=t+s*(x-r)^ie

      SUBROUTINE GEN5b(g,s,t,r,ie,xi,nx,dx,c1,c2,xint,Ef,id)
      implicit real*8 (a-h,o-z)
      dimension Ef(1100,5)

      islope=0
      id=0
      int=0
      last=0

      DO i=1,1100
      DO j=1,5
      Ef(i,j)=0.d0
      ENDDO
      ENDDO

      if(ie.LT.0)then
      xj=r+dx
      it=1
      else
      xj=xi
      it=2
      endif

      DO 40 i=1,nx+1
      x=xj+(i-1.d0)*dx
      x2=xj+i*dx

      U1=0.5d0*g*x*x
      U12=0.5d0*g*x2*x2
      U2=t+s/it*(x-r)**(ie)
      U22=t+s/it*(x2-r)**(ie)

      if(x.LT.xint)then
      V12=c1
      else
      V12=c2
      endif

      if(x2.LT.xint)then
      V122=c1
      else
      V122=c2
      endif

      delta12=U2-U1

      if(dabs(delta12).lt.1.d-10)then
      int=int+1
      GO TO 40
      endif
```

```
      adelta12=dabs(delta12)
      Efull= 1.d0 + 4.d0*(V12/delta12)*(V12/delta12)
      Efull=dsqrt(Efull)
      Efull=(delta12 - adelta12*Efull)*0.5d0
      Efull=U1+Efull

      Ef(i-int,1)=x
      Ef(i-int,2)=U1
      Ef(i-int,3)=U2
      Ef(i-int,4)=Efull
      Ef(i-int,5)=V12

      delta22=U22-U12

      if(dabs(delta22).lt.1.d-10)GO TO 40

      adelta22=dabs(delta22)
      Efull2= 1.d0 + 4.d0*(V122/delta22)*(V122/delta22)
      Efull2=dsqrt(Efull2)
      Efull2=(delta22 - adelta22*Efull2)*0.5d0
      Efull2=U12+Efull2

      if(Efull-Efull2.GT.1.d-10)then
            if((islope.EQ.2).AND.(last.NE.2))then
            islope=1
            last=2
            id=id+1
            else if(islope.EQ.0)then
            islope=1
            endif
      endif

      if(Efull2-Efull.GT.1.d-10)then
            if((islope.EQ.1).AND.(last.NE.1))then
            islope=2
            last=1
            id=id+1
            else if(islope.EQ.0)then
            islope=2
            endif
      endif

40    CONTINUE

      RETURN
      END

C V12 discontinous in d/dx (non-smooth) U2=t+s*exp(-x)

      SUBROUTINE GEN6(g,s,t,xi,nx,dx,c1,a,xint,c2,Ef,id,ins10)
      implicit real*8 (a-h,o-z)
      dimension Ef(1100,5)
```

```
islope=0
id=0
int=0
last=0

DO i=1,1100
DO j=1,5
Ef(i,j)=0.d0
ENDDO
ENDDO

if(ins10.EQ.1)then
b=c1-a*xint
else if(ins10.EQ.2)then
b=c2-a*xint
else
b=xint
endif

xj=xi

DO 40 i=1,nx+1
x=xj+(i-1.d0)*dx
x2=xj+i*dx

U1=0.5d0*g*x*x
U12=0.5d0*g*x2*x2
U2= t+s*dexp(-x)
U22= t+s*dexp(-x2)

if(x.LT.(c1-b)/a)then
V12=c1
else if((x.GE.(c1-b)/a).AND.(x.LT.(c2-b)/a))then
V12=a*x+b
else
V12=c2
endif

if(x2.LT.(c1-b)/a)then
V122=c1
else if((x2.GE.(c1-b)/a).AND.(x2.LT.(c2-b)/a))then
V122=a*x2+b
else
V122=c2
endif

delta12=U2-U1

if(dabs(delta12).lt.1.d-10)then
int=int+1
GO TO 40
endif
```

```
      adelta12=dabs(delta12)
      Efull= 1.d0 + 4.d0*(V12/delta12)*(V12/delta12)
      Efull=dsqrt(Efull)
      Efull=(delta12 - adelta12*Efull)*0.5d0
      Efull=U1+Efull

      Ef(i-int,1)=x
      Ef(i-int,2)=U1
      Ef(i-int,3)=U2
      Ef(i-int,4)=Efull
      Ef(i-int,5)=V12

      delta22=U22-U12

      if(dabs(delta22).lt.1.d-10)GO TO 40

      adelta22=dabs(delta22)
      Efull2= 1.d0 + 4.d0*(V122/delta22)*(V122/delta22)
      Efull2=dsqrt(Efull2)
      Efull2=(delta22 - adelta22*Efull2)*0.5d0
      Efull2=U12+Efull2

      if(Efull-Efull2.GT.1.d-10)then
            if((islope.EQ.2).AND.(last.NE.2))then
            islope=1
            last=2
            id=id+1
            else if(islope.EQ.0)then
            islope=1
            endif
      endif

      if(Efull2-Efull.GT.1.d-10)then
            if((islope.EQ.1).AND.(last.NE.1))then
            islope=2
            last=1
            id=id+1
            else if(islope.EQ.0)then
            islope=2
            endif
      endif

40    CONTINUE

      RETURN
      END

C V12 discontinuous in d/dx, U2=t+s*(x-r)^ie

      SUBROUTINE GEN6b(g,s,t,r,ie,xi,nx,dx,c1,a,xint,c2,Ef,id,ins10)
      implicit real*8 (a-h,o-z)
      dimension Ef(1100,5)
```

```
islope=0
id=0
int=0
last=0

DO i=1,1100
DO j=1,5
Ef(i,j)=0.d0
ENDDO
ENDDO

if(ins10.EQ.1)then
b=c1-a*xint
else if(ins10.EQ.2)then
b=c2-a*xint
else
b=xint
endif

if(ie.LT.0)then
xj=r+dx
it=1
else
xj=xi
it=2
endif

DO 40 i=1,nx+1
x=xj+(i-1.d0)*dx
x2=xj+i*dx

U1=0.5d0*g*x*x
U12=0.5d0*g*x2*x2
U2=t+s/it*(x-r)**(ie)
U22=t+s/it*(x2-r)**(ie)

if(x.LT.(c1-b)/a)then
V12=c1
else if((x.GE.(c1-b)/a).AND.(x.LT.(c2-b)/a))then
V12=a*x+b
else
V12=c2
endif

if(x2.LT.(c1-b)/a)then
V122=c1
else if((x2.GE.(c1-b)/a).AND.(x2.LT.(c2-b)/a))then
V122=a*x2+b
else
V122=c2
endif
```

```
      delta12=U2-U1

      if(dabs(delta12).lt.1.d-10)then
      int=int+1
      GO TO 40
      endif

      adelta12=dabs(delta12)
      Efull= 1.d0 + 4.d0*(V12/delta12)*(V12/delta12)
      Efull=dsqrt(Efull)
      Efull=(delta12 - adelta12*Efull)*0.5d0
      Efull=U1+Efull

      Ef(i-int,1)=x
      Ef(i-int,2)=U1
      Ef(i-int,3)=U2
      Ef(i-int,4)=Efull
      Ef(i-int,5)=V12

      delta22=U22-U12

      if(dabs(delta22).lt.1.d-10)GO TO 40

      adelta22=dabs(delta22)
      Efull2= 1.d0 + 4.d0*(V122/delta22)*(V122/delta22)
      Efull2=dsqrt(Efull2)
      Efull2=(delta22 - adelta22*Efull2)*0.5d0
      Efull2=U12+Efull2

      if(Efull-Efull2.GT.1.d-10)then
            if((islope.EQ.2).AND.(last.NE.2))then
            islope=1
            last=2
            id=id+1
            else if(islope.EQ.0)then
            islope=1
            endif
      endif

      if(Efull2-Efull.GT.1.d-10)then
            if((islope.EQ.1).AND.(last.NE.1))then
            islope=2
            last=1
            id=id+1
            else if(islope.EQ.0)then
            islope=2
            endif
      endif

40    CONTINUE

      if((id.EQ.0).AND.(islope.EQ.1).AND.(ie.EQ.2))then
      id=1
```

```
else if((id.EQ.2).AND.(ie.EQ.2))then
id=3
endif

RETURN
END
```

A2. Fortran programme to create Gaussian 98 input for grid optimization

```
C234567891234567891234567891234567891234567891234567891234567891234567891
C This programme produces as output: a Gaussian input file
C to optimize grids of 7-11 orbital for HBN
C commented out statement are there to help replace input.txt
C should it get deleted.

      implicit real*8 (a-h,o-z)
      character*3 sym
      character*10 chk
      character*20 file1,file2,title,output,junk
      character*90 met1,met2
      character*60 set,basis
      dimension sym(11),basis(80,3),nl(3),r(11,3)

      DO i=1,11
      DO j=1,3
      r(i,j)=0.d0
      ENDDO
      ENDDO

      nw2=0
      nh2=0
      nx3=0
      ny3=0
      nz3=0
      nx2=0
      ny2=0
      nz2=0
      nx=0
      ny=0
      nz=0

      OPEN(20,file='input.txt',status='unknown')

      READ(20,*)file1
      READ(20,*)chk
      READ(20,600)met1,met2
      READ(20,*)title
      READ(20,*)iq,im
      READ(20,*)ins1

C ins1= 1. 7orb line 2. 9orb cross
C 3. 11orb “line-box” 4. trapezoid “line-box”
C             Bq______Bq
C3,4. Bq-H--B--|      |--Bq-N--Bq-Bq
C             Bq______Bq

      IF((ins1.EQ.2).OR.(ins1.EQ.4))THEN
      iorb=8
      ELSE
      iorb=7
```

```
      ENDIF

      IF(ins1.EQ.1)THEN
      io=7
      ELSE IF(ins1.EQ.2)THEN
      io=9
      ELSE
      io=11
      ENDIF

C read basis sets for H, B, N.

      DO i=1,3
      READ(20,*)file2
      OPEN(21,file=file2,status='unknown')
      nl(i)=0
      DO
      READ(21,601,END=300)set
      nl(i)=nl(i)+1
      basis(nl(i),i)=set
      ENDDO
300   close(21)
      ENDDO

C orbital positions

      sym(1)='H'
      sym(2)='B'
      sym(3)='N'
      sym(4)='Bq1'
      sym(5)='Bq2'
      sym(6)='Bq3'
      sym(7)='Bq4'
      sym(8)='Bq5'
      sym(9)='Bq6'
      sym(10)='Bq7'
      sym(11)='Bq8'

      DO i=1,iorb
      READ(20,*)(r(i,j),j=1,3)
      ENDDO

      IF(iorb.EQ.7)THEN
      READ(20,*)junk
      ENDIF

c #steps,increments x,y,z for active linear Bq

      READ(20,*)nx,dx
      READ(20,*)ny,dy
      READ(20,*)nz,dz

c #steps, increments x,y,z for 1pair of off-linear Bq (2,4)
```

```
c /centre of "line-box"(3)

      IF(ins1.NE.1)THEN
      READ(20,*)nx2,dx2
      READ(20,*)ny2,dy2
      READ(20,*)nz2,dz2

c "line-box" centre position, initial, steps, increments height & width
c position,steps, increment of 2nd side of "line-box"

            IF(ins1.EQ.3)THEN
            READ(20,*)xci,yci,zci
            READ(20,*)h2i,w2i
            READ(20,*)nh2,dh2
            READ(20,*)nw2,dw2
            ENDIF

            IF(ins1.EQ.4)THEN
            READ(20,*)(r(10,j),j=1,3)
            READ(20,*)nx3,dx3
            READ(20,*)ny3,dy3
            READ(20,*)nz3,dz3
            ENDIF
      ENDIF

      CLOSE(20)

      zi=r(4,3)
      yi=r(4,2)
      xi=r(4,1)

      IF((ins1.EQ.2).OR.(ins1.EQ.4))THEN
      zi2=r(8,3)
      yi2=r(8,2)
      xi2=r(8,1)
            IF(ins1.EQ.4)THEN
            zi3=r(10,3)
            yi3=r(10,2)
            xi3=r(10,1)
            ENDIF
      ENDIF

      OPEN(22,file=file1,status='unknown')

      ni=0
      nd=(nw2+1)*(nh2+1)*(nx2+1)*(ny2+1)*(nz2+1)
      nd=nd*(nx+1)*(ny+1)*(nz+1)*(nz3+1)*(ny3+1)
      nd=nd*(nx3+1)

      DO 400 i=1,nw2+1
      DO 401 i1=1,nh2+1
      DO 402 i2=1,nx3+1
      DO 403 i3=1,ny3+1
```

```
DO 404 i4=1,nz3+1
DO 405 i5=1,nx2+1
DO 406 i6=1,ny2+1
DO 407 i7=1,nz2+1
DO 408 i8=1,nx+1
DO 409 i9=1,ny+1
DO 410 j1=1,nz+1

ni=ni+1

r(4,3)=zi+(j1-1)*dz
r(4,2)=yi+(i9-1)*dy
r(4,1)=xi+(i8-1)*dx

h2=h2i+(i1-1)*dh2
w2=w2i+(i-1)*dw2

IF((ins1.EQ.2).OR.(ins1.EQ.4))THEN
      r(8,3)=zi2+(i7-1)*dz2
      r(8,2)=yi2+(i6-1)*dy2
      r(8,1)=xi2+(i5-1)*dx2
      r(9,3)=r(8,3)
      r(9,2)=-r(8,2)
      r(9,1)=r(8,1)
      IF(ins1.EQ.4)THEN
            r(10,3)=zi3+(i4-1)*dz3
            r(10,2)=yi3+(i3-1)*dy3
            r(10,1)=xi3+(i2-1)*dx3
            r(11,3)=r(10,3)
            r(11,2)=-r(10,2)
            r(11,1)=r(10,1)
            ENDIF
ELSE IF(ins1.EQ.3)THEN
      zc=zci+(i7-1)*dz2
      yc=yci+(i6-1)*dy2
      xc=xci+(i5-1)*dx2

      r(8,3)=zc-w2
      r(9,3)=r(8,3)
      r(10,3)=zc+w2
      r(11,3)=r(10,3)
      r(8,2)=yc+h2
      r(9,2)=yc-h2
      r(10,2)=r(8,2)
      r(11,2)=r(9,2)
ENDIF

WRITE(22,602)'%chk=',chk,ni,'.chk'
WRITE(22,603)'#n ', met1
WRITE(22,603)'#n ', met2
WRITE(22,*)' '
WRITE(22,*)title
WRITE(22,*)' '
```

```
      WRITE(22,604)iq,im
      WRITE(22,605)sym(1),' 0   ',(r(1,ir),ir=1,2),' zH'
      WRITE(22,606)sym(2),' 0   ',(r(2,ir),ir=1,3)
      WRITE(22,605)sym(3),' 0   ',(r(3,ir),ir=1,2),' zN'

      DO ir=4,io
      WRITE(22,606)sym(ir),' 0  ',(r(ir,is),is=1,3)
      ENDDO

      WRITE(22,*)'     Variables:'
      WRITE(22,*)'zH ',r(1,3)
      WRITE(22,*)'zN ',r(3,3)
      WRITE(22,*)' '

      DO il=1,3
      IF(il.EQ.1)THEN
            IF(ins1.EQ.1)THEN
            WRITE(22,*)' 1 4 5 7 0'
            ELSE IF(ins1.EQ.2)THEN
            WRITE(22,*)' 1 4 5 7 8 9 0'
            ELSE
            WRITE(22,*)' 1 4 5 7 8 9 10 11 0'
            ENDIF
      ELSE IF(il.EQ.3)THEN
            WRITE(22,*)' 3 6 0'
      ELSE
            WRITE(22,*)' 2 0'
      ENDIF
      DO kl=1,nl(il)
      write(22,*)' ',basis(kl,il)
      ENDDO
      WRITE(22,607)'****'
      ENDDO

      IF(ni.NE.nd)THEN
      WRITE(22,*)' '
      WRITE(22,*)'--Link1--'
      ENDIF

410   CONTINUE
409   CONTINUE
408   CONTINUE
407   CONTINUE
406   CONTINUE
405   CONTINUE
404   CONTINUE
403   CONTINUE
402   CONTINUE
401   CONTINUE
400   CONTINUE

600   FORMAT(A90)
601   FORMAT(A60)
```

```
602   FORMAT(A5,A10,I2,A4)
603   FORMAT(A3,A90)
604   FORMAT(I2,1x,I2)
605   FORMAT(A3,A5,2(F8.4),A5)
606   FORMAT(A3,A5,3(F8.4))
607   FORMAT(1x,A4)

      CLOSE(22)

      END
```

A2.1 'input.txt'

In the comments the '/' symbol designates an alternative set of variables that can be written to the same line

```
BNH631c1-1.gjf
HBNb
uhf/gen scf=(conver=10,MaxCycle=2048) guess=(save,notranslate)
Opt=(z-matrix,MaxCycle=100,Calcall) nosymmetry pop=None
HBN                              |title
0 2                              |charge, multiplicity
2                                     |1.line 2.cross 3."line-box" 4.2sided
anchored "line-box"
631G-H.out
631G-B.out
631G-N.out
0.0000 0.0010 2.2099             |H x,y,z
0.0010 0.0000 0.0000             |B x,y,z
0.0010 0.0000 1.2309             |N
0.0010 0.0000 -1.213             |'active' Bq
0.0000 0.0010 1.5810             |H-like Bq
0.0000 0.0010 1.2445             |N-like Bq
0.0010 0.0000 -1.1597            |H-like Bq
0.0000 1.0000 0.0000              |for ins=2, off-lin H-like Bq/"line-box"
side1
0 0.3                            |nx dx for Bq active
0 0.01                           |ny dy
0 0.01                           |nz dz
0 0.01                                |nx dx for off-lin/"line-box" centre
Bq/"line-box" side1
5 0.1                            |ny dy
10 0.1                           |nz dz
0.0000 1.1000 0.0000             |"line-box" centre x,y,z/"line-box" side 2
0 0.0                            |1/2 "line-box" height, width/nx dx
0 0.1                            |nh,dh/ny dy
0 0.1                            |nw,dw/nz dz
```

A3. Fortran programme to analyze Gaussian 98 grid optimization output

```
C234567890123456789012345678901234567890123456789012345678901234567890123456789012
C This programme takes the grid optimization Gaussian output file and
C produces as output the position of each orbital and the energy
C of that configuration.

      character*20 line,hf,Egrid
      character*30 input,output
      character*8 xH,yH
      implicit real*8 (a-h,o-z)
      dimension r(11,3)

      DO i=1,11
      DO j=1,3
      r(i,j)=0.d0
      ENDDO
      ENDDO

      write(6,*)'Give grid input file'
      read(5,*)input
      write(6,*)'Give output file'
      read(5,*)output
      write(6,*)'1. 7orb line 2. 9orb cross'
      write(6,*)'3. 11orb "line-box" 4. 11orb anchored "line-box"'
      read(5,*)ins1

      if(ins1.EQ.1)then
      io=7
      else if(ins1.EQ.2)then
      io=9
      else
      io=11
      endif

      open(20,file=input,status='unknown')
      open(21,file=output,status='unknown')

301   read(20,602,end=300)line,hf

      if(line.EQ.' SCF Done:  E(UHF) =')then
      Egrid=hf
      endif

      if(line.EQ.' Charge =  0 Multipl')then
      read(20,*,end=300)line,a,r(1,1),r(1,2)
      read(20,*,end=300)line,a,r(2,1),r(2,2),r(2,3)
      read(20,*,end=300)line,a,r(3,1),r(3,2)
            DO i=4,io
            read(20,*,end=300)line,a,r(i,1),r(i,2),r(i,3)
            ENDDO
      endif
```

```
      if(hf.EQ.'   !   Optimized Par')then
      DO i=1,4
      read(20,*,end=300)line
      ENDDO

      read(20,600,end=300)r(1,3)
      read(20,600,end=300)r(3,3)

      if(ins1.EQ.2)then
      write(21,606)((r(i,j),j=1,3),i=1,9),Egrid
      else if(ins1.EQ.1)then
      write(21,605)((r(i,j),j=1,3),i=1,7),Egrid
      else if(ins1.EQ.3)then
      xc=r(8,1)
      yc=r(8,2)-(r(8,2)-r(9,2))/2
      zc=r(8,3)-(r(8,3)-r(10,3))/2
      h2=abs(r(8,2)-r(9,2))/2
      w2=abs(r(8,3)-r(10,3))/2
      write(21,607)((r(i,j),j=1,3),i=1,7),xc,yc,zc,h2,w2,Egrid
      else
      write(21,608)((r(i,j),j=1,3),i=1,11),Egrid
      endif

      endif

      go to 301

600   FORMAT(17x,F11.6)
601   FORMAT(19x,A8)
602   FORMAT(2A20)
605   FORMAT(21(F12.8,2x),A20)
606   FORMAT(27(F12.8,2x),A20)
607   FORMAT(21(F12.8,2x),5(F12.8,2x),A20)
608   FORMAT(33(F12.8,2x),A20)

300   close(20)
      close(21)
      end
```

A4. Fortran programme to produce Gaussian 98 input to build the diabatic potential energy curves

```
C23456789123456789123456789123456789123456789123456789123456789012
C This programme’s output is a Gaussian input file
C includes initializing the optimal grid
C moving the H nucleus along a prescribed trajectory

      implicit real*8 (a-h,o-z)
      character*3 sym,junk
      character*20 filename,chk,filename2,filename3,title
      character*20 filename4
      character*60 b1,b2,line,set,basis
      character*90 met1,met2,met3,met4
      dimension oc(11,3),qc(3,4),basis(80,3),sym(11),nl(3)
      dimension zH(3),yH(3),zN(3),a(3),b(3),rHN(100),rBN(100)
      dimension angle(100)

      pi=2*ACOS(0.0)

      DO i=1,11
            DO j=1,3
            oc(i,j)=0.0
            ENDDO
      ENDDO

      open(20,file='coordsc.txt',status='unknown')

      read(20,*)filename
      open(21,file=filename,status='unknown')

      read(20,*)chk
      write(21,*)'%chk=',chk

      read(20,601)met1,met2
      write(21,602)'#n ',met1
      write(21,602)'#n ',met2
      write(21,*)' '

c     method for FGO links
      read(20,601)met3,met4

      read(20,*)title
      write(21,*)title
      write(21,*)' '

      read(20,*)iq,im
      write(21,603)iq,im

      DO 304 i=1,3
      read(20,*)filename2
      open(22,file=filename2,status='unknown')
```

```
      nl(i)=0
            DO
            read(22,604,end=301)set
            nl(i)=nl(i)+1
            basis(nl(i),i)=set
            ENDDO
301   close(22)
304   CONTINUE

      read(20,*)iorb

      DO i=1,iorb
      read(20,*)sym(i),(oc(i,j),j=1,3)
      write(21,*)sym(i),' 0   ',(oc(i,j),j=1,3)
      ENDDO

      DO i=1,11-iorb
      read(20,*)junk
      ENDDO

      write(21,*)' '

      DO 300 i=1,3
      if(i.EQ.1)then
            if(iorb.EQ.7)then
            write(21,*)' 1 4 5 7 0'
            else if(iorb.EQ.9)then
            write(21,*)' 1 4 5 7 8 9 0'
            else
            write(21,*)' 1 4 5 7 8 9 10 11 0'
            endif
      else if(i.EQ.2)then
            write(21,*)' 2 0'
      else
            write(21,*)' 3 6 0'
      endif
            DO 303 j=1,nl(i)
            write(21,*)' ',basis(j,i)
303         CONTINUE

      write(21,605)'****'
300   CONTINUE

      iq2=iq

      DO i=1,3
      read(20,*)(qc(i,j),j=1,4)
      iq2=iq2-qc(i,4)
      ENDDO

c ins1: 1.ellipse  2.Newton polynomial 3.Fukui path 4.weighted ellipse
c 5. H parabolic N linear 6.H Fukui N fixed 7.H Fukui N linear
```

```
      read(20,*)ins1
      if((ins1.EQ.1).OR.(ins1.EQ.4))then
            read(20,*)thetai,ntheta,dtheta,zc,yc,zr,yr
            n=ntheta
      else if((ins1.EQ.2).OR.(ins1.EQ.5))then
            read(20,*)zH(1),zH(2),zH(3)
            read(20,*)yH(1),yH(2),yH(3)
                  DO i=1,3
                  s=0.0
                  p=1.0
                  DO j=1,i-1
                  p0=p
                  p=p*(zH(i)-zH(j))
                  s=s+a(j)*p0
                  ENDDO
                  a(i)=(yH(i)-s)/p
                  ENDDO
            if(ins1.EQ.2)then
            read(20,*)zN(1),zN(2),zN(3)
            b(1)=zN(1)
            b(2)=(zN(2)-b(1))/(zH(2)-zH(1))
            b(3)=zN(3)-b(1)-b(2)*(zH(3)-zH(1))
            b(3)=b(3)/((zH(3)-zH(2))*(zH(3)-zH(1)))
            else
            read(20,*)zN(1),zN(3)
            b(1)=zN(1)
            b(2)=(zN(3)-b(1))/(zH(3)-zH(1))
            b(3)=0.d0
            endif
            read(20,*)zi,nz,dz
            n=nz
      else if((ins1.EQ.3).OR.(ins1.EQ.6).OR.(ins1.EQ.7))then
            read(20,*)thetai,ntheta
            read(20,*)filename4
            open(23,file=filename4,status='unknown')
            n=ntheta

            DO
            read(23,*,end=306)rNH,rNB,theta
            if(theta.EQ.thetai)GO TO 305
            ENDDO

305         rHN(1)=rNH
            rBN(1)=rNB
            angle(1)=theta

            DO i=2,ntheta+1
            read(23,*,end=306)rHN(i),rBN(i),angle(i)
            ENDDO

306         close(23)
      else
            write(6,*)'CHARGE TRAJECTORY ERROR!'
```

```
      GO TO 333
      endif

      if(n.GT.60)then
      write(6,*)'TOO MANY LINKS!'
      GO TO 333
      endif

302   close(20)

      DO ii=1,n+1
      write(21,*)' '
      write(21,*)'--Link1--'
      write(21,*)'%chk=',chk
      write(21,602)'#n ',met3
      write(21,602)'#n ',met4
      write(21,*)' '
      write(21,*)title
      write(21,*)' '
      write(21,603)iq2,im

      DO ij=1,iorb
      write(21,*)'Bq  0   ',(oc(ij,j),j=1,3)
      ENDDO
      write(21,*)' '

      DO ik=1,3
      if(ik.EQ.1)then
            if(iorb.EQ.7)then
            write(21,*)' 1 4 5 7 0'
            else if(iorb.EQ.9)then
            write(21,*)' 1 4 5 7 8 9 0'
            else
            write(21,*)' 1 4 5 7 8 9 10 11 0'
            endif
      else if(ik.EQ.2)then
            write(21,*)' 2 0'
      else
            write(21,*)' 3 6 0'
      endif
            DO il=1,nl(ik)
            write(21,*)' ',basis(il,ik)
            ENDDO
      write(21,605)'****'
      ENDDO

      write(21,*)' '

      tb=oc(3,3)
      tm=(oc(6,3)-tb)/(oc(7,3)-oc(1,3))

      if((ins1.EQ.1).OR.(ins1.EQ.4))then
      theta=thetai*pi/180.0+(ii-1)*dtheta*pi/180.0
```

```
      qc(1,3)=zc+zr*cos(theta)
      qc(1,2)=yc+yr*sin(theta)
            if(ins1.EQ.4)then
            qc(3,3)=tb+tm*(qc(1,3)-oc(1,3))
            endif
      else if((ins1.EQ.2).OR.(ins1.EQ.5))then
      z=zi+(ii-1)*dz
      qc(1,3)=z
      qc(1,2)=a(1)+a(2)*(z-zH(1))+a(3)*(z-zH(1))*(z-zH(2))
      qc(3,3)=b(1)+b(2)*(z-zH(1))+b(3)*(z-zH(1))*(z-zH(2))

      else if((ins1.EQ.3).OR.(ins1.EQ.6).OR.(ins1.EQ.7))then
      qc(1,2)=rHN(ii)*sin(angle(ii)*pi/180)
      qc(1,3)=rBN(ii)-rHN(ii)*cos(angle(ii)*pi/180)
            if(ins1.EQ.3)then
            qc(3,3)=rBN(ii)
            else if(ins1.EQ.6)then
            qc(3,3)=oc(3,3)
            else
            qc(3,3)=tb+tm*(qc(1,3)-oc(1,3))
            endif
      endif

      write(21,606)((qc(k,j),j=1,4),k=1,3)

      ENDDO

601   FORMAT(A90)
602   FORMAT(A3,A90)
603   FORMAT(I3,1x,I1)
604   FORMAT(A60)
605   FORMAT(1x,A4)
606   FORMAT(4(F8.4,1x))
607   FORMAT(A90)
608   FORMAT(A3,A90)
609   FORMAT(1x,A13)
610   FORMAT(1x,A7)
      close(20)
333   end
```

A4.1 'coordsc.txt'

```
gedHBNkp1-1.gjf                              |Gaussian input filename
HBN6.chk                                     |checkpoint filename
uhf/gen       scf=(conver=10,MaxCycle=2048)       guess=(save,notranslate)
|met1 grid initialization
nosymmetry                                                        pop=None
|met2 grid initialization
uhf/gen                                        guess=(read,only,notranslate)
|met3 potential curves
charge                                                          nosymmetry
|met4 potential curves
HBN                                          |title
```

```
0 2                                     |charge,multiplicity
321difG-H.out                           |H basis set
321difG-B.out                           |B basis set
321difG-N.out                           |N basis set
11                                      |# of orbitals
H 0.0000 0.0010 -1.1637                 |H x,y,z
B 0.0010 0.0000 0.0000                  |B x,y,z
N 0.0010 0.0000 1.2601                  |N x,y,z
Bq 0.0010 0.0000 -1.206                 |H-like Bq
Bq 0.0000 0.0010 1.719                  |H-like Bq
Bq 0.0000 0.0010 1.2452                 |N-like Bq
Bq 0.0010 0.0000 2.2281                 |H-like Bq HBN-BNH alt H
Bq 0.0000 1.6520 0.1440                 |cross/"line-box" Bq
Bq 0.0000 -1.652 0.1440                 |cross/"line-box" Bq
Bq 0.0000 1.1420 1.1770                 |"line-box" Bq
Bq 0.0000 -1.142 1.1770                 |"line-box" Bq
0.0000 0.0010 -1.1637 1.0               |H nuclear x,y,z,q
0.0010 0.0000 0.0000 5.0                |B nuclear x,y,z,q
0.0010 0.0000 1.2601 7.0                |N nuclear x,y,z,q
2                                       |trajectory 1.ellipse 2.parabola
3.Fukui path 4.weighted ellipse 5.H parabola N linear 6.Fukui N fixed
7.Fukui N linear
2.2281 0.2816 -1.1637                          |1.initial angle # steps
increment,zc yc zr yr
0.0000 1.2201 0.0010                             |2.zH(R,TS,P)/ yH/ zN/
H:zi,nz,dz
1.2601 1.2601 1.2601                    |3.theta(HNB),ntheta/ filename
2.4000 60 -0.0100                       |4. (1.)
1.2445 1.2309 1.2440                    |5.(2.)\zN(R,P)/(2.)
2.4 60 -0.01                            |6.(3.)
                                        |7.(3.)
```

A5. Fortran programme to analyze Gaussian 98 output for building diabatic potential energy curves.

```
C234567890123456789012345678901234567890123456789012345678901234567890123456789012
C This programme reads the diabatic curve building Gaussian output file
C and gives the position of each nucleus and the total energy

      implicit real*8 (a-h,o-z)
      character*20 input,output,line,ennc,eenc,ekec
      character*5 line1
      character*8 x,y,z,qc
      dimension qc(9),eee(2,2,2)

C the electronic energy is a constant determined by
C the grid type and the basis set

c BNH 3-21+G lin
      eee(1,1,1)=46.90622055007
c HBN 3-21+G lin
      eee(2,1,1)=45.40324417467
c BNH 6-31G lin
      eee(1,2,1)=47.35133933707
c HBN 6-31G lin
      eee(2,2,1)=45.80926018145
c BNH 3-21+G keb
      eee(1,1,2)=46.88458782187
c HBN 3-21G keb
      eee(2,1,2)=45.40775270576

      write(6,*)'Give input file'
      read(5,*)input
      write(6,*)'Give output file'
      read(5,*)output

      write(6,*)'ISOMER: 1. BNH 2. HBN'
      read(5,*)ins1
      write(6,*)'BASIS SET: 1. 3-21+G 2. 6-31G'
      read(5,*)ins2
      write(6,*)'GRID: 1.linear 2.”line-box”'
      read(5,*)ins3

      open(20,file=input,status='unknown')
      open(21,file=output,status='unknown')

301   n=0
302   read(20,601,end=304)line1,x,y,z
      if(line1.NE.' XYZ=')GO TO 302
      n=n+1
      qc(3*n-2)=x
      qc(3*n-1)=y
      qc(3*n)=z
      if(n.NE.3)GO TO 302
```

```
303   read(20,602,end=304)line1,ennc,eenc,ekec
      if(line1.NE.' N-N=')GO TO 303

      open(22,file='converter.txt',status='unknown')
      write(22,*)ennc,eenc,ekec
      close(22)

      open(23,file='converter.txt',status='unknown')
      read(23,*)enn,een,eke
      close(23)

      etot=eee(ins1,ins2,ins3)+enn+een+eke

      write(21,603)(qc(i),i=1,9),etot
      GO TO 301

304   close(20)
      close(21)

600   FORMAT(2A20)
601   FORMAT(A5,3(2X,A8))
602   FORMAT(A5,A20,4X,A20,4X,A20)
603   FORMAT(9(A8,2X),F19.12)

      end
```